Auto-regulatory J-domain interactions control Hsp70 recruitment in the oligomeric DNAJB8 co-chaperone

Bryan D. Ryder[1,2], Irina Matlahov[3], Sofia Bali[1,2], Jaime Vaquer-Alicea[2,4], Patrick C.A. van der Wel[3,5*], Lukasz A. Joachimiak[2,6*]

[1] Molecular Biophysics Graduate Program, University of Texas Southwestern Medical Center, Dallas, TX 75390, United States

[2] Center for Alzheimer's and Neurodegenerative Diseases, University of Texas Southwestern Medical Center, Dallas, TX 75390, United States

[3] Department of Structural Biology, University of Pittsburgh School of Medicine, Pittsburgh, PA 15213, USA

[4] Neuroscience Graduate Program, University of Texas Southwestern Medical Center, Dallas, TX 75390, United States

[5] Zernike Institute for Advanced Materials, University of Groningen, 9747 AG Groningen, Netherlands

[6] Department of Biochemistry, University of Texas Southwestern Medical Center, Dallas, TX 75390, United States

[*] Correspondence: Lukasz.Joachimiak@utsouthwestern.edu, p.c.a.van.der.wel@rug.nl

Summary

Molecular chaperones closely regulate cellular protein homeostasis, with the Hsp40/Hsp70 families managing to be both versatile and specific. Traditionally seen as "co-chaperones", Hsp40s are now recognized as crucially important, but their structure and function are still poorly understood. The oligomeric members have especially proven resistive to in-depth characterization. Here we present a hybrid structure-function study of a homo-oligomeric Hsp40, DnaJB8, which is known for its potent suppression of aggregation by polyglutamine and other amyloidogenic proteins. Using a combination of biochemical, NMR, crosslinking-mass spectrometry, and *in silico* approaches, we examine the architecture and dynamics of DnaJB8 oligomers. We identify an electrostatically driven intra-oligomer interaction between the DnaJ-characteristic J-Domain (JD) and DnaJB8's C-terminal domain (CTD). This inter-domain contact is autoinhibitory of Hsp70 interaction by occluding the JD surface essential for Hsp70 binding. Disruption of the JD-CTD interaction liberates and mobilizes the JD to facilitate Hsp70 binding. These results identify the JD-CTD interaction as an evolutionarily conserved built-in regulatory element that controls recruitment of Hsp70 to activated Hsp40 co-chaperones.

INTRODUCTION

Molecular chaperones play central roles in cellular homeostasis by facilitating protein folding, directing protein folding quality control, and refolding stress-denatured substrates. Structural descriptions of chaperone architecture and conformational cycles have been key to understanding their biological function. Thus, functional insight into chaperones relies on structural biology tools such as NMR, cryo-EM and X-ray crystallography[1-7]. This structural information has been used to identify substrate binding sites, key conformational changes that drive substrate release, and the role of ATP hydrolysis. A molecular view of chaperones is essential to explain chaperones' biological function in protein folding and suggest new avenues for treating protein misfolding diseases.

The cellular chaperone network needs to handle a wide variety of protein substrates in numerous different (mis)folded states. This demands a combination of broad versatility and specificity in terms of substrate recognition, even though the central players Hsp70 and Hsp90 are highly conserved. This apparent contradiction is resolved by the Hsp40 (DnaJ) family of proteins, which are co-chaperones that recruit and regulate the activity of Hsp70 chaperones in refolding misfolded proteins[8-11]. While the human Hsp70 family is highly conserved, the Hsp40 co-chaperone family encodes 47 diverse members, each with specialized functions in substrate recognition and presumed coordination with Hsp70[12-14]. DnaJ proteins feature a J-domain (JD), which binds to Hsp70s through a conserved electrostatic interaction to trigger ATP hydrolysis by the Hsp70[1, 14-16]. This in turn initiates a conformational rearrangement in the substrate binding domain of the Hsp70 that helps capture an unfolded substrate for folding, refolding, or disaggregation[17]. In cases when misfolded proteins cannot be refolded, some Hsp40s help direct proteins for degradation[18-19]. However, the mechanistic details of how different Hsp40s recruit Hsp70 or their substrates remain unknown. Furthermore, while it is known that the Hsp70 can interact with JDs through electrostatic surfaces it remains unclear how JD binding to Hsp70 is controlled to specific and/or activated Hsp40 proteins.

90 In humans, Hsp40s are classified into A, B, and C sub-families, in which members
91 typically function as monomers, dimers, or polydisperse oligomers. For example, the A
92 family Hsp40s (DnaJA1-A4) and a subset of B family Hsp40s (DnaJB1/B4/B5), all encode
93 a globular domain architecture similar to the bacterial Hsp40 DnaJ. These classical Hsp40
94 members assemble into homo-dimers through conserved C-terminal motifs and bind
95 unfolded substrates through conserved β-barrel C-terminal domains (CTD)[20]. Recent
96 evidence suggests that this subset of Hsp40s can form mixed hetero-dimers driven by
97 electrostatic contacts to expand the substrate recognition repertoire[21].
98
99 A different set of non-classical Hsp40 B family members (DnaJB2, DnaJB6b, DnaJB7 and
100 DnaJB8) encode a domain architecture that is distinct from the classical dimeric DnaJ
101 orthologs. Rather than encoding a classical β-barrel CTD, their C-terminus encodes a
102 different architecture [22-23]. Of these 4 members, the DnaJB8 and DnaJB6b proteins have
103 been shown to assemble into oligomers *in vitro* and *in vivo*[22, 24-25]. The role of the CTD in
104 these chaperones remains unclear, and the literature reveals conflicting results,
105 suggesting either that it drives oligomerization or that it mediates intramolecular
106 contacts[22-24, 26]. The functional role of the oligomeric state of DnaJB6b and DnaJB8
107 remains unclear, although it has been proposed to serve as a type of phase-separated
108 storage form capable of capturing substrates[25]. The characteristic structural and dynamic
109 heterogeneity of the oligomers has greatly hindered efforts to study them, with recent
110 structural studies resorting to deletion mutants to gain structural insight[22-23]. A
111 combination of variables, including large size and polydispersity, has made these
112 chaperones recalcitrant to both classical and modern structural biology methods,
113 including cryoEM[25].
114
115 The oligomeric chaperones DnaJB6b and DnaJB8 have been shown to be potent
116 suppressors of aggregation of amyloid proteins in cells and *in vitro* [22, 26]. Despite several
117 studies demonstrating a role for DnaJB6b in suppressing assembly of amyloid-prone
118 substrates it is unclear which domains directly interact with substrates, and how

119 oligomerization plays a role in this process. For example, the serine/threonine domain of
120 DnaJB6b is important for suppression of mutant huntingtin protein aggregation in cells,[27]
121 and its deletion limits oligomerization yielding a stable monomer at the expense of
122 activity[23]. In absence of a comprehensive understanding of the full-length structural
123 behavior for this class of DnaJ chaperones, it remains unclear how they fulfill their critical
124 function to protect the proteome from aggregation.
125
126 Here we examine in unprecedented detail the DnaJB8 variant. DnaJB8 was shown to be
127 particularly effective at preventing formation of polyglutamine deposits, even more so than
128 DnaJB6b, despite 63 % sequence identity[22, 27]. Notably, unlike other chaperones that
129 inhibit mutant huntingtin aggregation[28], DnaJB8 and DnaJB6b are thought to target and
130 bind the expanded polyglutamine domain itself and thus are active across the whole
131 family of polyglutamine diseases[22, 27]. The assembly of DnaJB8 into dynamic and
132 heterogeneous high molecular weight complexes (polydisperse oligomers) has thus far
133 prevented their detailed characterization by traditional structural biology approaches. To
134 address this challenge, we applied a hybrid structural biology approach to understand the
135 architecture and dynamics of the DnaJB8 oligomer. We observe that DnaJB8 assembles
136 into large oligomers *in vitro* and *in vivo*. We used crosslinking mass spectrometry (XL-
137 MS) to identify local intra-domain contacts and long-range contacts mediated by
138 complementary electrostatic surfaces. We show that changes in ionic strength modulate
139 the assembly and topology of oligomer, which points to the important role of charge-
140 charge interactions. Using multidimensional solid-state NMR (ssNMR) we probe the
141 structural and dynamic disorder of the solvated oligomers. Dramatic domain-specific
142 differences in line widths, resolution, and peak intensity indicate that the oligomers feature
143 a range of (dis)order, but lack highly flexible regions. The JD transitions between a
144 strikingly ordered immobilized state and a more mobilized state in response to
145 electrostatic disruption. We show that the JD and CTD terminal domains are monomeric
146 in isolation, but form heterodimers when mixed, reconstituting interactions observed in
147 oligomers. Finally, we demonstrate that the DnaJB8 JD-CTD contacts regulate the

148 recruitment of Hsp70. Thus, we identify and validate the first example of a DnaJ protein
149 encoding a built-in regulatory domain that controls its recruitment (and activation) of
150 Hsp70.
151

152 RESULTS

153 **DnaJB8 JD binds to HspA1A using a conserved electrostatic surface**

154 Recent crystallographic analysis of the bacterial DnaK:DnaJ complex revealed the
155 binding mode of the complex[16], which validated previous insight from NMR and
156 biochemical data[15]. The model proposed an electrostatically driven interaction between
157 the basic surfaces on helices 2 and 3 on the DnaJ and an acidic surface on the DnaK that
158 spans the Nucleotide Binding Domain (NBD) and the Substrate Binding Domain (SBD)[16].
159 The JD includes a conserved Histidine-Proline-Aspartic acid (HPD) motif between helices
160 2 and 3 that recruits Hsp70 and stimulates ATP hydrolysis for substrate capture[29]. Using
161 the DnaK model (PDB id: 5NRO) as a template we employed Rosetta to build a homology
162 model of the human HspA1A homolog[16]. The HspA1A model shows good structural
163 agreement with the DnaK homolog (Figure 1A) and also presents a conserved acidic
164 surface that spans the NBD and SBD (Figure S1A-C). Using the DnaK:DnaJ complex
165 structure, we modeled the binding interface between the HspA1A homology model and
166 the experimentally determined structure of the JD of DnaJB8[30] (Figure 1B-C). The basic
167 surface on the DnaJB8 JD (Figure 1B) contacts the conserved acidic surface on the
168 HspA1A (Figure 1C, S1D-E). Thus, conserved electrostatic contacts are likely to play a
169 key role in the interaction between Hsp70 and Hsp40.
170

171 The DnaJB8 co-chaperone is predicted to encode three domains C-terminal to the
172 N-terminal JD (Figure 1D): a phenylalanine and glycine (F/G) rich domain (Figure 1D,
173 blue), a serine/threonine rich (S/T) domain (Figure 1D, cyan) and a C-terminal CTD
174 (Figure 1D, green). Secondary structure analysis on the DnaJB8 sequence reveals the
175 N-terminal JD fold but also predicts the CTD to adopt a five-stranded β-pleated sheet,
176 consistent with the conformation observed in the homologous DnaJB6b[31-32](Figure 1E).

177 The basic surface on JD helix 2 in DnaJB8 mediates binding to Hsp70, but we see that
178 there is surface charge complementarity to the CTD, which is similar to the same
179 complementarity expected from the JD-Hsp70 interaction (Figure 1F). The middle F/G
180 and S/T domains are unstructured (Figure 1G) and contain sequences with lower
181 complexity, particularly in the S/T domain. The F/G domain does not bind directly to
182 Hsp70, but it is involved in regulation of the substrate binding activity of Hsp70[10]. In
183 patients, mutations in the F/G domain of the homologous DnaJB6b (Figure S1F)
184 (including F89I, F93L, P96R and F100V) cause autosomal limb-girdle muscular dystrophy
185 diseases that exhibit similar, but not identical clinical outcomes. Recent studies have
186 shown that the JD-proximal region of the F/G domain in DnaJB6b can adopt a short helix
187 that weakly interacts with the JD [23], which may be relevant to the disease-causing
188 mutations since they are found within this helix[24, 27]. The low complexity S/T domain has
189 been proposed to play a key role in the activity of DnaJB8 to inhibit polyglutamine
190 aggregation[27]. Altogether, it is clear that charge complementarity is important for the
191 Hsp70:Hsp40 interaction, but that there is also a role for DnaJB8 interactions and
192 domains beyond the JD.
193
194 **Interactions of oligomeric DnaJB8 in a cellular context**
195 Prior studies have highlighted the ability of DnaJB8 to assemble into oligomers but have
196 failed to provide insights into the interactions that drive oligomer formation [22, 26]. We first
197 asked whether DnaJB8 can form oligomers in cells by expressing DnaJB8 fused to a
198 green fluorescent protein (GFP) derivative: Clover (herein, DnaJB8-Cover) in HEK293
199 cells (Figure 2A). We observed the formation of fluorescent juxtanuclear puncta that
200 localize close to the nucleus (Figure 2B). Puncta were not observed in control cells
201 expressing Clover alone (Figure 2B). When quantified, 39.2±3.1% of the cells expressing
202 DnaJB8-Clover contain puncta while only 0.44±0.50% of the control cells contained
203 puncta (Figure 2C). To test the concentration dependence on puncta formation, we
204 assayed the frequency of puncta with different levels of expression and observed 4-fold
205 lower protein levels reduced the DnaJB8-Clover puncta frequency to 17.5±10.3% (Figure

206 2C). The puncta frequency for Clover alone remained below 1% in the two experiments
207 (Figure 2C). From microscopy images we estimate the DnaJB8-Clover puncta to have a
208 maximum diameter of 1.0µm (Figure 2B).
209
210 We next sought to characterize biochemical properties of DnaJB8-Clover expressed in
211 mammalian cells. To isolate the Clover protein, we used α-GFP nano-bodies[33-34] allowing
212 immunoprecipitation (IP) of the DnaJB8-Clover fusion and Clover from HEK293 cells.
213 Western blot analysis of the purified IP fractions confirms the presence of DnaJB8 and
214 Clover using α-GFP and α-DnaJB8 antibodies (Figure S2A) in the DnaJB8-Clover and
215 control cell lines. The IP purified samples were first analyzed by a proteomic mass
216 spectrometry approach to identify any candidate proteins associated with DnaJB8-Clover.
217 Using the CPFP[35] software we identified 60 proteins that were enriched in the DnaJB8-
218 Clover samples relative to the control Clover sample (Figure S2B and Supplementary
219 Data 1). Among the enriched proteins we found other chaperones including the eukaryotic
220 chaperonin TRiC/CCT, Hsp90A/B, HspD1, and two Hsp70 family members: HspA8 and
221 HspA1A (Figure S2C). *A priori*, one might expect to see an enrichment in Hsp70, but the
222 levels of Hsp70 enrichment in the IP were minor relative to the Clover controls, suggesting
223 that the DnaJB8:Hsp70 interaction is weak under the conditions used, despite the known
224 Hsp40:Hsp70 relationship.
225
226 Combining crosslinking with mass spectrometry can help define contact points in
227 proteins and protein complexes, with particular importance for systems not tractable for
228 classical structural biology methods[36-38]. After isolation of DnaJB8-Clover using an α-GFP
229 nanobody IP, we reacted the samples with a combination of adipic acid dihydrazide (ADH)
230 and 4-(4,6-dimethoxy-1,3,5-triazin-2-yl)-4-methyl-morpholinium chloride (DMTMM),
231 respectively. ADH covalently links carboxylate-carboxylate contacts via a 6-carbon
232 bridge, while DMTMM acts as a chemical intermediate to form a direct covalent bond
233 between lysine-carboxylate groups through dehydration[37]. The latter reaction is referred
234 to as a "zero-length" crosslink since no additional atoms are added in order to link the two
235 target groups. Crosslinking treatment yielded a high molecular weight species, consistent

236 with an oligomeric form (Figure 2D). To identify whether inter-domain contacts were
237 present in these oligomers, we employed XL-MS on the DnaJB8-Clover purified by IP
238 from mammalian cells. We identified 1 carboxylate-carboxylate and 20 lysine-carboxylate
239 crosslinks that parsed into three coarse regions: JD-JD, CTD-CTD and JD-CTD (Figure
240 2C, Supplementary Data 2). The three local JD contacts (Figure 2C; JD contacts in red
241 box) linking K25-D37, K34-D37 and E41-K34 are consistent with the known structural
242 model of the domain (Figure S2D). Local CTD contacts were also accompanied by inter-
243 domain JD-CTD contacts that localize to helices 2 and 3 (Figure 2C, JD-CTD contacts in
244 grey box). Additionally, we identified a contact between K34 in the JD and D97 that is
245 consistent with a weak interaction between the JD and a putative helix 5 of the F/G
246 domain identified in the homologous DnaJB6b[23]. DnaJB8-Clover oligomers isolated from
247 mammalian cells reveal an array of inter-domain interactions, including contacts between
248 the charge complementary JD and CTD.
249

250 **DnaJB8 JD-CTD contacts are preserved *in vitro***

251 To enable a more detailed understanding of DnaJB8 oligomerization, we sought to
252 reconstitute DnaJB8 oligomers *in vitro*. Full length DnaJB8 was produced recombinantly
253 and purified as previously described[22]. We used Dynamic Light Scattering (DLS) and
254 Transmission Electron Microscopy (TEM) to detect DnaJB8 oligomers forming in solution
255 over time. We initially observe DnaJB8 species with an average radius of hydration (R_h)
256 of 13.7±2.5nm which after 8 hours steadily increase in size, eventually reaching a
257 maximum average R_h of 91.9±12.6nm after 15 hours (Figure 3A, Supplementary Data 3).
258 While the average R_h is informative for interpretation of the kinetics of assembly, the
259 derived values do not reflect real species. Partitioning the scattering data into bins with
260 different radii reveals *bona fide* sizes: DnaJB8 primarily begins as a small species
261 (5.54±2.36nm) with a small (<%1 by mass) contribution of larger species (>100nm) but
262 as aggregation progresses the small species are converted into larger assemblies (30.6%
263 by mass) (Figure S3A). We next used negative-stain TEM to visualize the DnaJB8
264 oligomers at 15 hours where we first observed the formation of larger species by DLS.

265 Upon imaging the grids, we found elongated polydisperse oligomeric structures with
266 varying lengths around 90nm, and widths of approximately 20nm along with amorphous
267 oligomeric species (Figure 3B). These findings are consistent with prior studies on
268 DnaJB6b and DnaJB8 showing that it can form oligomers *in vitro*[22, 24-25, 27, 39].
269 Next, we aimed to better understand the topology of these *in vitro* oligomers by XL-MS,
270 using two parallel chemistries; disuccinimidyl suberate (DSS) and ADH/DMTMM (Figure
271 2D). Consistent with the formation of oligomers, we observe by SDS-PAGE a ladder of
272 bands indicating the covalent trapping of intermolecular contacts (Figure S3B). Notably,
273 the ADH/DMTMM chemistry yielded a higher efficiency of trapping oligomeric species
274 than DSS, which has been previously used to probe structure of the related DnaJB6b[25].
275 XL-MS analysis of these samples showed only three crosslinks in the DSS condition
276 (Figure 3C, Supplementary Data 2). In contrast, the ADH/DMTMM analysis yielded 18
277 lysine-carboxylate crosslinks and 6 carboxylate-carboxylate crosslinks that localize to
278 three main regions (Figure 3C, Supplementary Data 2): within the JD (Figure 3C, red
279 dashed box), within the CTD (Figure 3C, green dashed box), and contacts between JD
280 and CTD (Figure 3C, grey dashed box). This pattern closely matches those observed in
281 the assemblies recovered from the mammalian cells above. Within the JD, there are five
282 crosslinks; one carboxylate-carboxylate (D33-E43) and four lysine-carboxylate crosslinks
283 (K34-E40, K34-E41, D37-K45 and E54-K60) (Figure 3C). Out of these five crosslinks,
284 four of them are localized around the loop between helix 2 and helix 3, where the HPD
285 motif responsible for Hsp70 binding is located. Mapping the crosslinks onto the structure
286 of the JD showed that the C_α-C_α distances varied across zero-length crosslink pairs from
287 11.6Å to 14.7Å and the single ADH pair spanned 8.9Å (Figure S3C). These C_α-C_α
288 distances are consistent for each chemistry, with zero-length crosslink pair distances
289 falling under 16Å and ADH-derived distances spanning less than 20Å[37]. In addition, the
290 side chains in each amino acid pair are solvent accessible in the DnaJB8 JD structure
291 (Figure S3C). These data suggest that the local JD crosslinks are consistent with
292 intramolecular contacts within a JD monomer.
293

294 The CTD region of DnaJB8 yielded two ADH-based crosslinks (E208-E224 and E210-
295 E224) and six lysine-carboxylate zero-length crosslinks (E211-K227, E208-K227, E210-
296 K227, E211-K223, K193-E211, and E211-K232) (Figure 3C). Amongst these, the local
297 regions spanning E208-E211 and K223-K227 are central to the CTD and repeatedly react
298 to peripheral sites. The third cluster of contacts linked the distal JD and CTD through four
299 lysine-carboxylate crosslinks (K34-D212, K47-E208, K47-E211, and K60-E211) (Figure
300 3C, inset). These long-range crosslinks span an average sequence separation of 163.5
301 amino acids separated by the central unstructured F/G and S/T domains. The CTD
302 crosslink sites are exclusively mediated through acidic amino acids; D212, E209 and
303 E211. Interestingly, the crosslinked amino acids on the JD are all lysines (K34, K47 and
304 K60) that localize to basic surfaces along each helix (Figure S3D) and overlap the basic
305 Hsp70 binding surface[16]. Consistent with the *ex vivo* analysis we again identified an
306 isolated crosslink between the JD and the proposed helix 5 in the F/G domain. Clearly,
307 these XL-MS data point to an intricate network of inter-domain interactions in the
308 oligomeric DnaJB8.
309
310 To further test the apparent role of electrostatically driven inter-domain interactions, we
311 used a higher ionic strength buffer in an analogous series of experiments. Using DLS we
312 found the average R_h to remain stable at 13.7 ± 1.2 nm over time (Figure 3D,
313 Supplementary Data 3). A closer inspection of the scattering data reveals a predominance
314 of smaller species (7.75±0.7nm) alongside a small and unchanging contribution of larger
315 species (<1% by mass) (Figure S3E). TEM showed that the latter species are spherical
316 with 10-20nm in diameter (Figure 3E). Thus, increased ionic strength inhibits the
317 formation of the more heterogenous larger (>100 nm) structures. DLS also shows that
318 the predominant species are more collapsed (5.54±2.36nm) in the low ionic strength
319 condition compared to that found in the higher salt (7.75±0.7nm) (Figure S3F). XL-MS
320 demonstrates that while some short-range crosslinks within either the JD or the CTD are
321 preserved, the long-range inter-domain contacts have now been lost (Figure 3F). To
322 control for reactivity in each buffer condition we compared the frequency of ADH driven

323 monolinks. Monolinks occur when a chemical crosslinker reacts with a solvent exposed
324 residue on the target protein, but no other corresponding residues are in close physical
325 proximity to attack the other end of the crosslinker. These peptide fragments are useful
326 for identifying isolated surfaces, as well as validating the efficiency of the crosslinker
327 chemistry. The data show that the higher ionic strength has little effect on the chemistry
328 of DMTMM on acidic residues or the ability of ADH to target those same residues (Figure
329 S3G). Thus, we observe the disruption of electrostatically driven JD-CTD interactions
330 being accompanied by changes in the domain architecture as well as higher order
331 assembly of DnaJB8 oligomers.
332
333 **ssNMR on DnaJB8 oligomers reveals regions of disorder and order**
334 To gain additional insight into their molecular structure and dynamics, multidimensional
335 magic-angle-spinning (MAS) ssNMR was performed on the hydrated oligomers of U-
336 ^{13}C,^{15}N-labeled DnaJB8. The MAS ssNMR signals of hydrated protein assemblies allow
337 for the site- and domain-specific detection of mobility and (secondary) structure, even in
338 presence of considerable disorder and heterogeneity. In 2D ssNMR spectra we observe
339 many broad peaks, with linewidths up to 0.38 kHz, consistent with an oligomeric assembly
340 displaying structural disorder (Figure 4A). However, strikingly, distinct subsets of narrow
341 peaks are also detected, with 1D projections showing linewidths of 0.1 to 0.2 kHz (Figure
342 4C-D left). These experiments employ the cross-polarization (CP) technique, which
343 means that the observable residues must be rigid or immobilized, lacking high flexibility
344 [40]. This conclusion is reinforced by a lack of signals in INEPT-based ssNMR spectra that
345 are selective for highly dynamic peptide segments [41-43] (more below). Then, the observed
346 narrow signals must originate from an immobilized, well-ordered subset of DnaJB8
347 residues. Based on the characteristic NMR shifts of amino acid types (Figure S4A)[44], we
348 can attribute these narrow signals to residues in the JD (Table 1) while the broad peaks
349 are dominated by signals from residues common in other domains (Table 1). The narrow
350 signals reflect mostly α-helical structure, unlike the broader signals that are mostly
351 random coil and β-sheet [45]. Finally, with known chemical shifts of the DnaJB8 JD in

352 solution (see also below), we prepared a synthetic 2D spectrum (Figure S4B) that reveals
353 a striking correspondence to the narrow ssNMR peaks (Figure 4C-D). The
354 correspondence is such that we tentatively assign the strikingly narrow signals (Figure
355 S4A,B) to residues in helix 2 and helix 3 (10V, 13S, 14A, 15S, 19I, 22A, 27A, 42A, 52A).
356 In absence of experimental solution NMR data for the other domains, we predicted
357 estimated spectra based on their model structures. Figure 4C-D (green) shows Ala and
358 Ser regions of their combined simulated NMR spectrum[46], resembling qualitatively the
359 broader signals in our 2D ssNMR data. A particular strength of MAS ssNMR analyses of
360 such hydrated proteins is the ability to gauge local and global dynamics. Single pulse
361 excitation (SPE) and refocused INEPT ssNMR spectra, which enhance the more dynamic
362 parts of samples[42-43], show surprisingly little evidence of flexible residues (Figure 4E red).
363 The main INEPT signal at ~42ppm arises from Lys side chains, which are expected to be
364 solvent exposed and dynamic. Since the 1D CP and SPE spectra look similar, with higher
365 signal intensities in the former, the different domains of the protein must have a similar
366 degree of mobility (Fig. 4E). Combined, the ssNMR data reveal oligomers that are
367 heterogeneous in structure but lack extended flexible domains. In other words, the central
368 F/G and ST domains are heterogenous, but also substantially immobilized within the
369 oligomers. Uniquely ordered are parts of the JD (residues in helices 2 and 3), which
370 appear to be well-folded and immobilized.
371
372 **Interaction sites from ssNMR**
373 In the JD structure (Figure 4F-I) these "ordered" residues form a surface region rich in
374 positively charged amino acids, involving helix 2 and 3, as well as residues connecting
375 these helices. What is responsible for stabilizing and immobilizing this part of the JD? XL-
376 MS showed long-range contacts from the JD to the CTD, involving K34, K47, and K60 in
377 helices 2, 3 and 4, which disappeared at elevated ionic strengths. Analogous ssNMR
378 studies of the oligomers in PBS buffer with 285mM NaCl are shown in Fig. 4B and S4.
379 The 2D CP-based ssNMR spectrum reproduces the broad signals of the immobilized
380 oligomers, but the narrow JD peaks are strikingly absent. Comparing the CP and SPE

381 ssNMR spectra (Figure 4E), there is a clear increase in mobility, but again there is a lack
382 of INEPT signals from highly flexible regions. Notably, although the well-ordered JD
383 signals are no longer seen as immobilized (i.e., visible in CP ssNMR), no new "flexible"
384 ssNMR signals were identified under high salt conditions. We interpret this as indicating
385 that the JD gains increased mobility due to disruption of its long-range electrostatic
386 interactions but is still folded and partly immobilized by its covalent attachment to the
387 overall assembly. As a consequence, the JD is invisible due to intermediate timescale
388 dynamics[40, 47]. Since the broad signals from the other domains are preserved, it appears
389 that the core architecture of the oligomers persists even at high ionic strength, such that
390 it is primarily the JD that is dislodged as electrostatic long-range interactions are
391 weakened.
392
393 **Isolated JD and CTD are folded and monomeric**
394 To evaluate the potential inter- and intra-domain interactions of the JD and CTD, we
395 produced isolated JD (residues 1-77; JD_{1-77}) and CTD (residues 170-232; $CTD_{170-232}$)
396 (Figure 5A). By size exclusion chromatography (SEC) both constructs yielded
397 monodisperse peaks (Figure 5B), with an estimated molecular weight of 10kDa and 8kDa
398 for JD_{1-77} and $CTD_{170-232}$, respectively. The CTD has been proposed to drive dimerization
399 and multimerization in the homologous DnaJB6b[24-25], but by Size Exclusion
400 Chromatography - Multi Angle Light Scattering (SEC-MALS) the molecular weight for the
401 DnaJB8 $CTD_{170-232}$ is unambiguously a monomer with a molecular weight of 8,376±14
402 g/mol (Figure S5A). Also, by DLS in solution we estimated the JD_{1-77} to be 2.30±0.12 nm
403 and the $CTD_{170-232}$ to be 1.71±0.02 nm, with both stable over 15 hours (Figure S5B,
404 Supplementary Data 3). The purified constructs were used for XL-MS to probe the
405 structural similarities to the corresponding domains within the full-length protein. On an
406 SDS-PAGE gel, the crosslinked JD_{1-77} and $CTD_{170-232}$ remained monomeric following
407 crosslinking, while the bands broadened as a result of the chemical modification (Figure
408 5C). XL-MS analysis yielded 4 crosslinks for JD_{1-77} and 6 crosslinks for $CTD_{170-232}$ (Figure
409 5D, Supplementary Data 2). The identified crosslinks revealed good agreement between

410 the local domain crosslinks observed in the full-length DnaJB8 and the isolated JD_{1-77} and
411 to a lesser extent for $CTD_{170-232}$ (Figure 5D, S5C-D).
412 We built 5000 predictive models of the CTD using *ab initio* ROSETTA which
413 employed fragment libraries derived from experimental structures[40]. We calculated the R_h
414 for the ensemble using HYDROPPRO and the resulting values were consistent with the
415 DLS measurement of 1.7nm (Figure 5E). The models reproducibly formed a low contact
416 order 5-stranded β-sheet topology (Figure 5E) and the R_h variation can be attributed to
417 the more flexible termini (Figure 5E, inset). The CTD topology is defined by four β-turns
418 stabilized by conserved asparagine/aspartate-glycine sequences (N/DG). These
419 structures are consistent with the recently published conformation of the DnaJB6b CTD[23].
420 Circular dichroism (CD) on the CTD sample yields spectra consistent with a
421 predominantly β-sheet content, as predicted by our model (Figure S7E-F). We mapped
422 the 14 CTD-derived crosslinks from across experiments onto the monomeric ensemble,
423 finding that a majority of structures explain 10-11 crosslinks but only a single model
424 explains 13 of 14 (Figure 5F). These crosslink pairs map onto each face of the β-sheet
425 and the distances are compatible with the geometry of the crosslinking chemistry. The
426 crosslinks that fall outside of the distance cutoff localize to the more dynamic C-terminus
427 of CTD (Figure 5E, inset) at positions K227 and K223 (Figure 5F). Thus, our data support
428 that both the JD_{1-77} and $CTD_{170-232}$ domains are folded, monomeric and do not have
429 intrinsic assembly properties.
430
431 **Basic surface on JD drives interaction with CTD**
432 In our experiments on the full-length DnaJB8 oligomers we saw that the JD and CTD
433 interact through complementary electrostatic surfaces. We further probed this interaction
434 by mixing the individual JD_{1-77} and $CTD_{170-232}$ domains *in vitro* (Figure 6A). We incubated
435 Flourescein(FITC)-labelled JD_{1-77} with a series of $CTD_{170-232}$ concentrations and
436 measured binding affinity using a fluorescence polarization assay. The resulting binding
437 curve revealed that the JD_{1-77} binds to the $CTD_{170-232}$ with 0.575±0.115 μM affinity (Figure
438 6B). Preincubated JD_{1-77} and $CTD_{170-232}$ domains were crosslinked with ADH/DMTMM

439 and analyzed using XL-MS. We identified local crosslinked pairs consistent with pairs
440 observed in full length DnaJB8 and the isolated JD_{1-77} and $CTD_{170-232}$ samples (Figure
441 6C). Importantly, we also reconstitute intermolecular contacts between the JD_{1-77} and
442 $CTD_{170-232}$ observed in full length DnaJB8 experiments. However, an increased variance
443 in the crosslink profile may indicate that the missing proximal sequences help define the
444 proper architecture of the full-length DnaJB8 oligomers. Solution NMR-based chemical
445 shift mapping was used to identify the JD_{1-77} surface that interacts with the $CTD_{170-232}$
446 (Figure 6D). Titration of increasing amounts of unlabeled $CTD_{170-232}$ into ^{15}N-labeled JD_{1-}
447 $_{77}$ produced concentration-dependent shifts in a specific subset of peaks (Figure 6D-E);
448 33 peaks were strongly perturbed (>0.2 p.p.m.) and another 40 peaks were perturbed
449 weakly (>0.1 p.p.m; Fig 6F). Among the strongly perturbed peaks, 27 residues have
450 solvent accessible side chains of which fifteen are charged, with a notable overlap with
451 the basic face in helix 2 that is implicated in Hsp70 binding (Figure 6H-I). Other residues
452 that show strong perturbations are basic and acidic residues that wrap around the exterior
453 face of the JD loop and helix 3 (D33, K39, E40, E41, K44, K47, E51), and residues on
454 the charged face of helix 4 (K60, K61, R62, L64, Y65). While a few other hydrophobic
455 residues also show strong perturbations, all are in close proximity to charged residues
456 along each helix. Given the small size of the JD_{1-77}, it is likely that residues in the core
457 behind the basic surface involved in the interaction experience chemical shifts.
458
459 **Sequence properties driving interactions in DnaJB8**
460 Using Rosetta, we generated a full-length model of DnaJB8 combining the solution NMR
461 structure of the JD (PDBID: 2DMX) with the *ab initio* model for CTD while keeping the
462 F/G and S/T region expanded. Using the relax module in Rosetta we applied our JD-
463 CTD XL-MS crosslink pairs as constraints to collapse the expanded full-length DnaJB8
464 monomer (Figure 7A and Figure S7A). The constraints drive the collapse of the molecule
465 to decrease the distance between the crosslink pairs (Figure 7A and Figure S7A) from an
466 R_g of 6.65 nm in the expanded state to a much smaller 2.45 nm (Figure 7C and Figure
467 S7B). Using the Hydropro software[48], we obtain R_h values of 9.27 nm and 4.02 nm,

468 respectively, for each structural model. Comparing the DLS R_h size ranges for the small
469 species in the low and high ionic strength conditions to the structure-derived R_h values
470 suggests congruency in observed shapes dependent on presence or absence of JD:CTD
471 contacts. The calculated R_h values for the collapsed (JD:CTD engaged) Rosetta
472 monomer conformation is consistent with the lower end DLS size distribution obtained
473 under low ionic strength. This is further supported by comparing the R_h of our Rosetta
474 model to a theoretical disordered protein containing 232 amino acids to be 3.98 nm as
475 modeled by Marsh and Forman-Kay[49]. We calculated the spherical volume of our
476 collapsed model to be 271.78 nm^3. By using this smaller sphere and fitting multiple copies
477 of it into the predicted volumes for larger oligomeric species, we estimate that the small
478 species range from a monomer to 8-mer under low ionic strength conditions, which over
479 time assemble into larger polydisperse species.

480 Guided by the constraints, the final model "docks" the JD onto the CTD placing the
481 putative acidic surface on the CTD (E208-D212) in contact with the NMR-identified basic
482 surface on the JD (K20-R29) (Figure 7A and Figure S7B). The final model also docks
483 Helix 5 onto the JD:CTD interface (Figure 7A). The CTD has proximal basic surfaces that
484 flank the acidic surface, generating a characteristic alternating charge pattern that is
485 inverted on the JD (Figure 7B). Furthermore, in the collapsed monomer, the 17 aromatic
486 residues distributed in the F/G and S/T regions are exposed to solvent highlighting their
487 possible role in oligomerization (Figure 7A). Although the NMR results were not employed
488 as constraints, it is striking that the predicted interaction sites line up well with the solution
489 and solid-state NMR data. These simulations, in conjunction with our ionic strength
490 perturbation experiments support a model in which the JD-CTD interaction is coupled to
491 the conformation of the F/G and S/T region with the potential to sense substrate binding
492 and modulating the oligomer assembly.

493

494 **Evolutionary preservation and co-evolution**

495 If this interaction has biological relevance, we may expect it to be evolutionarily preserved.
496 To probe this, we computed the extent of conservation across DnaJB8 homologs (Figure

497 S7C). The JD is the most conserved domain. Particularly for DnaJB6b, DnaJB2 and
498 DnaJB7 homologs which also encode a five-stranded pleated β-sheet CTD, we found
499 specific sites on the CTD with an elevated degree of conservation, these residues map
500 to the N/D-G β-turns and the β-sheet surface of the CTD (Figure S7D). In the Rosetta-
501 generated model, the majority of these conserved CTD sites are participating in the JD-
502 CTD interface (Figure S7D-E). A similar sequence analysis for the homologous DnaJB6b
503 sequence reveals similar conservation patterns and charge distributions (Figure S7F).
504 This supports the idea that the JD-CTD interaction has a degree of conservation across
505 DnaJ sequences featuring homologous CTD-like domains.
506
507 Lastly, we incorporated co-evolution analysis using the Gremlin algorithm[50-52]. Employing
508 an alignment of DnaJB8 homologs we identified amino acid positions that covary,
509 restricting analysis to only pairs showing >70% probability of being in contact. While many
510 of the amino acid pairs covary within the JD and CTD domains, we additionally observe
511 pairs that reflect inter-domain contacts between the JD-CTD (Figure 7C). Comparison of
512 these long-range covariance sites reveals a striking resemblance to the XL-MS pairs
513 identified in the full length DnaJB8 experiments. The similarity between the predicted
514 covarying contacts (Figure 7C), conservation (Figure S7C-D) and the XL-MS
515 experimental contacts not only further strengthens our DnaJB8 JD-CTD model, but it also
516 suggests that XL-MS can detect functionally important yet lower affinity interaction sites.
517
518 **JD-CTD interaction competes with Hsp70 binding**
519 The conserved Hsp70-JD electrostatic contacts (Figure 1) that overlap with the JD-CTD
520 contact sites lead us to hypothesize that the observed JD-CTD interactions could regulate
521 the recruitment of Hsp70 (Figure 8A-B). To test this hypothesis, we employed a
522 competition experiment leveraging a fluorescence polarization binding assay to
523 discriminate the JD-CTD and JD-HspA1A interactions (Figure 8C). For the JD:HspA1A
524 titration we determine a binding constant of 0.257±0.029μM, consistent with values
525 observed in the literature[53] and similar to the JD:CTD interaction (Figure 8D, black and

526 green, respectively). Due to the large size difference of HspA1A (70 kDa) and the CTD
527 (8.7 kDa) the respective titrations saturate at different polarization values (Figure S8A,
528 black and green, respectively). Leveraging this signal difference, we designed an
529 experiment to measure the competition of HspA1A and CTD binding to the JD. We
530 preincubated the FITC-labeled JD with a fixed concentration of CTD (3.125 µM) and then
531 subsequently titrated increasing concentrations of HspA1A. The polarization signal was
532 consistent with the already measured CTD-JD complex, up until HspA1A concentrations
533 reached 3.125uM. Past this point, the signal more closely matched that seen for the larger
534 HspA1A-JD complex (Figure S8A, purple). Normalization of the polarization data reveals
535 a ~25-fold shift in the apparent binding constant between JD:HspA1A when preincubated
536 with CTD (Figure 8D). XL-MS using ADH/DMTMM was used to identify contact points
537 between the JD and HspA1A, revealing 3 zero-length cross-links (K41-E513, K51-D323,
538 and D65-K319) that are all consistent with the structural model of the JD_{1-77}-HspA1A
539 interaction (Figure 8E, Supplementary Data 2). Consistent with our findings in cells
540 (above), incubation of HspA1A with full-length DnaJB8 yielded intra-molecular cross-links
541 for DnaJB8 and HspA1A, but no intermolecular cross-links observed between the two
542 different proteins (Supplementary Data 2). Thus, the DnaJB8 JD uses the same basic
543 surface to bind to its own CTD and HspA1A. Based on our DLS data and Rosetta models
544 of DnaJB8, the oligomer shape changes with the engagement of the JD:CTD interaction.
545 When the JD:CTD interaction is preserved, DnaJB8 is capable of forming species ranging
546 from monomer to octamer, which proceed to larger oligomers over time (Figure 8F). The
547 disruption of this JD:CTD interaction liberates the HspA1A binding face of the JD and
548 reduces the oligomer size to a more uniform size. Considering the possible role of
549 substrates, our model proposes that *in vivo* it is the binding of Hsp40 client peptides and
550 proteins that acts as the driving force that disrupts the DnaJB8 oligomer and the JD:CTD
551 interaction, thus promoting HspA1A recruitment for substrate transfer. This then
552 represents an exciting new regulatory mechanism by which Hsp40s orchestrate the
553 recruitment of Hsp70 (Figure 8F).
554

555 DISCUSSION

556

557 **Structure and dynamics of oligomeric DnaJB8**

558 Using a hybrid structural approach, we described the key molecular interactions in the
559 oligomeric state of the Hsp40 co-chaperone DnaJB8. By DLS and TEM, we observed that
560 DnaJB8 forms oligomers that vary in size and shape. In cells, DnaJB8 forms small puncta
561 consistent with the size of our *in vitro* produced aggregates. We used XL-MS to capture
562 surface contacts within and between folded domains and saw that they were similar *in*
563 *vitro* and in cells. Independent of the conditions, the protein assembled into oligomeric
564 base units with a R_h range of ~4-8 nm, which is consistent with an assembly of at most
565 eight monomers. Under normal ionic buffer conditions these assembles mature into larger
566 polydisperse assemblies while in the presence of higher salt they stable. The collective
567 data reveal that the core of these assemblies is formed by immobilized F/G and S/T
568 domains, while the JD and CTD are engaged in electrostatic interactions at the surface
569 rendering them sensitive to changes in ionic strength (Figure 8F). With ssNMR of the
570 assembled oligomers, we showed that the F/G and S/T domains lack secondary structure,
571 consistent with computational predictions, but should not be seen as dynamic, flexible
572 regions in the oligomers. Dynamics-sensitive ssNMR instead showed them to be
573 immobilized and insensitive to the destabilizing effects of elevated ionic strength. We
574 propose a model in which self-assembly of these oligomer cores is driven by hydrophobic
575 clustering and pi-pi stacking of aromatic side chains in the F/G and S/T domains (Figure
576 8F). At the periphery of this hydrophobic core are charged and hydrophilic residues, with
577 the former engaged in electrostatic interactions that are critical for the DnaJB8 self-
578 assembly and function.

579

580 We combined a variety of XL-MS and NMR in the solid and solution states to probe these
581 inter-domain interactions. One of the most striking features was a newly identified
582 interaction between the distal JD and CTD driven by electrostatics, whose perturbation
583 had a dramatic effect on the structure, dynamics and higher order assembly of the

584 oligomers. Analysis of the isolated JD and CTD showed a reduced mutual interaction,
585 revealing a distinct role for the intervening domains. Indeed, our data argue that the S/T
586 and F/G domains are central in the homo-oligomerization process, as the isolated JD and
587 CTD are surprisingly resistant to self-assembly. These findings are distinct from published
588 reports on the otherwise highly homologous DnaJB6b. The modeled structure of the CTD
589 is however very similar to its DnaJB6b counterpart, featuring a pleated β-sheet topology
590 absent of a hydrophobic core[23]. Consistent with prior observations from solution NMR
591 data we also observe weak contacts between the JD and a downstream helix in the FG
592 domain, similarly based on electrostatics. Supporting an electrostatically driven
593 immobilization of the JD, ssNMR analysis showed the JD mobility to be dependent on the
594 ionic strength. Thus, we conclude that the JD is bound to charged groups on the
595 oligomers' surface.
596
597 **Functional role of the CTD in the oligomeric co-chaperones**
598 Multiple analyses reveal the isolated DnaJB8 CTD to be a monomer encoding a five-
599 stranded pleated β-sheet topology. Our structural models for the DnaJB8 CTD are in
600 agreement with recent cs-Rosetta simulations on the DnaJB6b CTD[23]. This topology
601 resembles the negatively charged β-sheet surface on Hsp70 that is known to interact with
602 the JD[16]. Interestingly, outside of inter-strand hydrogen bonding and polar side-chain
603 contacts, it is not clear what forces stabilize this domain. This may explain the apparent
604 CTD heterogeneity (unlike the JD) seen in the ssNMR spectra. In DnaJB6b the CTD itself
605 has been implicated in driving the assembly of oligomers, even though the literature has
606 conflicting results[22-24, 26]. Söderberg *et al* have proposed that the minimal assembly is a
607 dimer mediated by inter-CTD contacts[25]. A recent solution NMR study showed that
608 truncating the entire S/T region or partial truncation of the CTD blocks oligomerization[23].
609 Our data show that the DnaJB8 CTD is not prone to dimer formation, presumably implying
610 a need for the other DnaJB8 domains. Considering the size of the DnaJB8 oligomeric
611 assembly, the inability of the CTD to self-assemble indicates that this domain alone is not
612 the driving force behind DnaJB8 oligomerization. While more experiments are required,

613 our data suggest a possible alternate mechanism where the JD-CTD interaction is
614 coupled strongly to the disordered F/G and S/T domains, with them together modulating
615 oligomerization. Mimicking the effect of ionic strength modulation, it is worth noting that
616 the lysines in the DnaJB8 and DnaJB6b CTD can be acetylated and deacetylated (via
617 Histone Deacetylases (HDACs)) to modify these proteins' self-assembly and function[22,
618 26]. The CTD architecture is conserved in a subset of B family member Hsp40s including
619 DnaJB2, DnaJB6b, and DnaJB7, of which DnaJB6b has also been shown to oligomerize.
620 It is tempting to speculate that the CTD in these DnaJB family members similarly serves
621 a regulatory role in which post-translational modifications could alter the affinity for the
622 JD, and thus indirectly alters assembly properties or Hsp70 recruitment.
623

624 **Implications for Hsp70 recruitment and substrate binding.**

625 DnaJB8 is responsible for the recognition and binding of particular misfolded substrates
626 such as expanded polyglutamine domains and Aβ[22,26-27,39]. Aside from inhibiting
627 aggregation on its own, DnaJB8 also recruits Hsp70 for further processing of bound
628 substrates. This necessitates a mechanism that connects Hsp70 recruitment to substrate
629 recognition and binding. Our current findings offer a potential molecular rationale,
630 involving auto-inhibitory interactions of the Hsp70-binding JDs within the DnaJB8 native
631 oligomer state. The recently solved structure of the JD of DnaJ in complex with DnaK·ATP
632 showed that the JD binds between the NBD and SBDβ domains of DnaK[16]. The
633 interaction surface is characterized by charge complementarity, involving a highly
634 negative side of DnaK and a highly positive region of the JD. The bacterial protein
635 interface is recapitulated in our modeling of HspA1A and the DnaJB8 JD (Figure 8B-C).
636 This involves residues involved in the DnaJB8 JD-CTD interactions, explaining the lack
637 of Hsp70 recruitment by oligomeric DnaJB8 in cells and *in vitro*. This is validated by the
638 observed competition between Hsp70 and CTD binding to the JD (Figure 8F). In terms of
639 the functional mechanism of DnaJB8 substrate recognition and Hsp70 recruitment, we
640 propose the following mechanism based on these findings.
641

642 In the non-stressed native state, the DnaJB8 forms oligomers in which the JD is engaged
643 in electrostatic interactions and thus not available for very effective Hsp70 binding.
644 Substrate binding to DnaJB8 is expected to disrupt the normal state of the oligomer
645 complex and could cause the release of the immobilized JD (in a manner analogous to
646 the ionic strength experiments). As a consequence, the Hsp70-binding helix-turn-helix
647 motif of the JD becomes available. This would enable the recruitment of Hsp70 to the
648 loaded DnaJB8 protein (Figure 8F). The substrate could do so by disrupting the oligomer
649 structure altogether. However, our data illustrate that complete loss of the oligomers is
650 not required for a mobilization of the JD. The oligomers must be stabilized by self-self
651 interactions that are not disrupted by ionic strength, and do not require the involvement
652 of the JD. We propose that the more hydrophobic F/G domain may form this salt-resistant
653 core structure, with the CTD and JD being more surface exposed. Thus, it may be
654 possible to recruit Hsp70 to an oligomeric state of DnaJB8, without a need for complete
655 solubilization of the protein. Although we employed ionic strength to manipulate the
656 sequestration of the JD helix-turn-helix motif, it is tempting to speculate that this could
657 also be affected by changes in the S/T and/or F/G domains. Here, it is noteworthy that
658 negative residues in helix 5 (E97/D98) in the F/G domain interact with the JD (XL-MS
659 data). A disruption of the JD-CTD interaction may therefore be coupled to low complexity
660 sequences located in the S/T domain that are thought to mediate substrate binding.
661 Future mechanistic and structural studies on this complex co-chaperone with substrates
662 will reveal the interplay between oligomer dynamics, substrate binding and recruitment of
663 Hsp70.
664

665 CONCLUSIONS

666 We present a hybrid structural biology studies of DnaJB8 oligomers to reveal a new role
667 for specific electrostatic contacts that mediate the homo-oligomeric assembly *in vitro* and
668 *in vivo*. Despite a heterogeneous structure of the oligomers, our use of complementary
669 XL-MS, (ss)NMR studies and *in silico* analyses provided a novel perspective on the
670 fundamental structure of the protein complex and its function. We show an exciting

671 interplay between contacts that drive self-assembly and regulate recruitment of Hsp70 to
672 the JD, pointing to an orchestrated auto-inhibitory mechanism involving the latter. Future
673 studies will be focused on the interplay between DnaJB8 conformation, substrate binding,
674 and Hsp70 recruitment. This study highlights how hybrid structural methods can reveal
675 novel insight in a dynamic and polydisperse oligomeric chaperone.
676

677 MATERIALS AND METHODS

678

679 **Sequence and structural analysis**

680 Analysis of protein sequences was performed using Local CIDER[54]. Secondary structure
681 prediction was calculated using PSIPRED[31-32] and the extent of disorder was calculated
682 using DISOPRED[55]. An ensemble of 5000 HspA1A structural models was produced using
683 *ab initio* Rosetta using the DnaK (PDB:5NRO) conformation as a template[16]. Briefly, the
684 HspA1A sequence was aligned to the DnaK sequence to identify regions with loop
685 insertions and deletions. The HspA1A fragment library was produced using the fragment
686 picker. The lowest scoring model was used to produce a complex between HspA1A and
687 the DnaJB8 JD. The structural images were produced using PyMOL.
688

689 **Cell biological and biochemical analysis of DnaJB8-Clover cell lines**

690 The human *DNAJB8* protein-coding sequence was cloned using Gibson assembly into a
691 modified FM5 lentiviral expression plasmid[56] in which the *UbC* promoter was replaced by
692 a *CMV* promoter, the linker sequence was replaced by "GSAGSAAGSGEF" and
693 the *YFP* was replaced by *mClover3*. The resulting gene produced a DNAJB8-mClover3
694 fusion protein. In parallel, we produced a construct that expresses the fluorescent protein
695 (mClover3) but lacks DNAJB8. Both plasmids we separately co-transfected into HEK293T
696 cells along with helper plasmids (pCMV-VSV-G and psPAX2) to produce lentivirus, which
697 was harvested after 48hrs and used to produce polyclonal cell lines that expressed either
698 DNAJB8-mClover3 or mClover3. For crosslinking experiments, cells from a confluent
699 10cm^2 cell culture dish were pelleted and lysed using an insulin syringe in 1xPBS with
700 1mM DTT, 1mM PMSF, 1x EDTA-free Protease Inhibitor Cocktail (Roche), and 1%
701 Digitonin. After spinning at 1000xg for 10min., the lysate was recovered and incubated

702 with a polyhistidine tagged GFP-nanobody (purified as described previously[34]) for 2.5
703 hours at 4ºC. The lysate was then incubated with 25µL NiNTA beads (Clontech) (for 1
704 hour at 4ºC for binding. The beads were washed five times with 300µL 1xPBS. The buffer
705 for each wash was removed after pulse spinning the beads via centrifugation. The beads
706 were preincubated for 5 minutes at 37ºC and a final concentration of 57mM ADH and
707 36mM DMTMM were added to each sample. Following a one-minute incubation with
708 chemical crosslinkers, the reaction was quenched with 1mM ammonium bicarbonate.
709 After another pulse spin to remove the buffer, the beads were resuspended in elution
710 buffer, (8M Urea, 0.5M imidazole, pH 7.5). After a final pulse spin, the supernatant was
711 retained and analyzed by mass spectrometry.
712

713 **Analysis of Mass Spectrometry Results**

714 Each Thermo .raw file was converted to .mzXML format for analysis using an in-house
715 installation of xQuest[57]. Score thresholds were set through xProphet[57], which uses a
716 target/decoy model. The search parameters were set as follows. For grouping light and
717 heavy scans (hydrazide crosslinks only): Precursor mass difference for isotope-labeled
718 hydrazides = 8.05021 Da for ADH-d_0/d_8; maximum retention time difference for
719 light/heavy pairs = 2.5 min. Maximum number of missed cleavages = 2, peptide length =
720 5-50 residues, fixed modifications = carbamidomethyl-Cys (mass shift = 57.02146 Da),
721 mass shift of light crosslinker = 138.09055, mass shift of monolinks = 156.1011 Da, MS^1
722 tolerance = 15 ppm, and MS^2 tolerance = 0.2 Da for common ions and 0.3 Da for crosslink
723 ions; search in enumeration mode. For zero-length crosslink search: maximum number
724 of missed cleavages = 2, peptide length = 5-50 residues, fixed modifications
725 carbamidomethyl-Cys (mass shift = 57.02146 Da), mass shift of crosslinker = -18.010595
726 Da, no monolink mass specified, MS^1 tolerance = 15 ppm, and MS^2 tolerance = 0.2 Da
727 for common ions and 0.3 Da for crosslink ions; search in enumeration mode. The FDRs
728 of all *in vitro* experiments range from 0.05 to 0.33.
729
730

731 **Western blot analysis**

732 10µL aliquots of the HEK control, Clover, and DnaJB8-Clover cell-lines were removed
733 from the elution and loaded onto a 4-12% Bis-Tris SDS-PAGE gel for western blotting.
734 Upon running the gel to completion, the gel transferred onto a transfer membrane soaked
735 in Novoblot transfer buffer. Following the transfer, the membrane was soaked in milk
736 blocking buffer for 1 hour at room temperature. For immunolabelling, we added 1:2000
737 dilution of polyclonal Anti-GFP (rabbit) (Rockland) in milk and incubated the membrane
738 shaking at room temperature for 2 hours. The primary antibody solution was dumped and
739 the membrane washed three times for 10 minutes each with 1xTBST before adding the
740 polyclonal Anti-Rabbit Peroxidase (Rockland) at a 1:5000 dilution in milk. The membrane
741 was incubated with secondary antibody at room temperature for 1 hour before removing
742 the antibody solution. The membrane was washed 3 times in 5-minute intervals with
743 1xTBST and finally one 5-minute wash with 1xTBS. The membrane was soaked in 1mL
744 of Luminol enhancer and peroxide solution for 1 minute before imaging.
745
746 **In cell analysis of DnaJB8-Clover and Clover cell lines**
747 HEK293T cells expressing either DNAJB8-mClover3 or mClover alone were plated at
748 300,000 cells per well in media (10%FBS, 1%Pen/Strep, 1%GlutaMax in DMEM) in a 6-
749 well glass bottom plate (Cellvis, P06-1.5-N). After 30 hours, cells were stained with
750 Hoescht33342 at a final concentration of 2ug/mL in cell media for 30 minutes at 37C and
751 5%CO2. The plate was placed on an InCell6000 with a heated stage and fifty fields of
752 view were imaged under DAPI and FITC channels at 60X magnification (Nikon 60X/0.95,
753 Plan Apo, Corr Collar 0.11-0.23, CFI/60 lambda). Images were exported as TIFF files for
754 downstream analysis.
755
756 **Identification of factors bound to DnaJB8**
757 DnaJB8-Clover was purified from HEK293 cells as described previously[34] using a GFP-
758 nanobody construct with a His tag. The pulldown was analyzed via LC-MS/MS, resulting
759 in mass spectra with mass peaks for all proteins in solution. The resulting data was
760 submitted to the CPFP[35] server for peak assignment and protein identification. The UTSW

761 CPFP server assigns protein peptides to peaks in submitted mass spectra by searching
762 the NCBI and EBI protein databases for mass spectra matches to known protein
763 sequences. The output results assign each identified protein a value in sequence
764 coverage, peptide-spectrum match (PSM), unique peptide hits, and matched isotope
765 pattern chromatograms (MICs). Using a Clover only cell line as a control, we compared
766 MIC scores for relative protein abundance in the DnaJB8-Clover sample to determine
767 which proteins were more abundant in the presence of DnaJB8 during the pulldown and
768 used sequence coverages >70% and PSMs>50 to restrict the list. Hits identified in the
769 DnaJB8-Clover pull downs that were enriched relative to the Clover controls were input
770 into the string database[58] to build network interaction maps based on interactions
771 described in the literature.
772
773 **Recombinant expression and purification of DnaJB8**
774 The vector used for DnaJB8 expression was a pET-29b vector containing the gene for
775 human DnaJB8, a T7 promoter to activate DnaJB8 expression, a His tag region at the
776 end of the gene, and a gene for kanamycin resistance. This vector construct was
777 transformed into *E. coli* BL-21 (DE3) cells and plated onto 2xLB plates containing
778 0.05mg/mL Kanamycin. 12mL of 2xLB, 0.05mg/mL Kanamycin were prepared and
779 inoculated with a single colony from the plate. This small culture was incubated overnight
780 at 37°C while shaking at 220rpm. In the morning, the 12mL culture was added to 1L of
781 2xLB supplemented with 0.05mg/mL Kanomycin and incubated at 37°C while shaking at
782 220rpm. Once OD600 reached 0.6-0.8 A.U., 1mL of 1M IPTG was added to induce
783 DnaJB8 expression. After incubation for an additional 4 hours, the cells were harvested
784 by spinning down the culture at 4,000g for 20 minutes.
785 The resulting cell pellet was resuspended in 25mL 1xPBS and 1mM PMSF in preparation
786 for insoluble separation. The resuspended cells were sonicated at 30% power, 5X pulse
787 for 10 minutes using an Omni Sonic Ruptor 4000 (Omni International). The lysed cells
788 were pelleted at 10,000g for 30 minutes and the supernatant was discarded. The

789 insoluble pellet was rinsed with 1xPBS, 0.75%Tween-20 and again pelleted at 10,000g
790 for 30 minutes.
791 The insoluble cell pellet was resuspended in 50mL lysis buffer (8M Guanidinium HCl,
792 50mM HEPES, 20mM Imidazole, 1mM DTT pH 7.5) and sonicated at 30% power, 3X
793 pulse for 1 minute to solubilize the DnaJB8 from the insoluble pellet. After a 30-minute
794 incubation at room temperature, the cellular debris was pelleted at 15,000g for 30
795 minutes. The resulting supernatant was mixed with 2mL HisPur™ Ni-NTA Resin (Thermo
796 Scientific) for 1 hour before being loaded onto a gravity column. The column was washed
797 with an additional 50mL of lysis buffer, followed by 50mL of a second wash buffer (50mM
798 HEPES, 20mM Imidazole, 1mM DTT pH 7.5 in H_2O). The protein was eluted with 30mL
799 of elution buffer (50mM HEPES, 500mM Imidazole, 1mM DTT pH 7.5 in H_2O) and
800 collected in 2mL fractions. After selecting for fractions with high purity, the DnaJB8
801 solution was loaded into 3.5kDa cutoff Biotech CE Dialysis Tubing (Spectrum Labs) and
802 dialyzed overnight at 4ºC in 50mM ammonium formate to minimize assembly. The protein
803 was then lyophilized and stored at -80°C for future use.
804
805 **Dynamic Light Scattering**
806 All samples were prepared at 1.2mg/mL in 1xPBS, 1mM DTT, pH 7.4. All protein samples
807 were filtered through a 0.22µm PES sterile filter and loaded in triplicate onto a 384 well
808 clear flat-bottom plate. The plate was loaded into a Wyatt DynaPro Plate Reader III and
809 set to run continuously at room temperature at a scanning rate of 1 scan per 15 minutes,
810 with 1 scan composed of 10 acquisitions. The data were analyzed using the Wyatt
811 Dynamics software version 7.8.2.18. Light scattering results were filtered by Sum of
812 Squares (SOS) <20 to eliminate statistical outlier acquisitions within each scan. For
813 DnaJB8 in 1xPBS(150mM) buffer, one of the triplicates contains partial data due to high
814 SOS values. This is a result of increasing polydispersity and heterogeneity, which is
815 consistent with oligomers of that size. Average R_h readings at each time point were
816 reported and further averaged across triplicate wells. Data for the smallest particles was
817 reported by filtering out any signal that was greater than 10nm for runs with JD_{1-77} and

818 $CTD_{170-232}$, while more broad analyses such as the full DnaJB8 protein did not consider
819 size cutoffs.
820
821 **Transmission Electron Microscopy**
822 5µL of sample at 200µM was loaded onto grids. 200 mesh formvar grids are prepared
823 through glow discharge followed by the application of each 5µL sample onto each grid.
824 After 30 seconds, the grid is blotted by filter paper followed by washing the grid with 5µL
825 of ddH_2O. After another 30 seconds, the grid is blotted again followed by the addition of
826 5µL of 2% uranyl acetate for negative staining. After 1 minute, the grid was dried for the
827 final time and loaded into a FEI Tecnai G2 Spirit Biotwin TEM. All images were captured
828 using a Gatan 2Kx2K multiport readout post column CCD. The images were acquired at
829 the UT Southwestern EM Core Facility.
830
831 **Cross-Linking Reagents**
832 All crosslinking reagents used are commercially available: ADH (Sigma-Aldrich), and
833 mixed light and deuterated ADH (ADH-h_8/d_8) (Creative Molecules). DMTMM (Sigma-
834 Aldrich). For all crosslinking experiments, stock solutions were made of each crosslinking
835 reagent. A 1:1 ADH-d_0/ADH-d_8 solution was made at 100mg/mL in 1xPBS pH 7.4 (Sigma-
836 Aldrich). DMTMM (Sigma-Aldrich) was prepared at a 120mg/mL concentration in 1xPBS
837 pH 7.
838
839 **Cross-Linking Mass Spectrometry**
840 The *ex-vivo* purified DnaJB8 was dialyzed to remove excess imidazole, and transferred
841 into 1xPBS pH 7.4 buffer. For the full-length DnaJB8 experiments, lyophilized DnaJB8
842 was resuspended in either 1xPBS(150mM) or 1xPBS(285mM) to a concentration of
843 100µM. The JD_{1-77} and $CTD_{170-232}$ constructs were purified into 1xPBS buffer, and were
844 prepared for XLMS experiments at 100µM each. 2µM HspA1A in 1xPBS pH 7.4 buffer
845 and mixed with either 40µM DnaJB8 or 40µM JD_{1-77} for XLMS experiments. All samples
846 were incubated at 37°C while shaking at 350 rpm for 30 minutes. Final concentrations of

847 57mM ADH d_0/d_8 (Creative Molecules) and 36mM DMTMM (Sigma-Aldrich) were added
848 to the protein samples with final concentrations of 8.3 mg/mL and 12 mg/mL respectively,
849 and incubated at 37°C with shaking at 350 rpm for 30 minutes. The reactions were
850 quenched with 100mM ammonium bicarbonate and incubated at 37°C for 30 min.
851 Samples were lyophilized and resuspended in 8M urea. Samples were reduced with
852 2.5mM TCEP incubated at 37°C for 30 min followed by alkylation with 5mM iodoacetimide
853 for 30 minutes in the dark. Samples were diluted to 1M urea using a stock of 50mM
854 ammonium bicarbonate and trypsin (Promega) was added at a 1:50 enzyme-to-substrate
855 ratio and incubated overnight at 37°C shaking at 600 rpm. 2% (v/v) formic acid was added
856 to acidify the samples following overnight digestion. All samples were run on reverse
857 phase Sep-Pak tC18 cartridges (Waters) eluted in 50% acetonitrile with 0.1% formic acid.
858 10µL of the purified peptide fractions was injected for LC-MS/MS analysis on an Eksigent
859 1D-NanoLC-Ultra HPLC system coupled to a Thermo Orbitrap Fusion Tribrid system.
860 Peptides were separated on self-packed New Objective PicoFrit columns (11cm x
861 0.075mm I.D.) containing Magic C18 material (Michrom, 3µm particle size, 200Å pore
862 size) at a flow rate of 300nL/min using the following gradient. 0-5min = 5 %B, 5-95min =
863 5-35 %B, 95-97min = 35-95 %B and 97-107min = 95 %B, where A =
864 (water/acetonitrile/formic acid, 97:3:0.1) and B = (acetonitrile/water/formic acid, 97:3:0.1).
865 The mass spectrometer was operated in data dependent mode by selecting the five most
866 abundant precursor ions (m/z 350-1600, charge state 3+ and above) from a preview scan
867 and subjecting them to collision-induced dissociation (normalized collision energy = 35%,
868 30ms activation). Fragment ions were detected at low resolution in the linear ion trap.
869 Dynamic exclusion was enabled (repeat count 1, exclusion duration 30sec).
870

871 **Solid state NMR analysis**

872 Chaperone oligomers were prepared in PBS buffer with different NaCl concentrations.
873 Lyophilized DnaJB8 uniformly labeled with ^{13}C and ^{15}N (U-^{13}C,^{15}N) was re-suspended in
874 1ml of PBS buffer in which the final NaCl concentration was 100mM or 285mM. Each
875 sample was packed into a 3.2mm MAS NMR rotor (Bruker Biospin) by sedimentation,

876 using a previously described ultracentrifugal packing tool[59] . Sedimentation was done at
877 175,000 x g force in an Optima L-100 XP Ultracentrifuge using a SW-32 Ti centrifuge
878 rotor for 1 hour. Subsequently, excess of the supernatant fluid was removed. Sample
879 tubes were washed with another 1mL buffer solution after which a second packing step
880 using same parameters was performed. Finally, supernatant was removed, spacers were
881 placed on the top of the hydrated sedimented protein oligomers, and rotors were closed
882 with the cap, sealed with a small amount of epoxy to avoid sample dehydration.
883
884 Experiments were performed on Bruker 600 MHz and 750 MHz spectrometers, at 277 K
885 temperature using triple-channel (HCN) 3.2mm MAS EFree probes. Single pulse
886 excitation (SPE) measurements were performed using a 6μs 90˚ pulse on ^{13}C, 3s recycle
887 delay, 4k scans and TPPM[60] proton decoupling of 83 kHz during acquisition.
888 1D Cross-Polarization experiments (CP) were performed using a 3.1μs 90˚ ^{1}H pulse, 2ms
889 contact time, recycle delay of 3s, 4k scans and TPPM proton decoupling of 83 kHz during
890 acquisition. Both SPE and CP experiments ran for 3.4 hours.
891 The ^{13}C-^{13}C 2D CP-DARR experiments were performed using 25ms mixing time, 0.4ms
892 contact time, 3.1μs 90° proton pulse, 6μs 90°pulse on ^{13}C, TPPM proton decoupling of
893 83 kHz, recycle delay of 2.8s, 1k scans. This experiment took 4 days and 20 hours. The
894 amino acid type and secondary structure were predicted using the PLUQ program[45]
895 based on the to chemical shifts in the 2D experiment. Linewidth calculation was done
896 using the SPARKY program[61].

897 **Simulations and synthetic NMR spectra**

898 The structure of the DnaJB8 JD in solution was determined previously using solution
899 NMR[30]. The synthetic spectrum of this domain was generated using the corresponding
900 solution NMR chemical shifts from the BMRB (entry 11417). To simulate 2D NMR spectra
901 of the other three domains MD simulations were performed on full length DnaJB8. The
902 starting DNAJB8 conformation was produced using rosetta with a fully expanded
903 conformation of the F/G and S/T domains while keeping the JD and CTD in the folded
904 conformations. MD simulations were carried out in Desmond and the simulation box was

905 prepared in Maestro[62-63]. Estimated chemical shifts of the resulting structural models were
906 generated using the SPARTA+ package[46].
907
908 **Recombinant Expression and Purification of J Domain and C-Terminal Domain**
909 Both vector constructs containing DnaJB8 JD and CTD respectively were cloned into
910 pET-29b using Gibson assembly. These vectors were transformed into *E. coli* BL-21
911 (DE3) cells and plated onto 2xLB plates with 0.05mg/mL Kanamycin. 12mL of 2xLB with
912 0.05mg/mL Kanamycin were prepared and inoculated with a single colony from each
913 plate. These small cultures were incubated overnight at 37°C while shaking at 220rpm.
914 In the morning, the 12mL culture was added to 1L of 2xLB supplemented with 0.05mg/mL
915 Kanamycin and incubated at 37°C while shaking at 220rpm. Once OD600 reached 0.6-
916 0.8 A.U., 1mL of 1M IPTG was added to induce protein expression. After incubation for
917 an additional 4 hours, the cells were harvested by spinning down the culture at 4,000g for
918 20 minutes. For preparing ^{15}N JD, a single colony was inoculated into 10mL 2xLB
919 supplemented with 0.05mg/mL Kanamycin and incubated for 7-8 hours at 37°C while
920 shaking at 220rpm. The 10mL culture was then mixed into 100mL of M9 minimal media
921 (42mM Na_2HPO_4, 22mM KH_2PO_4, 8.5mM NaCl, 0.1mM CaCl, 2mM Mg_2SO_4, 1E-4%
922 Thiamine, 0.4% Glucose, 187mM NH_4Cl, 0.05mg/mL Kanamycin) and incubated
923 overnight at 37°C while shaking at 220rpm. In the morning of the following day, the cells
924 were spun down at 2,000g for 10minutes and resuspended in 20mLs of M9 minimal media
925 containing 15N labeled NH_4Cl in place of the unlabeled molecule. This was immediately
926 added to 1L of M9 minimal media with ^{15}N labeled NH_4Cl and allowed to incubate at 37°C
927 shaking at 220rpm. Once OD600 reached 0.6-0.8 A.U., 1mL of 1M IPTG was added to
928 induce protein expression. After incubation for an additional 4 hours, the cells were
929 harvested by spinning down the culture at 4,000g for 20 minutes. The cell pellets were
930 resuspended in 20mL of soluble wash buffer (SWB) (50mM KPO_4, 300mM NaCl, 10%
931 glycerol, 1mM PMSF, 10mM BME, pH 8) and sonicated at 30% power, 5X pulse for 10
932 minutes using an Omni Sonic Ruptor 4000 (Omni International). After incubation at room
933 temperature for 1 hour, the cell lysate was spun down at 15,000g for 30 minutes to

934 separate the soluble supernatant from the insoluble pellet. The supernatant was mixed
935 with 2mL TALON® Metal Affinity Resin (Clontech) and incubated shaking at 4°C for 1
936 hour. The protein-resin slurry was loaded onto a gravity column and washed with an
937 additional 40mL of SWB. This was followed by subsequent washes: 20mL SWB with 0.5%
938 tritonX-100, 20mL SWB with adjusted 700mM NaCl, 20mL SWB with 0.1mM ATP and
939 5mM $MgCl_2$, and an additional 40mL of SWB. The protein was eluted with 16mL SWB
940 with 200mM Imidazole into 2mL fractions. After selecting for fractions with high purity, the
941 protein solution was loaded into 3.5kDa cutoff Biotech CE Dialysis Tubing (Spectrum
942 Labs) and dialyzed overnight at 4°C in 1xPBS to restore native folding. Both domain
943 constructs were further enriched by running on a GE Superdex 200 Increase 10/300
944 column in 1xPBS 1mM DTT pH 7. The protein was aliquoted and flash frozen in liquid
945 nitrogen and stored at -80°C for future use.
946
947 **Solution NMR with ^{15}N-labeled JD and CTD**
948 The ^{15}N-labeled JD was exchanged into 20mM Tris 100mM NaCl 1mM DTT pH 7 buffer
949 in preparation for solution NMR. Each HSQC run was done for 4 hours at 1 scans/min
950 with the temperature fixed at 299K. After each run, unlabeled CTD was titrated into the
951 sample at 1:1, 1:3, and 1:6 ratios sequentially. All scans were collected on an Agilent DD2
952 600MHz instrument at the UT Southwestern Biomolecular NMR Facility. Each spectrum
953 was converted into a readable format and phase corrected using NMRPipe[64]. Peak
954 assignments were based on the deposited information from BMRB (11417). The software
955 Sparky[61, 65] was used to analyze the peak shifts across all spectra.
956
957 **Circular Dichroism**
958 Recombinant $CTD_{170-232}$ domain constructs were transferred into 10mM $NaPO_4$, 150mM
959 NaF, pH 7.4 buffer at a concentration of 40µM. The experiment was run using a Jasco J-
960 815 Circular Dichroism instrument with a PMT detector using a 10 mm quartz cuvette. 6
961 accumulations were taken at a speed of 50 nm/min along the UV spectrum from 190 nm

962 to 300 nm. Spectra analysis was done using the BeStSel online software[66-67] to determine
963 secondary structural composition.
964
965 **SEC-MALS**
966 $CTD_{170-232}$ construct at a concentration of 6.6 mg/mL in 1xPBS was filtered through a 0.1
967 µm filter to remove larger impurities. The sample was further filtered using a 0.22 µm
968 centrifugal filter before 100 µL was applied to a Superdex 200 Increase 10/300 column
969 equilibrated in 1xPBS. The column was inline with a Shimadzu UV detector, a Wyatt
970 TREOS II light-scattering detector, and a Wyatt Optilab tREX differential-refractive-index
971 detector. The flow rate was 0.5 mL/min. The data were analyzed with Wyatt's ASTRA
972 software version 7.1.0.29. SEDFIT was used to calculate the dn/dc of the protein.
973
974 **CTD model generation**
975 Fragment libraries for the CTD sequence were generated using the Robetta server. 5000
976 models were produced using the *ab initio* protocol and clustered to identify unique
977 conformations. Lowest scoring models from the top clusters showed high structural
978 similarity. The identified crosslinks from the CTD in full length DnaJB8 or isolated CTD
979 were evaluated for consistency with each model in the ensemble. For acid-acid and acid-
980 lysine crosslinks a distance threshold of 21 and 16 Å, respectively, was considered as
981 satisfied and consistent with the chemistry. Distances were calculated using a custom
982 script in MATLAB ver.R2019a and the crosslink pairs were visualized using PyMOL. The
983 HYDROPRO software was used to calculate radii of hydration from structural models.
984
985
986 **Fluorescence polarization**
987 JD_{1-77} was labelled with 10x FITC-maleimide in 1xPBS 1mM TCEP for 2 hours at room
988 temperature. Excess dye was removed and the reaction quenched using a Zeba™ spin
989 desalting column. For all experiments, 0.2µM JD_{1-77} was incubated in triplicate with a
990 titration gradient of Hsp70(150µM-0µM) or $CTD_{170-232}$(150µM-0µM) in 1xPBS, 1mM

991 TCEP, pH 7.4. For competition experiments, labelled JD_{1-77} was mixed with 3.125µM CTD
992 in triplicate and incubated at room temperature for 1 hour before adding a titration gradient
993 of Hsp70(150µM-0µM). Fluorescence polarization readings were taken with excitation at
994 494nm and emission at 525nm.
995
996 **Modeling of full length DNAJB8 using Rosetta and XL-MS restraints**
997 Given the globular conformations of the JD and CTD we considered how the crosslinks
998 identified for the full-length protein could guide the JD-CTD interaction. Using Rosetta we
999 assembled a monomeric conformation leveraging the JD and CTD conformations while
1000 keeping the F/G and S/T regions full expanded. This starting model was then used in a
1001 relax protocol in conjunction with crosslinks as constraints to produce an ensemble of
1002 collapsed conformations. For acid-acid and acid-lysine contacts 21 and 16 Å distance
1003 thresholds were used as restraints.
1004
1005 **Conservation mapping**
1006 DnaJB8 homolog sequences were identified using Blast[68-69] and the sequences were
1007 aligned using Clustal Omega[70]. The protein sequence alignment and structure of DnaJB8
1008 JD (PDBID 2DMX) were used as input in Al2Co[71] to map the conservation onto the
1009 structural models. The conservation was mapped onto the models in PyMOL.
1010
1011 **Coevolutionary variation analysis**
1012 The GREMLIN software[50-52] was used to identify covarying amino acid pairs from a
1013 DnaJB8 protein sequence alignment. A probability of 0.7 was used to threshold the data
1014 to identify amino acids with strong coupling.
1015
1016 **Recombinant expression and purification of HspA1A**
1017 HspA1A gene was cloned into the pMCSG7 plasmid[72] and transformed into BL-21 (DE3)
1018 cells and plated onto 2xLB plates with 0.1mg/mL ampicillin. 12mL of 2xLB with 0.1mg/mL
1019 ampicillin were prepared and inoculated with a single colony from each plate. These small

1020 cultures were incubated overnight at 37ºC while shaking at 220rpm. In the morning, the
1021 12mL culture was added to 1L of 2xLB supplemented with 0.1mg/mL ampicillin and
1022 incubated at 37°C while shaking at 220rpm. Once OD600 reached 0.6-0.8 A.U., 1mL of
1023 1M IPTG was added to induce protein expression. The cells continued to incubate
1024 overnight at 12ºC shaking at 220rpm. After incubation, the cells were lysed using a
1025 PandaPlus 2000 homogenizer (GEA) by pressing the cells with 10,000p.p.m pressure.
1026 The lysate was spun at 15,000xg for 45 minutes to remove insoluble cell components,
1027 and the resulting supernatant was mixed with 2mL TALON® Metal Affinity Resin
1028 (Clontech) and incubated at 4ºC for 1 hour. The slurry was spun down at 700xg for 2 min
1029 to remove the majority of the buffer and the beads were added onto a gravity column. The
1030 beads were washed with 6CV of wash buffer (50mM Tris, 500mM NaCl, 10mM imidazole,
1031 5mM βME, pH 8) and eluted with 5mL of elution buffer (50mM Tris, 500mM NaCl, 300mM
1032 imidazole, 5mM βME, pH 8). HspA1A containing fractions were confirmed by SDS-PAGE
1033 and pooled together for desalting. Desalting/buffer exchange was performed using a PD-
1034 10 desalting column (GE Healthcare), where HspA1A fractions were transferred into
1035 anion-exchange wash buffer (50mM Tris, 20mM NaCl, 1mM DTT, pH 8.75). The protein
1036 was loaded onto a HiTrap Q HP anion exchange column (GE Healthcare) and eluted
1037 across a gradient of anion-exchange elution buffer (50mM Tris, 1M NaCl, 1mM DTT, pH
1038 8.75). HspA1A-containing fractions were once again combined and loaded onto a
1039 Superdex™ 200 Increase 10/300 GL (GE Life Sciences) size exclusion column, where
1040 HspA1A was further purified and transferred into 1xPBS, 1mM DTT, pH 7.4 buffer for all
1041 subsequent experiments.
1042
1043 **Code availability**

1044 All DnaJB8 simulations were carried out with ROSETTA (available at
1045 https://www.rosettacommons.org/). All DNAJB8 molecular dynamics simulations were
1046 performed using Desmond (available at
1047 https://www.deshawresearch.com/resources_desmond.html). Sequence charge
1048 distributions were calculated using localCIDER (available at
1049 https://pappulab.github.io/localCIDER/).
1050

1051 **Acknowledgements**

1052 This work was supported by grants from the Welch Foundation and the Effie Marie Cain
1053 Endowed Scholarship (L.A.J.) and NIGMS R01 GM112678 (P.V.D.W.). We appreciate
1054 the help of the Structural Biology Laboratory, Biomolecular Nuclear Magnetic Resonance
1055 Facility, Electron Microscopy Core Facility, and Proteomics Core Facility at the University
1056 of Texas Southwestern Medical Center.

1057

1058 **Author Contributions**

1059 B.D.R., I.M., P.V.D.W., and L.A.J. conceived and designed the overall study. B.D.R. performed *in*
1060 *vitro* protein assays, cell models, crosslink mass spectrometry, and ROSETTA simulations. I.M.
1061 and P.V.D.W. performed ssNMR experiments and analyzed the data. S.B. performed DNAJB8
1062 CTD experiments and ROSETTA simulations. J.V.A produced mammalian cell lines and collected
1063 microscopy images. B.D.R. performed electron microscopy. B.D.R., I.M., P.V.D.W., and L.A.J.
1064 wrote the manuscript, and all authors contributed to its improvement.

1065

1066 **Competing Interests**

1067 The authors declare no competing interests.

1068
1069

1070

1071

1072 **References**

1073

1074 1. Flaherty, K. M.; DeLuca-Flaherty, C.; McKay, D. B., Three-dimensional structure of the
1075 ATPase fragment of a 70K heat-shock cognate protein. *Nature* **1990,** *346* (6285), 623-8.

1076 2. Wang, H.; Kurochkin, A. V.; Pang, Y.; Hu, W.; Flynn, G. C.; Zuiderweg, E. R., NMR solution
1077 structure of the 21 kDa chaperone protein DnaK substrate binding domain: a preview of
1078 chaperone-protein interaction. *Biochemistry* **1998,** *37* (22), 7929-40.
1079 3. Bertelsen, E. B.; Chang, L.; Gestwicki, J. E.; Zuiderweg, E. R., Solution conformation of
1080 wild-type E. coli Hsp70 (DnaK) chaperone complexed with ADP and substrate. *Proc Natl Acad Sci*
1081 *U S A* **2009,** *106* (21), 8471-6.
1082 4. Pellecchia, M.; Szyperski, T.; Wall, D.; Georgopoulos, C.; Wuthrich, K., NMR structure of
1083 the J-domain and the Gly/Phe-rich region of the Escherichia coli DnaJ chaperone. *J Mol Biol*
1084 **1996,** *260* (2), 236-50.
1085 5. Szyperski, T.; Pellecchia, M.; Wall, D.; Georgopoulos, C.; Wuthrich, K., NMR structure
1086 determination of the Escherichia coli DnaJ molecular chaperone: secondary structure and
1087 backbone fold of the N-terminal region (residues 2-108) containing the highly conserved J
1088 domain. *Proc Natl Acad Sci U S A* **1994,** *91* (24), 11343-7.
1089 6. Pellecchia, M.; Guntert, P.; Glockshuber, R.; Wuthrich, K., NMR solution structure of the
1090 periplasmic chaperone FimC. *Nat Struct Biol* **1998,** *5* (10), 885-90.
1091 7. Choudhury, D.; Thompson, A.; Stojanoff, V.; Langermann, S.; Pinkner, J.; Hultgren, S. J.;
1092 Knight, S. D., X-ray structure of the FimC-FimH chaperone-adhesin complex from uropathogenic
1093 Escherichia coli. *Science* **1999,** *285* (5430), 1061-6.
1094 8. Minami, Y.; Hohfeld, J.; Ohtsuka, K.; Hartl, F. U., Regulation of the heat-shock protein 70
1095 reaction cycle by the mammalian DnaJ homolog, Hsp40. *J Biol Chem* **1996,** *271* (32), 19617-24.
1096 9. Wall, D.; Zylicz, M.; Georgopoulos, C., The NH2-terminal 108 amino acids of the
1097 Escherichia coli DnaJ protein stimulate the ATPase activity of DnaK and are sufficient for lambda
1098 replication. *J Biol Chem* **1994,** *269* (7), 5446-51.
1099 10. Wall, D.; Zylicz, M.; Georgopoulos, C., The conserved G/F motif of the DnaJ chaperone is
1100 necessary for the activation of the substrate binding properties of the DnaK chaperone. *J Biol*
1101 *Chem* **1995,** *270* (5), 2139-44.
1102 11. Hartl, F. U., Molecular chaperones in cellular protein folding. *Nature* **1996,** *381* (6583),
1103 571-9.
1104 12. Cheetham, M. E.; Caplan, A. J., Structure, function and evolution of DnaJ: conservation
1105 and adaptation of chaperone function. *Cell Stress Chaperones* **1998,** *3* (1), 28-36.
1106 13. Muchowski, P. J.; Wacker, J. L., Modulation of neurodegeneration by molecular
1107 chaperones. *Nat Rev Neurosci* **2005,** *6* (1), 11-22.
1108 14. Kampinga, H. H.; Craig, E. A., The HSP70 chaperone machinery: J proteins as drivers of
1109 functional specificity. *Nat Rev Mol Cell Biol* **2010,** *11* (8), 579-92.
1110 15. Ahmad, A.; Bhattacharya, A.; McDonald, R. A.; Cordes, M.; Ellington, B.; Bertelsen, E. B.;
1111 Zuiderweg, E. R. P., Heat shock protein 70 kDa chaperone/DnaJ cochaperone complex employs
1112 an unusual dynamic interface. *Proc Natl Acad Sci U S A* **2011,** *108*, 18966-18971.
1113 16. Kityk, R.; Kopp, J.; Mayer, M. P., Molecular Mechanism of J-Domain-Triggered ATP
1114 Hydrolysis by Hsp70 Chaperones. *Mol Cell* **2018,** *69* (2), 227-237 e4.
1115 17. Rampelt, H.; Kirstein-Miles, J.; Nillegoda, N. B.; Chi, K.; Scholz, S. R.; Morimoto, R. I.;
1116 Bukau, B., Metazoan Hsp70 machines use Hsp110 to power protein disaggregation. *EMBO J*
1117 **2012,** *31* (21), 4221-35.

1118 18. Wagner, I.; Arlt, H.; van Dyck, L.; Langer, T.; Neupert, W., Molecular chaperones
1119 cooperate with PIM1 protease in the degradation of misfolded proteins in mitochondria. *EMBO*
1120 *J* **1994,** *13* (21), 5135-45.
1121 19. Nakatsukasa, K.; Huyer, G.; Michaelis, S.; Brodsky, J. L., Dissecting the ER-associated
1122 degradation of a misfolded polytopic membrane protein. *Cell* **2008,** *132* (1), 101-12.
1123 20. Jiang, Y.; Possi, P.; Kalodimos, C. G., Structural basis for client recognition and activity of
1124 Hsp40 chaperones. *Science* **2019,** *365* (6459), 1313-1319.
1125 21. Nillegoda, N. B.; Stank, A.; Malinverni, D.; Alberts, N.; Szlachcic, A.; Barducci, A.; De Los
1126 Rios, P.; Wade, R. C.; Bukau, B., Evolution of an intricate J-protein network driving protein
1127 disaggregation in eukaryotes. *Elife* **2017,** *6*.
1128 22. Hageman, J.; Rujano, M. A.; van Waarde, M. A.; Kakkar, V.; Dirks, R. P.; Govorukhina, N.;
1129 Oosterveld-Hut, H. M.; Lubsen, N. H.; Kampinga, H. H., A DNAJB chaperone subfamily with
1130 HDAC-dependent activities suppresses toxic protein aggregation. *Mol Cell* **2010,** *37* (3), 355-69.
1131 23. Karamanos, T. K.; Tugarinov, V.; Clore, G. M., Unraveling the structure and dynamics of
1132 the human DNAJB6b chaperone by NMR reveals insights into Hsp40-mediated proteostasis.
1133 *Proc Natl Acad Sci U S A* **2019**.
1134 24. Månsson, C.; Kakkar, V.; Monsellier, E.; Sourigues, Y.; Härmark, J.; Kampinga, H. H.;
1135 Melki, R.; Emanuelsson, C., DNAJB6 is a peptide-binding chaperone which can suppress amyloid
1136 fibrillation of polyglutamine peptides at substoichiometric molar ratios. *Cell Stress and*
1137 *Chaperones* **2014,** *19*, 227-239.
1138 25. Söderberg, C. A. G.; Månsson, C.; Bernfur, K.; Rutsdottir, G.; Härmark, J.; Rajan, S.; Al-
1139 Karadaghi, S.; Rasmussen, M.; Höjrup, P.; Hebert, H.; Emanuelsson, C., Structural modelling of
1140 the DnaJB6 oligomeric chaperone shows a peptide-binding cleft lined with conserved S/T-
1141 residues at the dimer interface. *Scientific Reports* **2018,** *8* (5199).
1142 26. Gillis, J.; Schipper-Krom, S.; Juenemann, K.; Gruber, A.; Coolen, S.; van den Nieuwendijk,
1143 R.; van Veen, H.; Overkleeft, H.; Goedhart, J.; Kampinga, H. H.; Reits, E. A., The DNAJB6 and
1144 DNAJB8 protein chaperones prevent intracellular aggregation of polyglutamine peptides. *J Biol*
1145 *Chem* **2013,** *288* (24), 17225-37.
1146 27. Kakkar, V.; Mansson, C.; de Mattos, E. P.; Bergink, S.; van der Zwaag, M.; van Waarde,
1147 M. A.; Kloosterhuis, N. J.; Melki, R.; van Cruchten, R. T.; Al-Karadaghi, S.; Arosio, P.; Dobson, C.
1148 M.; Knowles, T. P.; Bates, G. P.; van Deursen, J. M.; Linse, S.; van de Sluis, B.; Emanuelsson, C.;
1149 Kampinga, H. H., The S/T-Rich Motif in the DNAJB6 Chaperone Delays Polyglutamine
1150 Aggregation and the Onset of Disease in a Mouse Model. *Mol Cell* **2016**.
1151 28. Shahmoradian, S. H.; Galez-Montoya, J. G.; Schmid, M. F.; Cong, Y.; Ma, B.; Spiess, C.;
1152 Frydman, J.; Ludtke, S. J.; Chiu, W., TRiC's tricks inhibit huntingtin aggregation. *eLife* **2013,** *2*
1153 (e00710).
1154 29. Genevaux, P.; Schwager, F.; Georgopoulos, C.; Kelley, W. L., Scanning mutagenesis
1155 identifies amino acid residues essential for the in vivo activity of the Escherichia coli DnaJ
1156 (Hsp40) J-domain. *Genetics* **2002,** *162* (3), 1045-53.
1157 30. Ohnishi, S.; Tochio, N.; Koshiba, S.; Inoue, M.; Kigawa, T.; Yokoyama, S., Solution
1158 structure of the J domain of DnaJ homolog subfamily B member 8. TO BE PUBLISHED, 2006.
1159 31. D.W.A., B.; Jones, D. T., The PSIPRED Protein Analysis Workbench: 20 years on. *Nucleic*
1160 *Acids Research* **2019**.

1161 32. Jones, D. T., Protein secondary structure prediction based on position-specific scoring
1162 matrices. *J. Mol. Bio.* **1999,** *292*, 195-202.
1163 33. Kirchhofer, A.; Helma, J.; Schmidthals, K.; Frauer, C.; Cui, S.; Karcher, A.; Pellis, M.;
1164 Muyldermans, S.; Casas-Delucchi, C. S.; Cardoso, M.; Leonhardt, H.; Hopfner, K. P.; Rothbauer,
1165 U., Modulation of protein properties in living cells using nanobodies. *Nat. Struc. and Mol. Bio.*
1166 **2010,** *17* (1), 133-138.
1167 34. Kubala, M. H.; Kovtun, O.; Alexandrov, K.; Collins, B. M., Structural and thermodynamic
1168 analysis of the GFP:GFP-nanobody complex. *Protein Sci.* **2010,** *19* (12), 2389-2401.
1169 35. Trudgian, D. C.; Thomas, B.; McGowan, S. J.; Kessler, B. M.; Salek, M.; Acuto, O., CPFP: a
1170 central proteomics facilities pipeline. *Bioinformatics* **2010,** *26* (8), 1131-1132.
1171 36. Leitner, A.; Faini, M.; Stengel, F.; Aebersold, R., Crosslinking and Mass Spectometry: An
1172 Integrated Technology to Understand the Structure and Function of Molecular Machines. *Cell*
1173 *Press* **2016,** *41* (1), 20-32.
1174 37. Leitner, A.; Joachimiak, L. A.; Unverdorben, P.; Walzthoeni, T.; Frydman, J.; Förster, F.;
1175 Aebersold, R., Chemical cross-linking/mass spectometry targeting acidic residues in proteins
1176 and protein complexes. *Proc Natl Acad Sci U S A* **2014,** *111* (26), 9455-9460.
1177 38. Walzthoeni, T.; Joachimiak, L. A.; Rosenberger, G.; Röst, H. L.; Malmström, L.; Leitner, A.;
1178 Frydman, J.; Aebersold, R., xTract: software for characterizing conformational changes of
1179 protein complexes by quantitative cross-linking mass spectometry. *Nat Methods* **2015,** *12* (12),
1180 1185-1190.
1181 39. Månsson, C.; Arosio, P.; Hussein, R.; Kampinga, H. H.; Hashem, R. M.; Boelens, W. C.;
1182 Dobson, C. M.; Knowles, T. P.; Linse, S.; Emanuelsson, C., Interaction of the molecular
1183 chaperone DNAJB6 with growing amyloid-beta 42 (Abeta42) aggregates leads to sub-
1184 stoichiometric inhibition of amyloid formation. *J Biol Chem* **2014,** *289* (45), 31066-76.
1185 40. Matlahov, I.; van der Wel, P. C. A., Hidden motions and motion-induced invisibility:
1186 Dynamics-based spectral editing in solid-state NMR. *Methods* **2018,** *148*, 123-135.
1187 41. Morris, G. A.; Freeman, R., Enhancement of Nuclear Magnetic-Resonance Signals by
1188 Polarization Transfer. *J Am Chem Soc* **1979,** *101* (3), 760-762.
1189 42. Lin, H. K.; Boatz, J. C.; Krabbendam, I. E.; Kodali, R.; Hou, Z. P.; Wetzel, R.; Dolga, A. M.;
1190 Poirier, M. A.; van der Wel, P. C. A., Fibril polymorphism affects immobilized non-amyloid
1191 flanking domains of huntingtin exon1 rather than its polyglutamine core. *Nat Commun* **2017,** *8*.
1192 43. Hoop, C. L.; Lin, H. K.; Kar, K.; Magyarfalvi, G.; Lamley, J. M.; Boatz, J. C.; Mandal, A.;
1193 Lewandowski, J. R.; Wetzel, R.; van der Wel, P. C., Huntingtin exon 1 fibrils feature an
1194 interdigitated beta-hairpin-based polyglutamine core. *Proc Natl Acad Sci U S A* **2016,** *113* (6),
1195 1546-51.
1196 44. Fritzsching, K. J.; Hong, M.; Schmidt-Rohr, K., Conformationally selective
1197 multidimensional chemical shift ranges in proteins from a PACSY database purged using
1198 intrinsic quality criteria. *J Biomol NMR* **2016,** *64* (2), 115-30.
1199 45. Fritzsching, K. J.; Yang, Y.; Schmidt-Rohr, K.; Hong, M., Practical use of chemical shift
1200 databases for protein solid-state NMR: 2D chemical shift maps and amino-acid assignment with
1201 secondary-structure information. *J Biomol NMR* **2013,** *56* (2), 155-67.
1202 46. Shen, Y.; Bax, A., SPARTA+: a modest improvement in empirical NMR chemical shift
1203 prediction by means of an artificial neural network. *J Biomol NMR* **2010,** *48* (1), 13-22.

1204 47. Mandal, A.; Hoop, C. L.; DeLucia, M.; Kodali, R.; Kagan, V. E.; Ahn, J.; van der Wel, P. C.
1205 A., Structural Changes and Proapoptotic Peroxidase Activity of Cardiolipin-Bound Mitochondrial
1206 Cytochrome c. *Biophys. J.* **2015,** *109*, 1873-1884.
1207 48. Ortega, A.; Amoros, D.; Garcia, J., Prediction of hydrodynamic and other solution
1208 properties of rigid proteins from atomic and residue-level models. *Biophys. J.* **2011,** *101*, 892-
1209 898.
1210 49. Marsh, J. A.; Forman-Kay, J. D., Sequence determinants of compaction in intrinsically
1211 disordered proteins. *Biophys. J.* **2010,** *98*, 2383-2390.
1212 50. Ovchinnikov, S.; Kamisetty, H.; Baker, D., Robust and accurate prediction of residue-
1213 residue interactions across protein interfaces using evolutionary information. *Elife* **2014,** *3*.
1214 51. Kamisetty, H.; Ovchinnikov, S.; Baker, D., Assessing the utility of coevolution-based
1215 residue-residue contact predictions in a sequence- and structure-rich era. *Proc Natl Acad Sci U S*
1216 *A* **2013,** *110* (39), 15674-15679.
1217 52. Balakrishnan, S.; Kamisetty, H.; Carbonell, J. G.; Lee, S.; Langmead, C. J., Learning
1218 generative models for protein fold families. *Proteins: Structure, Function, and Bioinformatics*
1219 **2011,** *79* (4), 1061-1078.
1220 53. Mayer, M. P.; Laufen, T.; Paal, K.; McCarty, J. S.; Bukau, B., Investigation of the
1221 interaction between DnaK and DnaJ by surface plasmon resonance spectroscopy. *J Mol Biol*
1222 **1999,** *289* (4), 1131-1134.
1223 54. Holehouse, A. S.; Ahad, J.; Das, R. K.; Pappu, R. V., CIDER: Classification of Intrinsically
1224 Disordered Ensemble Regions. *Biophys. J.* **2015,** *108*, 228a.
1225 55. Jones, D. T.; Cozzetto, D., DISOPRED3: precise disordered region predictions with
1226 annotated protein-binding activity. *Bioinformatics* **2105,** *31* (6), 857-863.
1227 56. Sanders, D. W.; Kaufman, S. K.; DeVos, S. L.; Sharma, A. M.; Mirbaha, H.; Li, A.; Barker, S.
1228 J.; Foley, A.; Thorpe, J. R.; Serpell, L. C.; Miller, T. M.; Grinberg, L. T.; Seeley, W. W.; Diamond, M.
1229 I., Distinct tau prion strains propagate in cells and mice and define different tauopathies.
1230 *Neuron* **2014,** *82* (6), 1271-1288.
1231 57. Leitner, A.; Walzthoeni, T.; Aebersold, R., Lysine-specific chemical cross-linking of
1232 protein complexes and identification of cross-linking sites using LC-MS/MS and the
1233 xQuest/xProphet software pipeline. *Nat. Protocols* **2014,** *9*, 120-137.
1234 58. Szklarczyk, D.; Gable, A. L.; Lyon, D.; Junge, A.; Wyder, S.; Huerta-Cepas, J.; Simonovic,
1235 M.; Doncheva, N. T.; Morris, J. H.; Bork, P.; Jensen, L. J.; von Mering, C., STRING v11: protein–
1236 protein association networkswith increased coverage, supporting functionaldiscovery in
1237 genome-wide experimental datasets. *Nucleic Acids Research* **2019,** *47*, D607-D613.
1238 59. Mandal, A.; Boatz, J. C.; Wheeler, T. B.; van der Wel, P. C., On the use of ultracentrifugal
1239 devices for routine sample preparation in biomolecular magic-angle-spinning NMR. *J Biomol*
1240 *NMR* **2017,** *67* (3), 165-178.
1241 60. Bennett, A. E.; Rienstra, C. M.; Auger, M.; Lakshmi, K. V.; Griffin, R. G., Heteronuclear
1242 Decoupling in Rotating Solids. *J Chem Phys* **1995,** *103* (16), 6951-6958.
1243 61. D., G. T.; G., K. D. *SPARKY 3*, 3.110; University of California, San Francisco: San Francisco,
1244 CA, 2004.
1245 62. *Schrödinger Release 2019-3*, D.E. Shaw Research: New York, NY, 2019.

63. Bowers, K. J.; Chow, E.; Xu, H.; Dror, R. O.; Eastwood, M. P.; Gregersen, B. A.; Klepeis, J. L.; Kolossvary, I.; Moraes, M. A.; Sacerdoti, F. D.; Salmon, J. K.; Shan, Y.; Shaw, D. E. In *Scaleable Algorithms for Molecular Dynamics Simulations on Commodity Clusters*, Proceedings of the ACM/IEEE Conference on Supercomputing (SC06), Tampa, FL, November 11-17; ACM: Tampa, FL, 2006.
64. Delaglio, F.; Grzesiek, S.; Vuister, G. W.; Zhu, G.; Pfeifer, J.; Bax, A., NMRPipe: A multidimensional spectral processing system based on UNIX pipes. *Journal of Biomolecular NMR* **1995,** *6*, 277-293.
65. Lee, W.; Tonelli, M.; Markley, J. L., NMRFAM-SPARKY: enhanced software for biomolecular NMR spectroscopy. *Bioinformatics* **2015,** *31* (8), 1325-1327.
66. Micsonai, A.; Wien, F.; Bulyáki, E.; Kun, J.; Moussong, E.; Lee, Y.; Goto, Y.; Réfrégiers, M.; Kardos, J., BeStSel: a web server for accurate protein secondary structure predicition and fold recognition from the circular dichroism spectra. *Nucleic Acids Research* **2018,** *46* (W), 315-322.
67. Micsonai, A.; Wien, F.; Kernya, L.; Lee, Y.; Goto, Y.; Réfrégiers, M.; Kardos, J., Accurate scondary structure prediction and fold recognition for circular dichroism spectroscopy. *Proc Natl Acad Sci U S A* **2015**.
68. Altschul, S. F.; Gish, W.; Miller, W.; Myers, E. W.; Lipman, D. J., Basic Local Alignment Search Tool. *J. Mol. Bio.* **1990,** *215*, 403-410.
69. Altschul, S. F.; Madden, T. L.; Schäffer, A. A.; Zhang, Z.; Miller, W.; Lipman, D. J., Gapped BLAST and PSI-BLAST: a new generation of protein database search programs. *Nucleic Acids Research* **1997,** *25*, 3389-3402.
70. Madeira, F.; Park, Y. M.; Lee, J.; Buso, N.; Gur, T.; Madhusoodanan, N.; Basutkar, P.; Tivey, A. R. N.; Potter, S. C.; Finn, R. D.; Lopez, R., The EMBL-EBI search and sequence analysis tools APIs in 2019. *Nucleic Acids Research* **2019,** *47* (W1), 636-641.
71. Pei, J.; Grishin, N. V., AL2CO: calculation of positional conservation in a protein sequence alignment. *Bioinformatics* **2001,** *17* (8), 700-712.
72. Eschenfeldt, W. H.; Lucy, S.; Millard, C. S.; Joachimiak, A.; Mark, I. D., A family of LIC vectors for high-throughput cloning and purification of proteins. *Methods Mol. Biol.* **2009,** *498*, 105-115.

Tables

Table 1. Residue distribution per domain with net charge for each domain.

Domain aa. length	Domain	Residue																				Net charge for the domain
		A	R	N	D	Q	E	G	H	I	L	K	M	F	P	S	T	Y	V	W	C	
1-75	**JD**	8	5	3	6	1	7	2	1	1	6	10	1	1	3	7	0	5	4	2	1	+2
76-148	**F/G**	6	5	2	5	0	5	13	2	1	2	0	1	14	6	6	3	2	0	1	0	-5
149-185	**S/T**	0	0	1	0	0	1	7	1	0	1	1	3	4	0	15	4	0	1	0	1	0
186-232	**CTD**	0	2	3	2	3	6	4	7	2	2	6	1	0	0	2	3	0	6	1	0	0

1308 **Figure Legends**

1309

1310 **Figure 1. Electrostatic interactions drive chaperone and co-chaperone interactions. (A)**
1311 Structural superposition of a HspA1A structural model (blue) with a crystal structure of DnaK-
1312 DnaJ (green and cyan, respectively; PDBID: 5NRO) shows good agreement. **(B-C)** Electrostatic
1313 surface potential of DnaJB8 JD docked into the JD binding site on HspA1A is shown in cartoon
1314 representation and is colored in black. Binding mode is based on the DnaJ-DnaK coordinates.
1315 Basic surface on helix 2 docks onto the HspA1A surface. Electrostatic surface potential of
1316 HspA1A with docked DnaJB8 JD is shown in cartoon representation and is colored in black. The
1317 HspA1A surface presents an acidic face that complements the basic DnaJB8 JD surface. Highly
1318 acidic potential is shown in red and highly basic is shown in blue. **(D)** Cartoon schematic of
1319 DnaJB8 colored according to domain annotation: JD (red), F/G rich(blue), S/T rich (cyan), and
1320 CTD (green). **(E)** PSIPRED secondary structure analysis of the DnaJB8 sequence. Probabilities
1321 for helix, sheet, and random coil assignments are colored pink, yellow and blue, respectively. **(F)**
1322 Charge-based analysis of the DnaJB8 sequence. Sequence charge distribution of DnaJB8 is
1323 shown using Net Protein Charge per Residue (NPCR). Basic regions are shown in blue and acidic
1324 regions are shown in red. Basic face of helix 2 is highlighted along with the corresponding acidic
1325 face of the CTD. The helices for JD are shown as grey rectangles. **(G)** DISOPRED analysis of
1326 the DnaJB8 sequence. Regions above the red-dashed line are predicted to be disordered.

1327

1328 **Figure 2. DnaJB8 forms oligomers in cells.** (**A**) Cartoon schematics for the DnaJB-Clover and
1329 Clover constructs used in the mammalian experiments. DnaJB8 is colored as in Figure 1. Clover
1330 is colored in green. (**B**) Representative images of cells expressing DnaJB8-Clover and Clover.
1331 Clover and DAPI fluorescence signal are shown in green and blue, respectively. 5um scale bar is
1332 shown in white. (**C**) Quantification of DnaJB8-Clover and Clover puncta in high and low protein
1333 level expressing cell lines. In each analysis at least 2000 cells were counted. (**D**) Western blot
1334 analysis of DnaJB8-Clover and Clover proteins isolated from mammalian cell lines. Total (T),
1335 elutions (E) and crosslinked elutions (XL) of each condition are shown. Western blot was probed
1336 with GFP antibodies. (**E**) XL-MS contact map of DnaJB8-Clover crosslinks (orange boxes)
1337 identified using DMTMM and ADH. The axes are colored in red and green for JD and CTD,
1338 respectively. Crosslink pairs between JD-CTD, JD-JD and CTD-CTD are shown in dashed boxes
1339 colored grey, red and green, respectively.

1340

1341 **Figure 3. DnaJB8 forms oligomers *in vitro*. (A)** DLS time-course of DnaJB8. Average radius of
1342 hydration (R_h) of triplicate samples starts at ~15nm and increases over time to ~90nm. An arrow
1343 indicates the time point where DnaJB8 was observed under TEM. **(B)** TEM image of DnaJB8
1344 oligomers. 200nm scale bar is shown in black. Length of oligomeric assemblies is ~90nm with a
1345 ~20nm width. **(C)** XL-MS contact map of DnaJB8 crosslinks identified using DMTMM and ADH
1346 (black) and DSS (grey). The axes are colored in red and green for JD and CTD, respectively.
1347 Crosslink pairs between JD-CTD, JD-JD and CTD-CTD are shown in dashed boxes colored grey,
1348 red and green, respectively. **(D)** DLS time-course of DnaJB8 under elevated ionic strength
1349 conditions (285mM NaCl). Average R_h of triplicate samples is ~13.7±1.2 nm. **(E)** TEM image of
1350 DnaJB8 oligomers. 50nm scale bar is shown in black. The oligomers appear as spherical masses
1351 with an average diameter of ~15nm. **(F)** Contact map of DnaJB8 crosslinks identified using
1352 ADH/DMTMM in the presence of high ionic strength. The axes are colored in red and green for
1353 JD and CTD, respectively. JD-JD and CTD-CTD crosslinks are shown in dashed boxes colored
1354 in red and green, respectively.

1355

1356 **Figure 4. Solid-state NMR of DnaJB8 oligomers at physiological and high ionic strength.**

(A) 2D ^{13}C-^{13}C ssNMR spectrum of U-^{13}C,^{15}N-labeled DnaJB8 oligomers in PBS, using 25 ms DARR mixing. **(B)** Corresponding 2D ssNMR spectrum at elevated ionic strength (285mM NaCl). **(C-D)** Boxed Ala and Ser regions from panel "A". The experimental peak pattern (black) is well resolved and is similar to the expected pattern of the folded JD in solution (red; middle). Green spectra (right) represent simulated signals predicted for Ala and Ser in our models of the non-JD domains, shown with enhanced broadening reflecting the heterogeneity seen in the experiments. 1D spectra on far left show slices through the experimental 2D data, along with selected peak widths (in kHz). **(E)** ^{13}C 1D spectra at physiological (top) and elevated ionic strength (bottom) that show rigid residues (black, CP), rigid and mobile residues (green, SPE) and only mobile residues (red, INEPT). See also text. **(F)** Electrostatic surface potential of the DnaJB8 JD. Strongly positive area surrounding helix 2 is highlighted by the grey ellipse. Highly positive and negative potentials are colored blue and red, respectively. White color represents neutral charge. **(G)** The same view showing the location of Ala with narrow peaks at physiological salt levels (panel "A") which disappear at high ionic strength (panel "B"). **(H,I)** Same model after 90° y-rotation showing two additional smaller positively charged regions and the nearby location of Alanines that disappear at high ionic strength.

Figure 5. Isolated JD and CTD proteins are monomeric. (A) Cartoon schematic for the full length DnaJB8 and the two domain fragments: JD_{1-77} and $CTD_{170-232}$. Domains are colored as in Figure 1. **(B)** SEC chromatograms of JD_{1-77}(red), $CTD_{170-232}$(green) and LMW standards (blue). JD_{1-77} and $CTD_{170-232}$ elute at apparent molecular weights of 14kDa and 6.5kDa, respectively. **(C)** SDS-PAGE coomassie gel of crosslinked JD_{1-77} and $CTD_{170-232}$ crosslinked with either DMTMM only or additionally with ADH. **(D)** Contact map of ADH/DMTMM crosslinks identified for JD_{1-77}(red), $CTD_{170-232}$(green) and full length DnaJB8 (black). The axes are colored in red and green for JD and CTD, respectively. Crosslink pairs between JD-JD and CTD-CTD are shown in dashed boxes colored in red and green, respectively. **(E)** Rosetta *ab initio* models of CTD. The structural models are consistent with R_h values derived from DLS (dashed line). Structural overlay of low energy scoring models reveals consistent pleated β-sheet fold. Models are shown in cartoon representation and are colored in green. **(F)** Histogram of the number of intra-domain crosslinks that are consistent with crosslink chemistry geometry ("satisfied") in the ensemble of 5000 models. One model satisfies 13 out of 14 possible crosslinks identified in our experiments. Crosslinks are mapped onto best matching CTD structural model. CTD is shown in cartoon representation and is colored in white. Sites of crosslink are shown as spheres and are colored red or blue for D/E and K, respectively. Dashed yellow lines connect linked amino acid pairs.

Figure 6. JD and CTD interact through charge complementary surfaces.
(A) Schematic of the JD_{1-77} and $CTD_{170-232}$ constructs used in fluorescence polarization and XL-MS binding experiments. **(B)** Fluorescence polarization (FP) titration measuring interaction between JD_{1-77}-FITC and a concentration range of unlabeled $CTD_{170-232}$. FP experiments were performed in triplicate and shown as averages with standard deviation. Non-linear regression fit of the binding curve reveals a $K_{d,app}$ of 0.575μM for this interaction. **(C)** Contact map of ADH/DMTMM crosslinks identified from an incubated JD_{1-77} and $CTD_{170-232}$ sample (grey) and full length DnaJB8 (black). The axes are colored in red and green for JD and CTD, respectively. Helix 2 and 3 are shown in grey on the x-axis. Crosslink pairs between JD-CTD are shown in a dashed box colored in grey. **(D)** Schematic for the chemical shift experiment with U-^{15}N JD and titrated with unlabeled CTD. Domains are colored as in Figure 1. HSQC solution NMR spectrum of ^{15}N-labelled JD_{1-77} against a titration of $CTD_{170-232}$: 0x (yellow), 1x (red), 3x (purple), 6x (blue). DnaJB8 JD peak assignments were transferred from deposited data (BMRB:11417). **(E)** Insets of peaks with highest observed chemical shifts: H31, L28, L26, R29. Peaks were colored as in **D**. **(F)** Histogram of chemical shifts by residue from 1-77. Average chemical shift value of ~0.019ppm is

denoted by the red line (excludes prolines). **(G)** DnaJB8 JD structure illustrating the location of helix 2 (pdbid:2DMX). Structure is shown in cartoon representation and colored in white. **(H)** Mapping chemical shifts onto the DnaJB8 JD structure. JD is shown in surface representation and is colored according to chemical shifts from low (0.0 ppm) colored in yellow to high colored in red (0.04 ppm). **(I)** Electrostatic potential mapping onto DnaJB8 JD structure. JD is shown in surface representation and colored according to electrostatic. Highly acidic potential is shown in red and highly basic is shown in blue.

Figure 7. Sequence and structural properties of the JD-CTD interaction. (**A**) XL-MS-based refinement of full length expanded DnaJB8 monomer. Cartoon representation of DnaJB is shown in fully expanded conformation and collapsed conformation, colored by domain as in Figure 1. Aromatic amino acids in the F/G and S/T domains are shown as spheres and colored according to the domain. Residues in Helix 5 (H5) are shown as spheres and colored in magenta. (**B**) Charge complementary surfaces on the JD and CTD in the full-length DnaJB8 model mediate the interaction. Highly acidic potential is shown in red (- sign) and highly basic is shown in blue (+ sign) and colored by conservation. **(C)** GREMLIN sequence-based covariance analysis identified high confidence covarying amino acids on DnaJB8 that localize within the JD (red sector), within CTD (green sector) and across JD-CTD (grey sector). XL-MS identified for full length DnaJB8 (black) overlap with the covarying regions. Covarying positions localizing to amino acids in F/G domain are shown in brown and co-localize with crosslinks to this surface (black). **(D)** Three amino acids: D37, E43, and S50 are shown to covary with the CTD (red spheres).

Figure 8. CTD and HSPA1A compete for the same basic binding surface on DnaJB8 JD. (A-B) Acidic surfaces on HspA1A and CTD interact with basic surface on DnaJB8 JD. In the fully extended DnaJB8 conformation, the CTD (green) is not engaged with the DnaJB8 JD (red) and is accessible to HspA1A binding. In the collapsed DnaJB8 conformation, the CTD (green) is with the engaged DnaJB8 JD and not accessible to HspA1A binding. DnaJB8 is shown in cartoon and is colored according to domains as in Figure 1. HspA1A is shown in cartoon representation and is colored in blue. **(C)** Experimental workflow of experiments to determine competition between Hsp70 and CTD for JD binding. **(D)** Normalized FP binding curves measuring affinity between JD-CTD (green) and JD-Hsp70 (grey). Preincubation of JD-CTD followed by addition of Hsp70 (purple) shows delay in binding consistent with a competitive binding model. FP experiments were performed in triplicate and shown as averages with standard deviation. Fit was performed using non-linear regression analysis in GraphPad Prism. **(E)** JD-HspA1A crosslinks mapped onto JD-Hsp70 model. JD and HspA1A are shown in cartoon representation and colored white and black respectively. Sites of crosslink are shown as spheres and are colored red or blue for aspartic/glutamic and lysines, respectively. Dashed yellow lines connect linked amino acid pairs. **(F)** Schematic of proposed DnaJB8 model. Individual domains are shown as JD (red spheres), CTD (green spheres), F/G+S/T (light blue spheres), and both Hsp70 (dark blue spheres) and substrate (purple line) are shown. DnaJB8 domains are displayed relative to the R_h values derived from DLS experiments (Hsp70 not drawn to scale). DnaJB8 forms a fundamental oligomeric species through aromatic contacts in the F/G and S/T domains ranging from monomer to octamer. In the JD:CTD engaged state, these structures grow over time to form larger polydisperse oligomers(>100nm). The JD:CTD disengaged state (bottom) demonstrates our hypothesis where substrate bound to a uniform minimal unit of DnaJB8 disrupts the JD:CTD interaction. This leads to the recruitment of Hsp70 along the JD-CTD binding face, and the handoff of substrate to Hsp70.

Figure 1

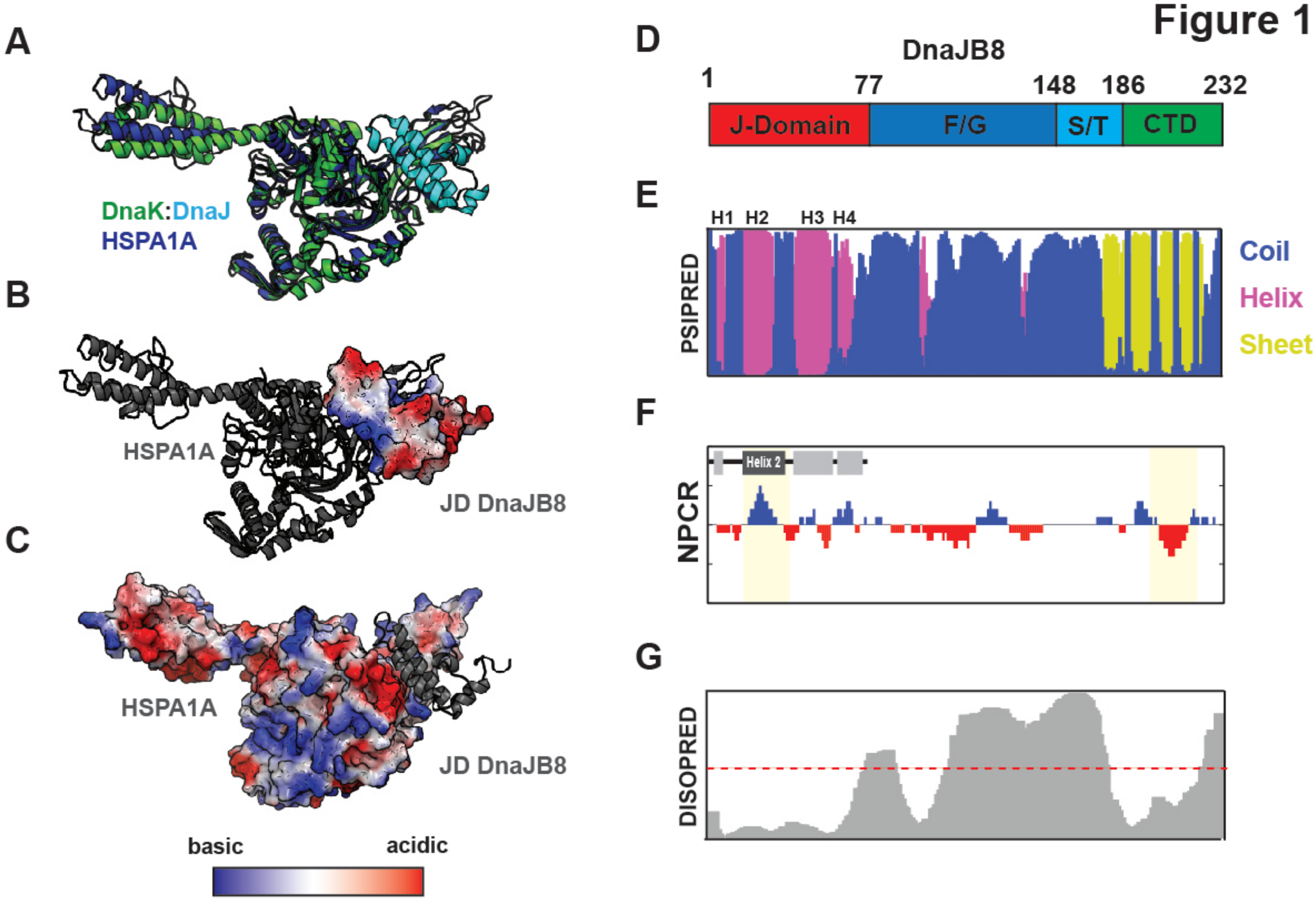
A
DnaK:DnaJ
HSPA1A
B
HSPA1A
JD DnaJB8
C
HSPA1A
JD DnaJB8
basic
acidic
D
DnaJB8
1
77
148
186
232
J-Domain
F/G
S/T
CTD
E
H1 H2 H3 H4
PSIPRED
Coil
Helix
Sheet
F
Helix 2
NPCR
G
DISOPRED

Figure 2

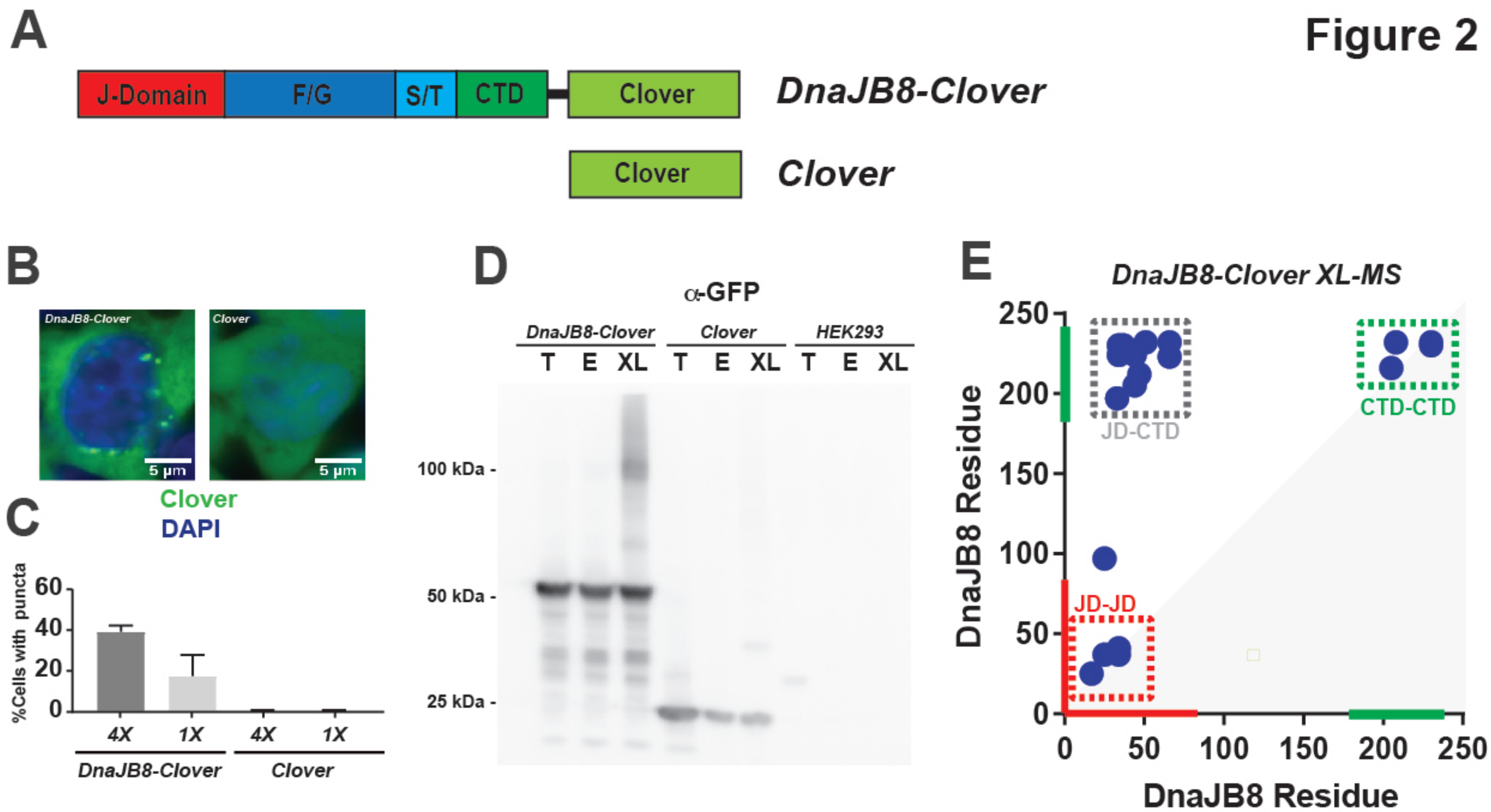
A
J-Domain
F/G
S/T
CTD
Clover
DnaJB8-Clover
Clover
Clover
B
DnaJB8-Clover
Clover
5 µm
5 µm
Clover
DAPI
C
%Cells with puncta
60
40
20
0
4X
1X
4X
1X
DnaJB8-Clover
Clover
D
α-GFP
DnaJB8-Clover
Clover
HEK293
T E XL T E XL T E XL
100 kDa -
50 kDa -
25 kDa -
E
DnaJB8-Clover XL-MS
DnaJB8 Residue
250
200
150
100
50
0
JD-CTD
CTD-CTD
JD-JD
0 50 100 150 200 250
DnaJB8 Residue

Figure 3

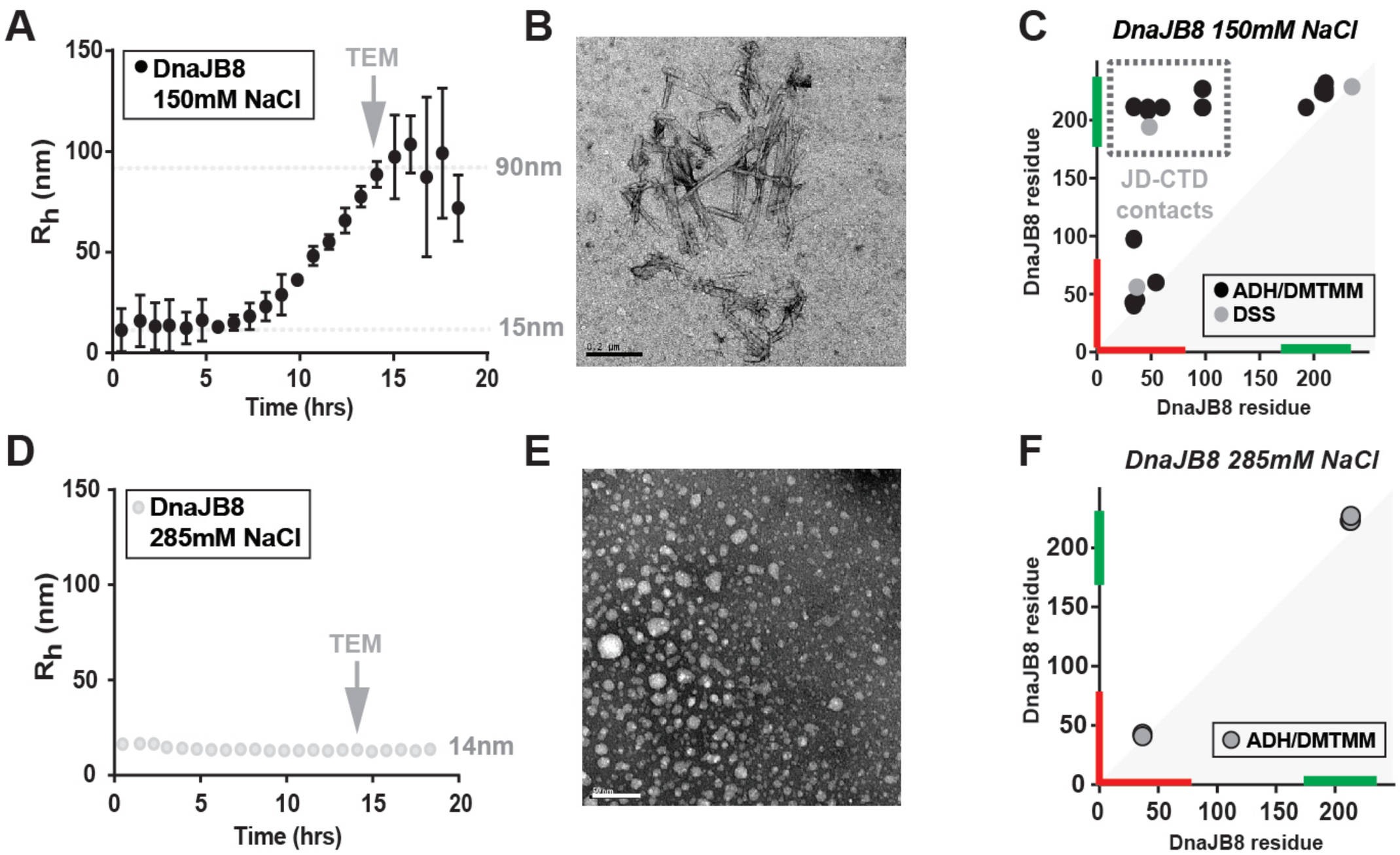
A
DnaJB8
150mM NaCl
TEM
90nm
15nm
R_h (nm)
Time (hrs)
B
C
DnaJB8 150mM NaCl
JD-CTD
contacts
ADH/DMTMM
DSS
DnaJB8 residue
DnaJB8 residue
D
DnaJB8
285mM NaCl
TEM
14nm
R_h (nm)
Time (hrs)
E
F
DnaJB8 285mM NaCl
ADH/DMTMM
DnaJB8 residue
DnaJB8 residue

Figure 4

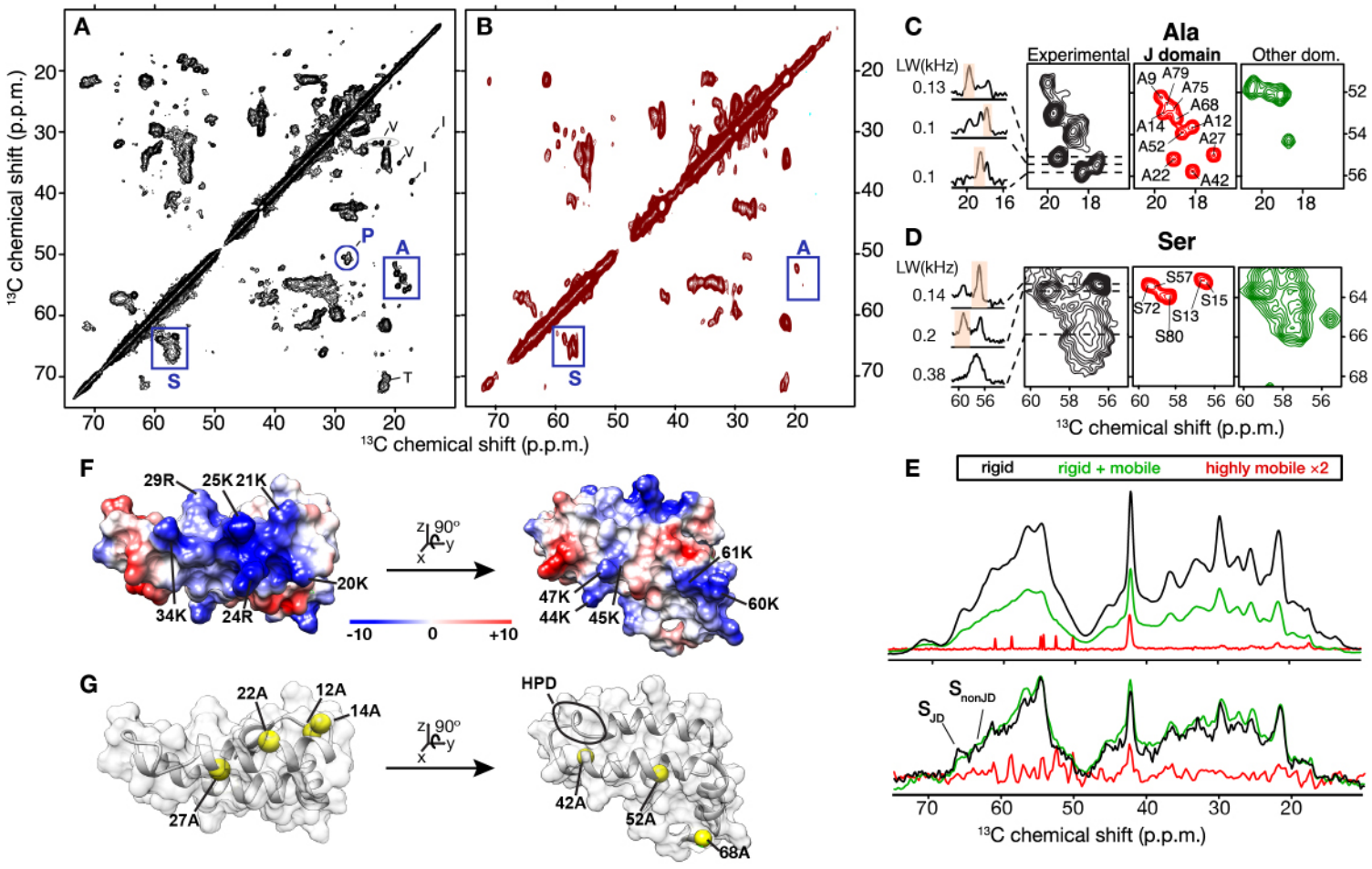
A
B
C
D
E
F
G
^{13}C chemical shift (p.p.m.)
P
A
S
V
I
T
Ala
Experimental
J domain
Other dom.
LW(kHz)
A9
A79
A75
A68
A14
A12
A52
A27
A22
A42
Ser
S57
S72
S15
S13
S80
rigid
rigid + mobile
highly mobile ×2
S_{JD}
S_{nonJD}
29R
25K
21K
20K
34K
24R
61K
47K
44K
45K
60K
-10
0
+10
22A
12A
14A
27A
HPD
42A
52A
68A
90°

Figure 5

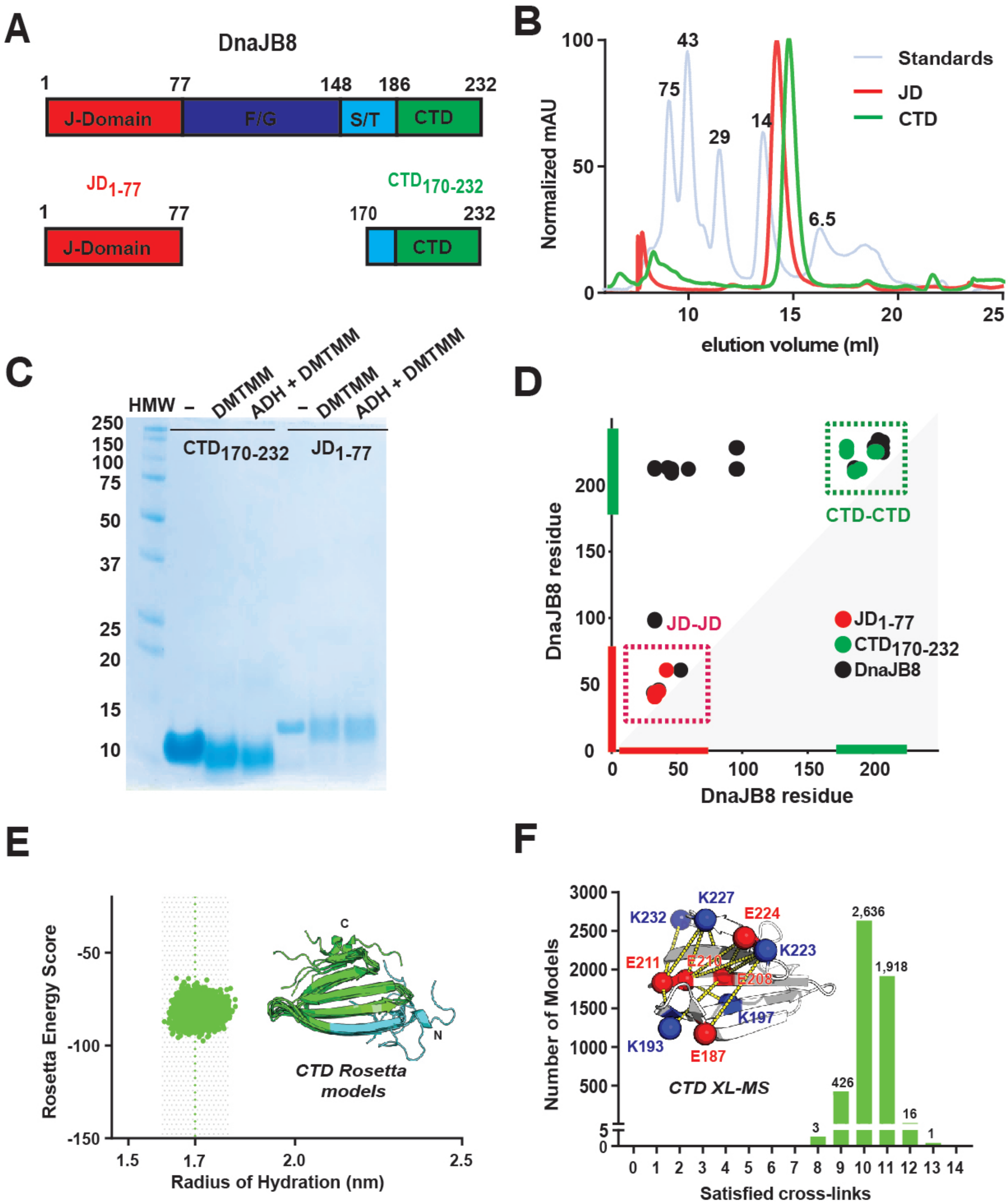
A
DnaJB8
1
77
148
186
232
J-Domain
F/G
S/T
CTD
JD1-77
CTD170-232
J-Domain
CTD
B
Standards
JD
CTD
Normalized mAU
elution volume (ml)
43
75
29
14
6.5
C
HMW
–
DMTMM
ADH + DMTMM
CTD170-232
JD1-77
250
150
100
75
50
37
25
20
15
10
D
DnaJB8 residue
CTD-CTD
JD-JD
JD1-77
CTD170-232
DnaJB8
E
Rosetta Energy Score
Radius of Hydration (nm)
CTD Rosetta models
C
N
F
Number of Models
Satisfied cross-links
K227
K232
E224
K223
E211
E210
E208
K197
K193
E187
CTD XL-MS
2,636
1,918
426
3
16
1

Figure 6

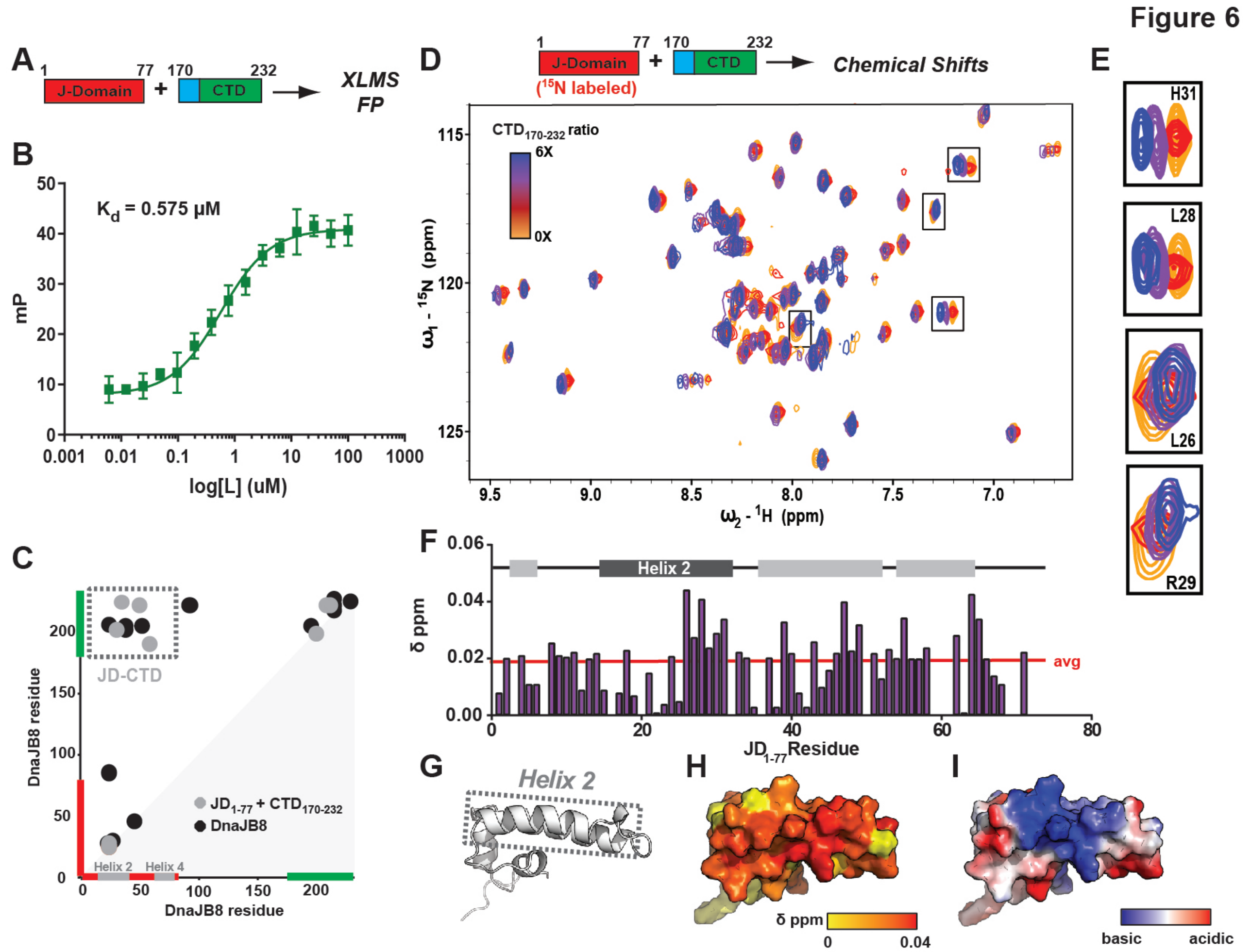
A
1
77
170
232
J-Domain
CTD
XLMS
FP
B
K_d = 0.575 μM
mP
log[L] (uM)
C
JD-CTD
DnaJB8 residue
JD_{1-77} + $CTD_{170-232}$
DnaJB8
Helix 2
Helix 4
D
(^{15}N labeled)
Chemical Shifts
$CTD_{170-232}$ ratio
6X
0X
ω_1 - ^{15}N (ppm)
ω_2 - ^{1}H (ppm)
E
H31
L28
L26
R29
F
Helix 2
δ ppm
avg
JD_{1-77} Residue
G
Helix 2
H
δ ppm
I
basic
acidic

Figure 7

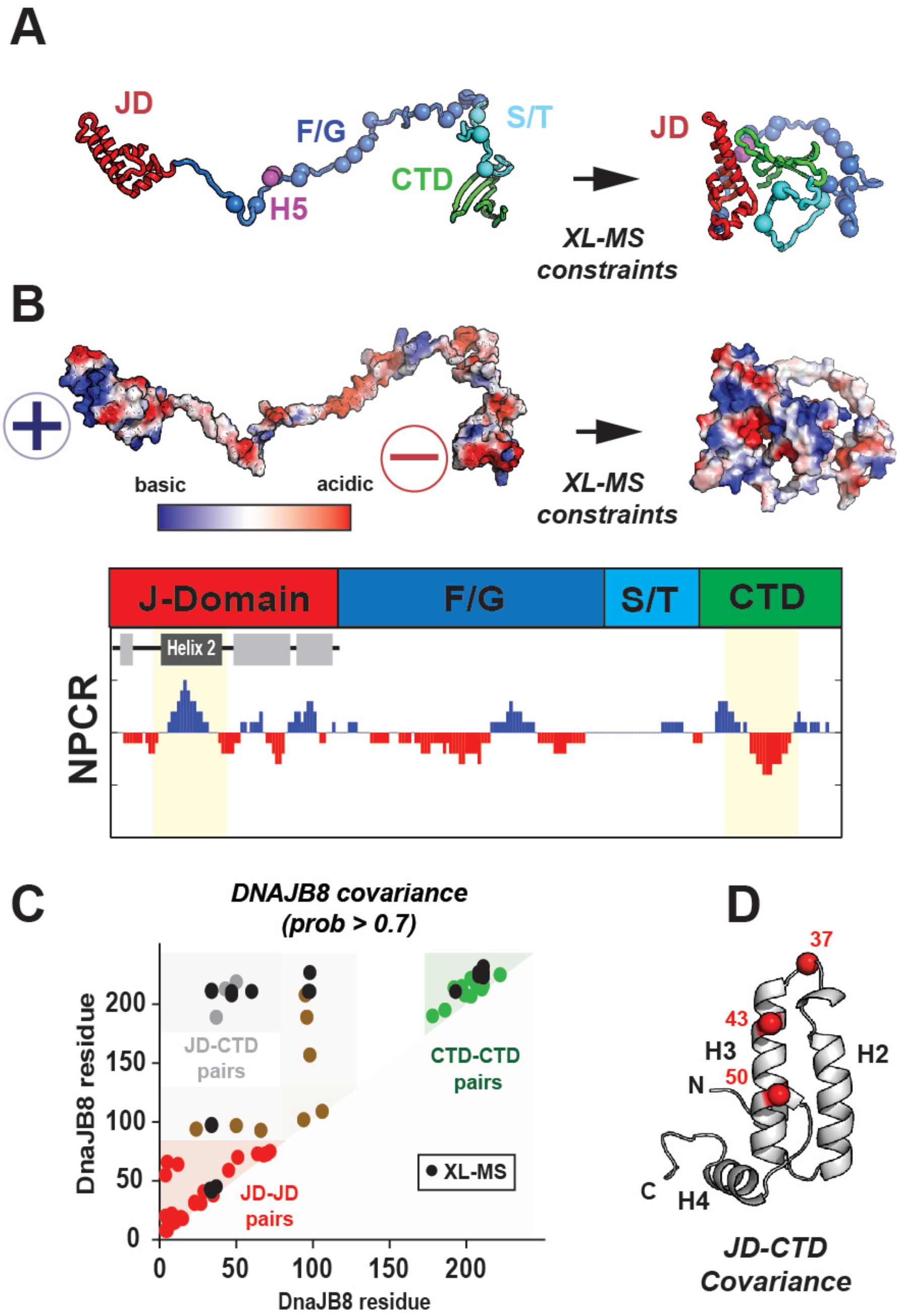
A
JD
F/G
S/T
CTD
H5
JD
XL-MS
constraints
B
basic
acidic
XL-MS
constraints
J-Domain
F/G
S/T
CTD
Helix 2
NPCR
C
DNAJB8 covariance
(prob > 0.7)
DnaJB8 residue
JD-CTD
pairs
CTD-CTD
pairs
XL-MS
JD-JD
pairs
0
50
100
150
200
DnaJB8 residue
D
37
43
H3
H2
N
50
C
H4
JD-CTD
Covariance

Figure 8

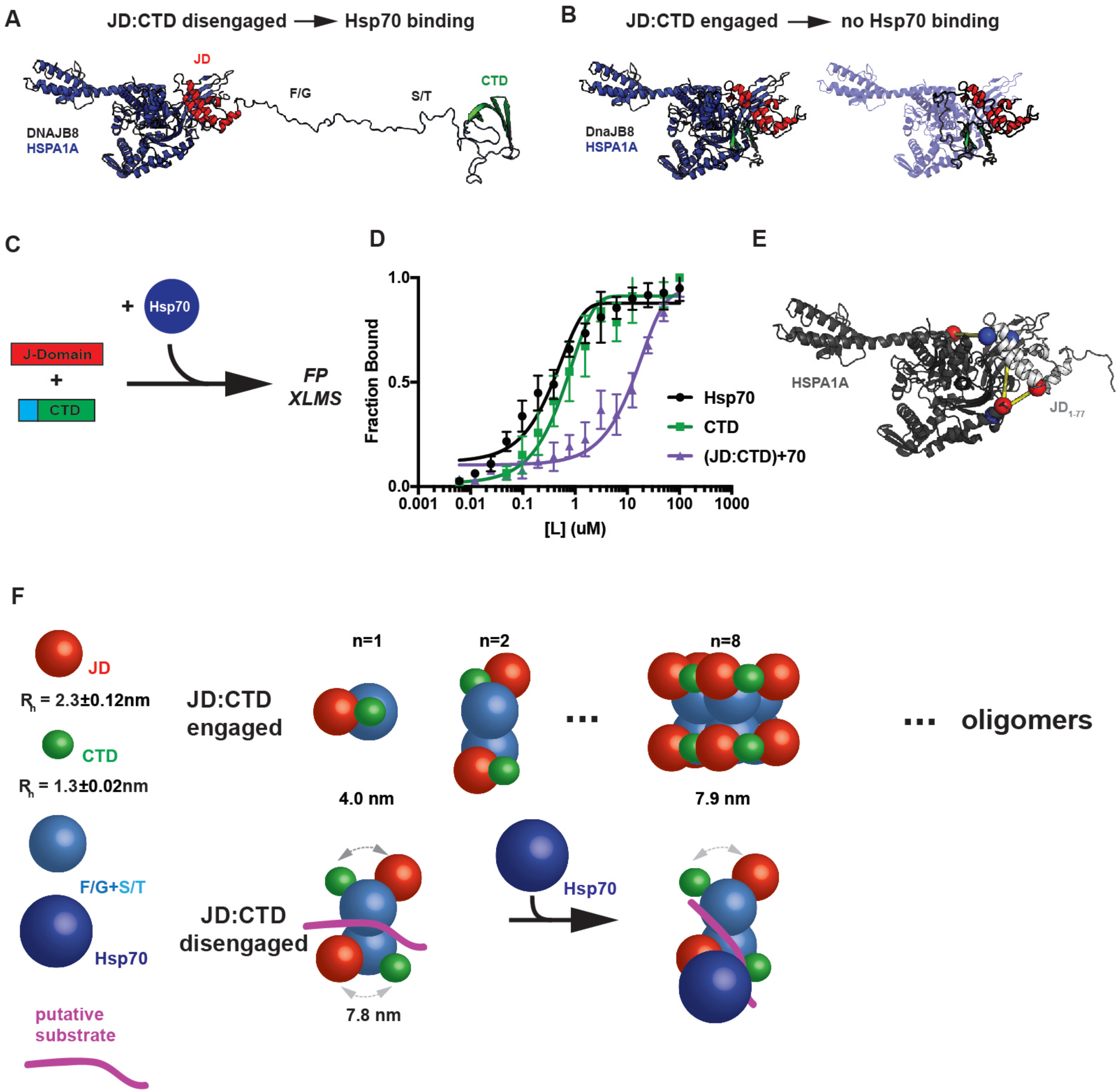
A
JD:CTD disengaged → Hsp70 binding
JD
F/G
S/T
CTD
DNAJB8
HSPA1A
B
JD:CTD engaged → no Hsp70 binding
DnaJB8
HSPA1A
C
Hsp70
J-Domain
CTD
FP
XLMS
D
Fraction Bound
1.0
0.5
0.0
0.001
0.01
0.1
1
10
100
1000
[L] (uM)
Hsp70
CTD
(JD:CTD)+70
E
HSPA1A
JD1-77
F
JD
Rh = 2.3±0.12nm
CTD
Rh = 1.3±0.02nm
F/G+S/T
Hsp70
putative
substrate
JD:CTD
engaged
n=1
n=2
n=8
4.0 nm
7.9 nm
... oligomers
JD:CTD
disengaged
7.8 nm
Hsp70

1457 **SUPPLEMENTAL INFORMATION**

1458

1459 **Auto-regulatory J-domain interactions control Hsp70 recruitment in the**

1460 **oligomeric DNAJB8 co-chaperone**

1461

1462 Bryan Ryder, Irina Matlahov, Sofia Bali, Jaime Vaquer-Alicea, Patrick C.A. van der Wel, Lukasz

1463 A. Joachimiak

1464
1465
1466
1467
1468
1469
1470
1471
1472
1473
1474
1475
1476
1477

1478 **Supplementary Data**

1479

1480 **Supplementary Data 1. Primary mass spectrometry data acquired for proteomic analysis**

1481 **of DnaJB8-Clover and Clover samples.**

1482 **Supplementary Data 2. Primary XL-MS data for DnaJB8 and its domains.**

1483 **Supplementary Data 3. Primary DLS measurements for DnaJB8 oligomers.**

1484

1485

1486

1487

1488

1489

1490

1491

1492

1493 **Supplementary Figure Legends**

1494

1495 **Figure S1. Structural analysis of HspA1A and DnaJB6b. (A)** HspA1A contains two domains,
1496 a nucleotide binding domain (NBD; turquoise) and a substrate binding domain (SBD; grey). (**B)**
1497 NPCR map of the HspA1A sequence. The surfaces in the NBD and SBD implicated in Hsp40 JD
1498 binding are highlighted. (**C)** HspA1A is a highly conserved Hsp70 chaperone throughout the
1499 sequence. (**D)** Structure of HspA1A colored by domain with the NBD in turquoise and SBD in
1500 grey. (**E)** Electrostatic surface mapped onto the HspA1A structure with the negatively charged
1501 Hsp40 JD binding site circled in yellow. (**F**) DnaJB6b is comprised of a JD (red), F/G rich domain
1502 (blue), S/T rich domain (cyan), and CTD (green). PSIPRED secondary structure prediction
1503 correctly identifies the 4 α-helices in the JD (purple), and predicts a five strand β-sheet within the
1504 CTD (yellow). DISOPRED results predict two highly disordered regions within the F/G and S/T
1505 domains.
1506
1507 **Figure S2. Biochemical and mass spectrometry analysis of DnaJB8-Clover proteins**
1508 **isolated from HEK293 cells.** (**A**) Western blot analysis of input and anti-GFP nanobody elutions
1509 DnaJB8-Clover, Clover and HEK293 cell lines as detected with anti-DnaJB8 and anti-GFP
1510 antibodies. Total (T) and elutions (E) for each condition are shown. (**B**) Analysis of proteins
1511 identified in the DnaJB8-Clover purification compared to the Clover cell lines. The data are shown
1512 as fold enrichment and are colored according to cellular activity. (**C**) String database network
1513 map of hits identified in the DnaJB8-Clover cell lines. Chaperones are shown in red and other
1514 proteins are shown in white. **(D)** JD intra-domain ADH/DMTMM crosslinks mapped onto the JD
1515 structure. JD is shown in cartoon representation and is colored in white. Sites of crosslink are
1516 shown as spheres and are colored red or blue for aspartic/glutamic and lysines, respectively.
1517 Dashed yellow lines connect linked amino acid pairs.
1518
1519 **Figure S3. Dynamics of DnaJB8 oligomer assembly.** (**A)** Histogram of overall R_h of DnaJB8 in
1520 1xPBS 150mM NaCl at times 0h (black), 10h (blue), and 20h (gold). Over time, there was a
1521 depletion in particle sizes <10nm and an increase in particles ~100-1000nm. **(B)** SDS-PAGE
1522 coomassie gel showing DnaJB8 in the absence of crosslinker (left), with DSS (middle), and with
1523 DMTMM and ADH (right). **(C)** JD intra-domain ADH/DMTMM crosslinks mapped onto the JD
1524 structure. JD is shown in cartoon representation and is colored in white. Sites of crosslink are
1525 shown as spheres and are colored red or blue for aspartic/glutamic and lysines, respectively.
1526 Dashed yellow lines connect linked amino acid pairs. **(D)** Three JD-CTD inter-domain
1527 ADH/DMTMM crosslinks mapped onto the JD structure. DnaJB8 JD is shown in cartoon
1528 representation and is colored in white. JD lysine sites that crosslink to CTD are shown as spheres
1529 and are colored blue. (**E**) Histogram of overall R_h of DnaJB8 in 1xPBS 285mM NaCl at times 0h
1530 (blue), 10h (black), and 20h (red). Over time, there is no change in the species of particle sizes
1531 <10nm and no appearance of particles ~100-1000nm. **(F)** Average R_h of DnaJB8 over time limited
1532 to particles <10nm for each experiment. Under 1xPBS 150mM NaCl conditions, the average size
1533 was consistently at 5.8±1.1nm while under 1xPBS 285mM NaCl the average size was
1534 7.75±0.05nm. **(G)** Histogram of frequency of ADH monolinks observed in normal and elevated
1535 ionic strength XLMS experiments.
1536
1537
1538 **Figure S4. DnaJB8 oligomer dynamics are perturbed by changes in ionic strength. (A)**
1539 Experimental 2D ^{13}C-^{13}C CP-DARR of DnaJB8 oligomers uniformly labeled with ^{13}C and ^{15}N**, (B)**
1540 Synthetic ^{13}C-^{13}C 2D spectrum of the DnaJB8 JD in solution generated from BMRB solution NMR
1541 chemical shifts. Amino acid residues are indicated alongside signals present in the experimental

ssNMR spectrum. Dashed lines mark two cross-peaks of proline 32 in the HPD motif present in the experimental data, **(C)** Partial simulated spectrum from three other domains (F/G, S/T and CTD). Green box represents broad signals present in the experimental data in (**A**).

Figure S5. JD and CTD are stable monomers. (A) SEC-MALS of $CTD_{170-232}$ shows a single peak that was calculated to have a molar mass of 8,376 ±14 g/mol. The single peak indicates that the construct elutes as a monomer. (**B)** DLS time course of both JD_{1-77} and $CTD_{170-232}$ constructs. The average R_h of JD_{1-77} and $CTD_{170-232}$ was calculated to be 2.30±0.12 nm and 1.71±0.02 nm, respectively. (**C)** Histogram of JD intra-domain crosslinks across XLMS experiments for DnaJB8(black), JD_{1-77}(red), and JD_{1-77} mixed with $CTD_{170-232}$(grey). All intra-domain crosslinks satisfy the physical constraint of <20nm for the ADH/DMTMM crosslinkers. (**D)** Intra-domain crosslinks from the JD_{1-77} XLMS experiment mapped onto the DnaJB8 JD structure (PDBID:2DMX). Acidic amino acids (red spheres) and K34(blue sphere) are shown. **(E, F)** CD spectra of CTD was analyzed and fit using the Bestsel server. Secondary structure analysis of the data shows high β-sheet character (yellow) with some helix character (purple) and no random coil (blue). The results are compared to the CTD model generated from ab initio.

Figure S6. JD_{1-77} construct spectra consistent with deposited chemical shifts. (A) Overlay of our HSQC spectra for JD_{1-77}(black) onto the submitted spectra for DnaJB8 JD (red) (BMRB:11417). 97% of assigned peaks in the published spectra were matched to our data. (**B)** Amino acid assignments mapped onto the HSQC spectra for JD_{1-77}.

Figure S7. Modeling the full length DnaJB8 monomer using crosslinks. (A) DnaJB8 ADH/DMTMM crosslinks mapped onto an expanded structure featuring the conserved JD and our predicted CTD model. The histogram of C_α-C_α distances shows 11 crosslinks that exceed the physical limitations for ADH/DMTMM. **(B)** Rosetta *ab initio* collapsed structure of DnaJB8 with ADH/DMTMM crosslinks mapped. The histogram of C_α-C_α distances shows that all crosslinks are satisfied when the JD and CTD are docked in this model. **(C)** Conservation-based analysis of the DnaJB8 sequence. DnaJB8 schematic is colored as in Figure 1. Sequence conservation is shown as a histogram mapping frequency of changes at each position, bars are colored in grey. Positions above the threshold shown in the red dotted line are defined as conserved. (**D**) Conserved surfaces on the JD and CTD in the full-length DnaJB8 model mediate the interaction. Highly conserved sites are colored in red (and highlighted by arrows) and variable positions are colored in yellow**.** Sequence-based conservation of DnaJB8 shows highly conserved faces along the JD, and some conserved faces in the CTD that overlap with the XL-MS identified surfaces. **(E)** Conservation map of the JD where amino acids are shown from least conserved(yellow) to most conserved(red). **(F)** Charge-based analysis of the DnaJB6 sequence and colored by domain as for the homologous DnaJB8. Sequence charge distribution of DnaJB6 is shown using NPCR. Basic regions are shown in blue and acidic regions are shown in red. Sequence conservation is shown as a histogram mapping frequency of changes at each position, bars are colored in grey.

Figure S8. Hsp70 proteins present a conserved acidic surface presented from NBS and SBD. (A) Raw FP binding curves of JD-Hsp70 (black), JD-CTD (green) and (JD-CTD)+Hsp70 (purple). FP experiments were performed in triplicate and shown as averages with standard deviation. Fit was performed using non-linear regression analysis in GraphPad Prism.

Figure S1

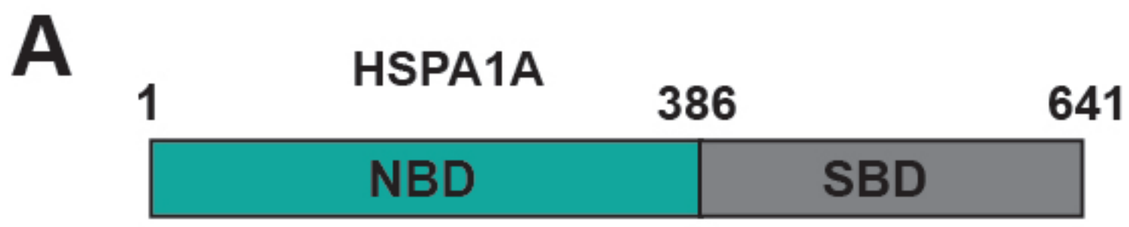
A
HSPA1A
1
386
641
NBD
SBD

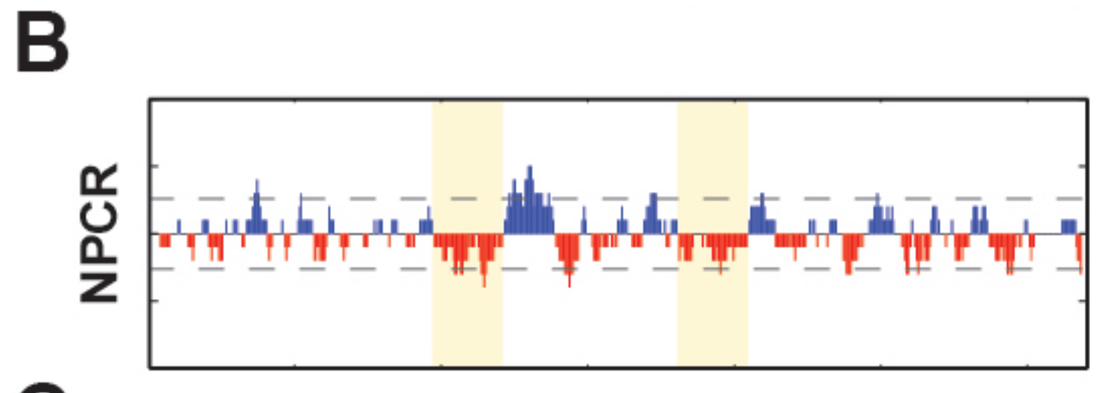
B
NPCR

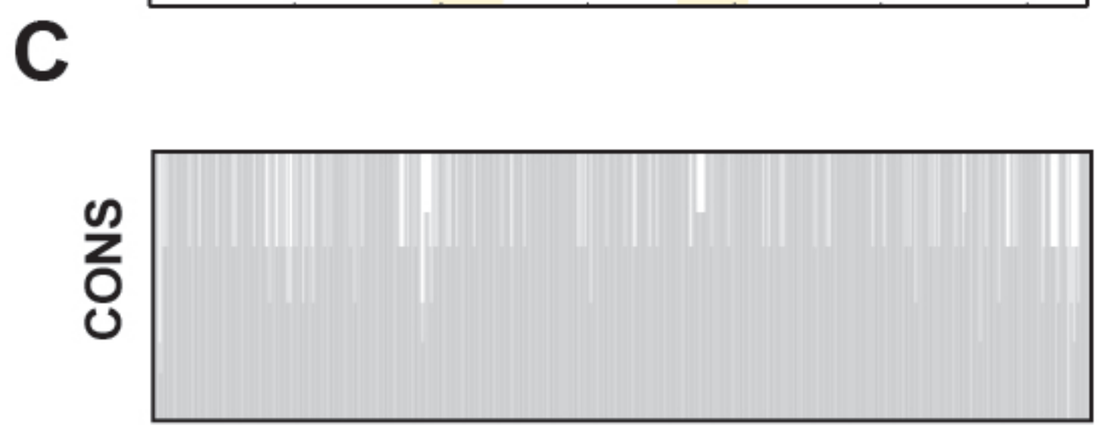
C
CONS

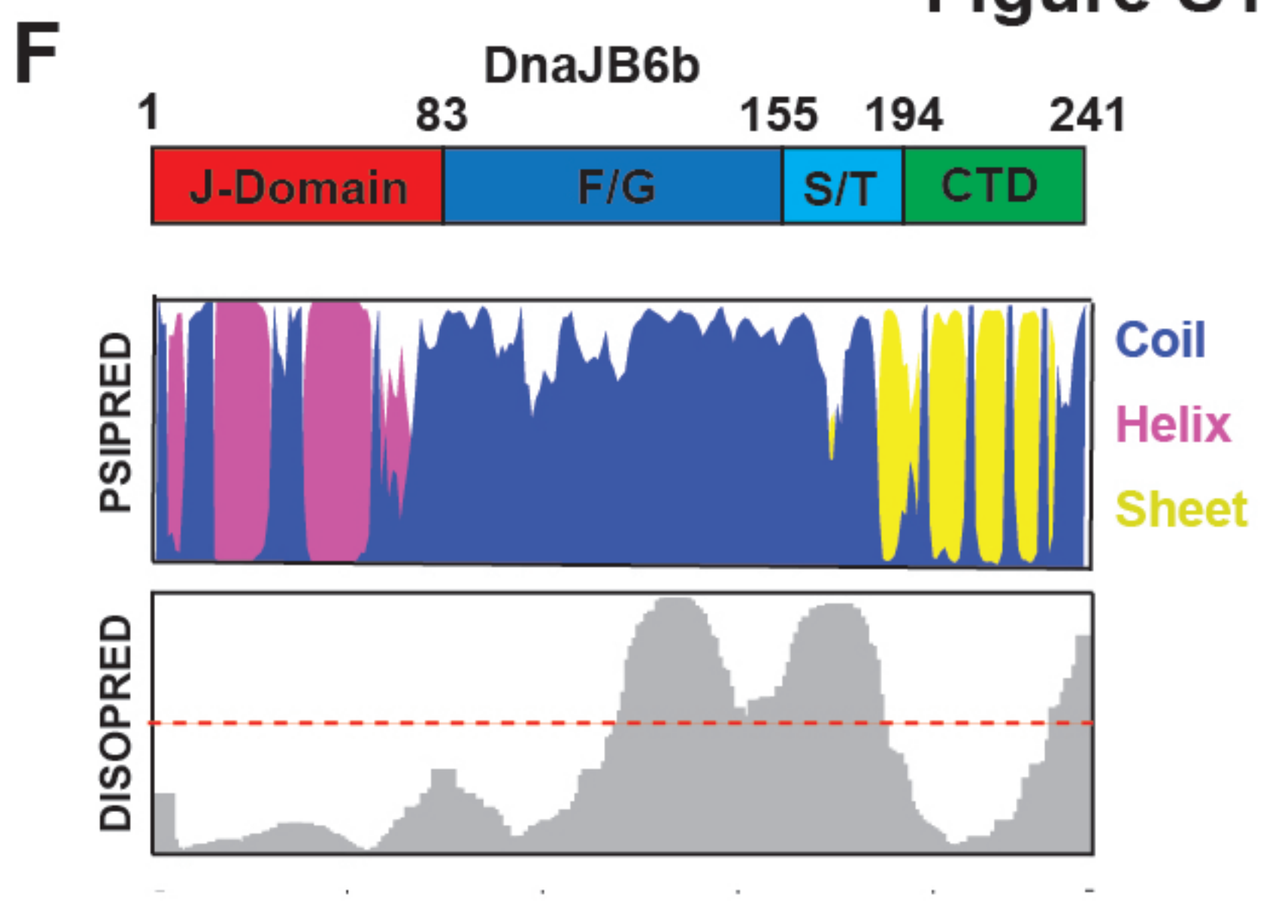
F
DnaJB6b
1
83
155
194
241
J-Domain
F/G
S/T
CTD
PSIPRED
Coil
Helix
Sheet
DISOPRED

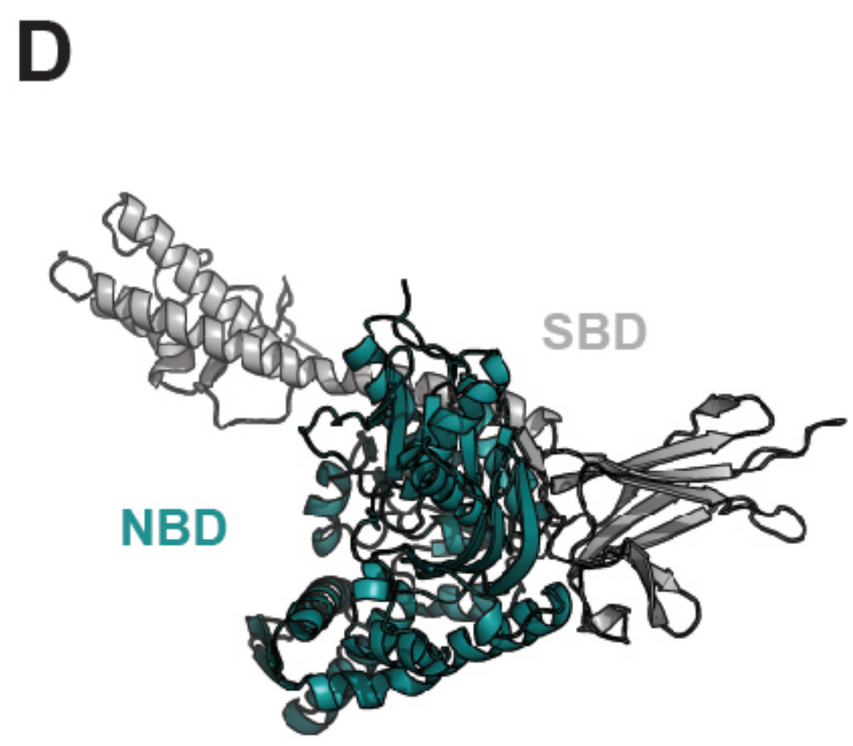
D
SBD
NBD

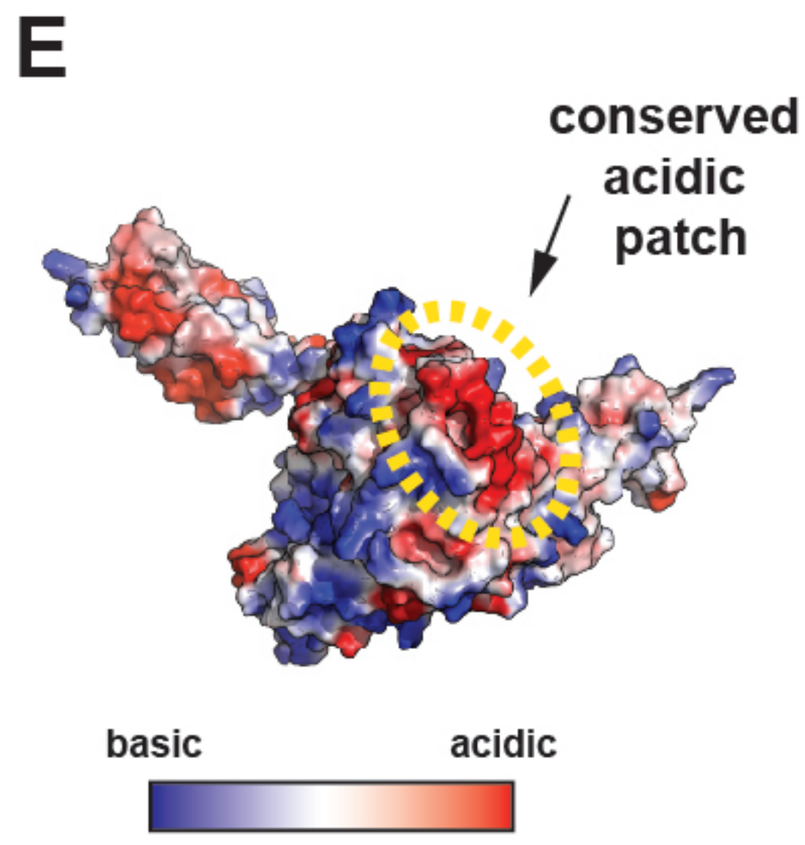
E
conserved
acidic
patch
basic
acidic

Figure S2

A

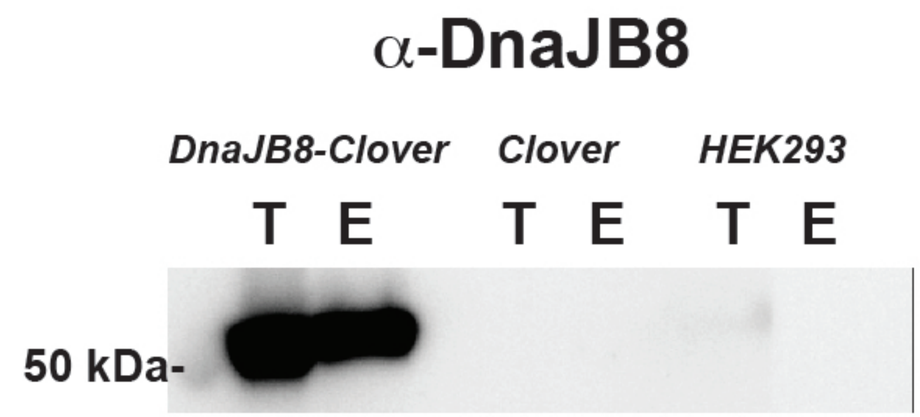

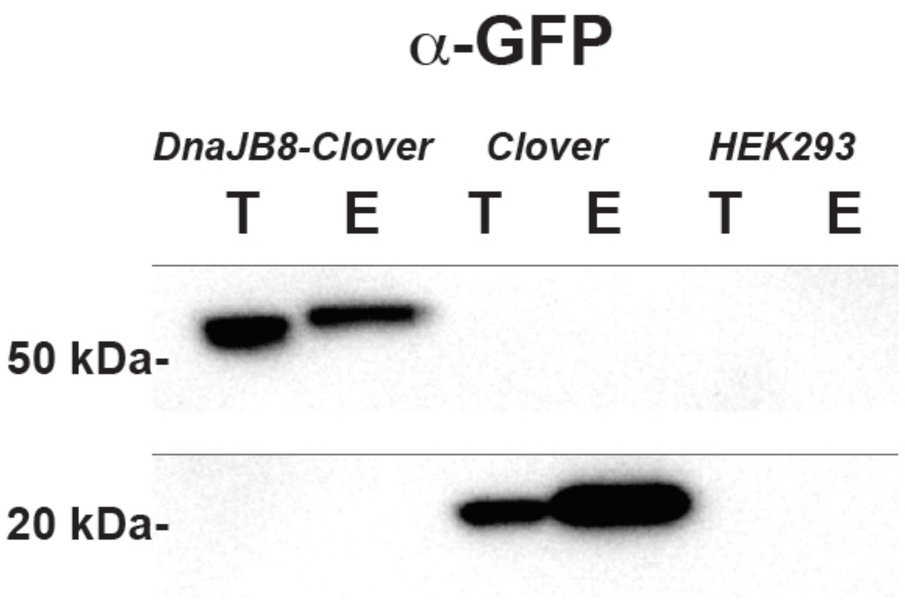

C

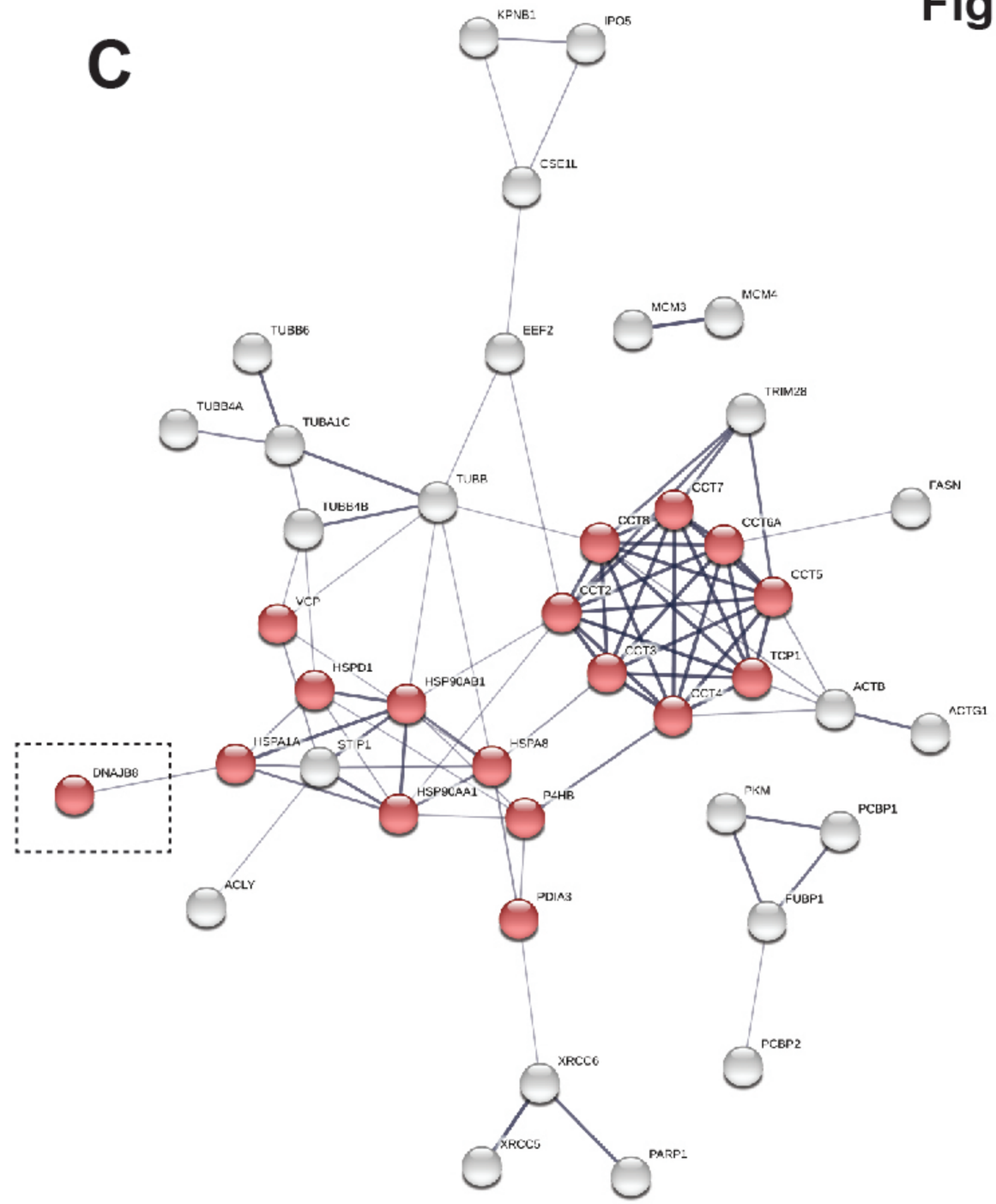

B

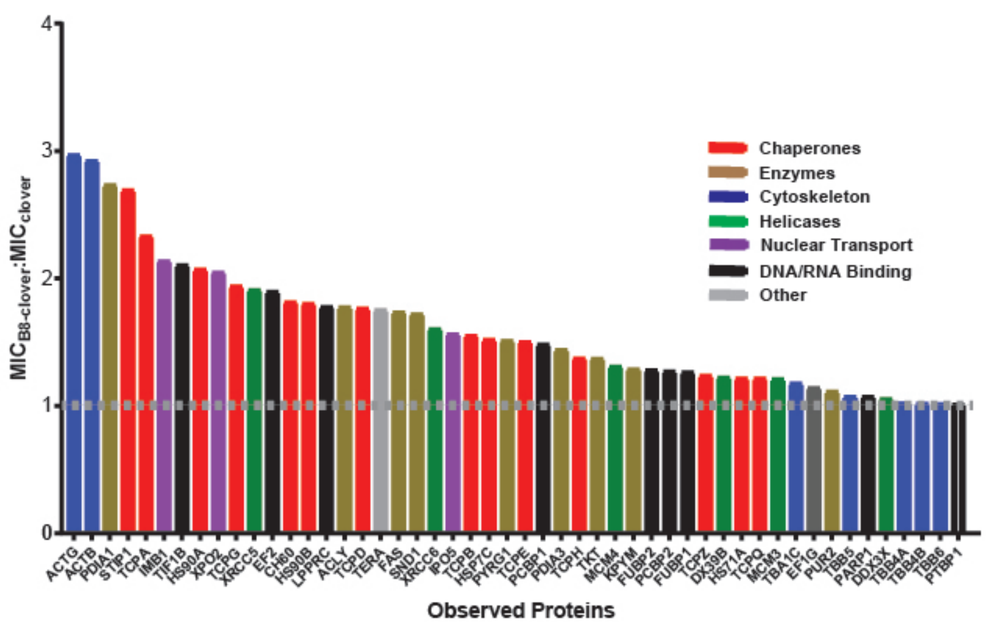

D

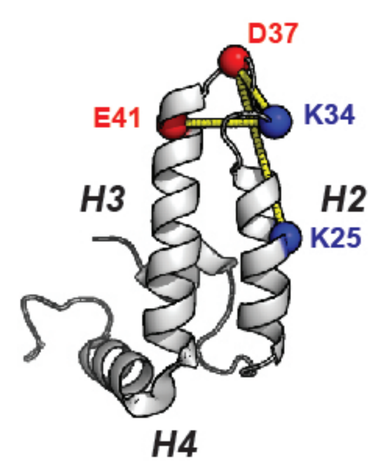

JD-JD
ex vivo Contacts

Figure S3

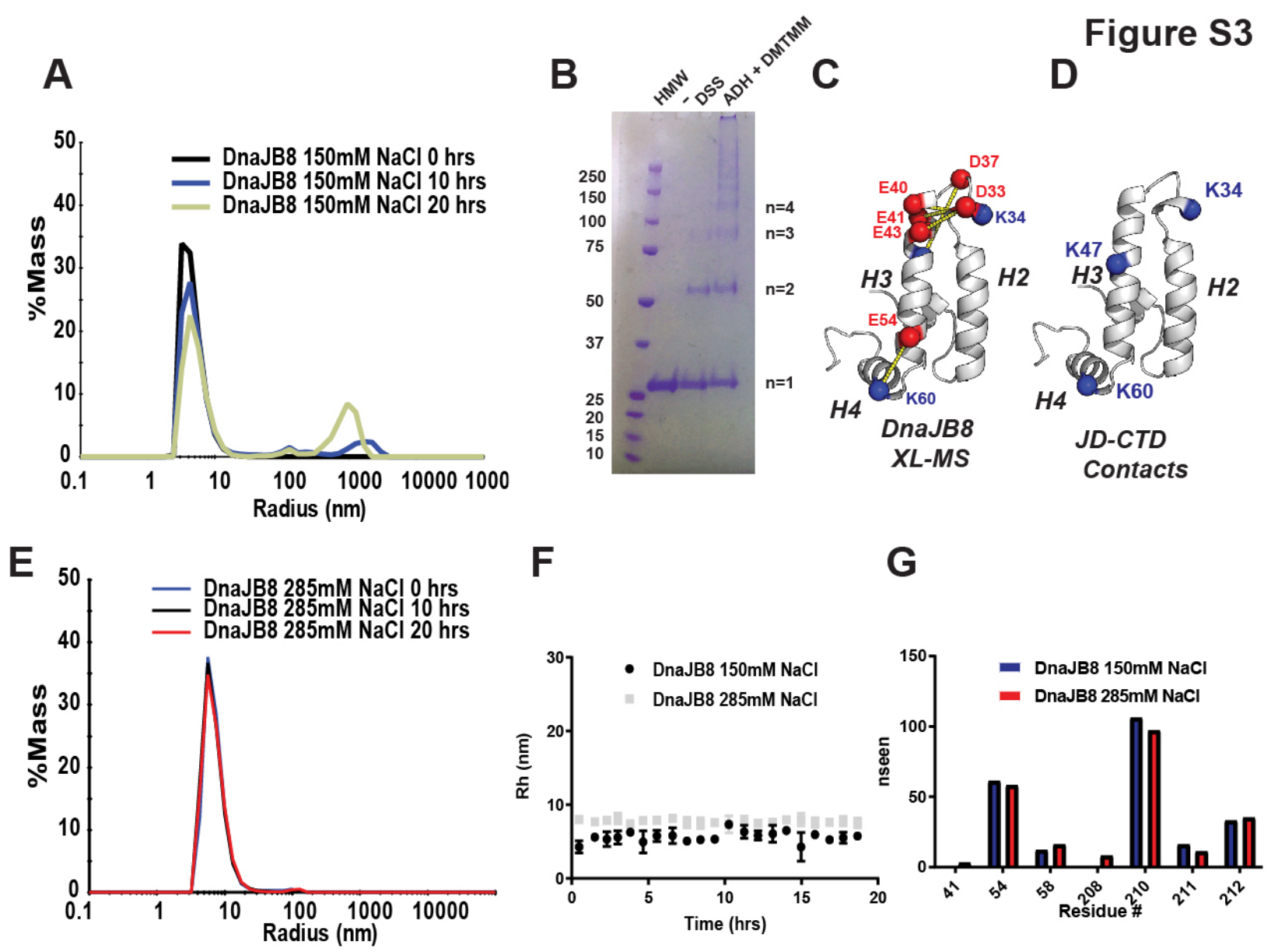
A
DnaJB8 150mM NaCl 0 hrs
DnaJB8 150mM NaCl 10 hrs
DnaJB8 150mM NaCl 20 hrs
%Mass
Radius (nm)
B
HMW
- DSS
ADH + DMTMM
250
150
100
75
50
37
25
20
15
10
n=4
n=3
n=2
n=1
C
D37
E40
D33
E41
E43
K34
H3
H2
E54
H4
K60
DnaJB8
XL-MS
D
K34
K47
H3
H2
H4
K60
JD-CTD
Contacts
E
DnaJB8 285mM NaCl 0 hrs
DnaJB8 285mM NaCl 10 hrs
DnaJB8 285mM NaCl 20 hrs
%Mass
Radius (nm)
F
DnaJB8 150mM NaCl
DnaJB8 285mM NaCl
Rh (nm)
Time (hrs)
G
DnaJB8 150mM NaCl
DnaJB8 285mM NaCl
nseen
Residue #
41
54
58
208
210
211
212

Figure S4

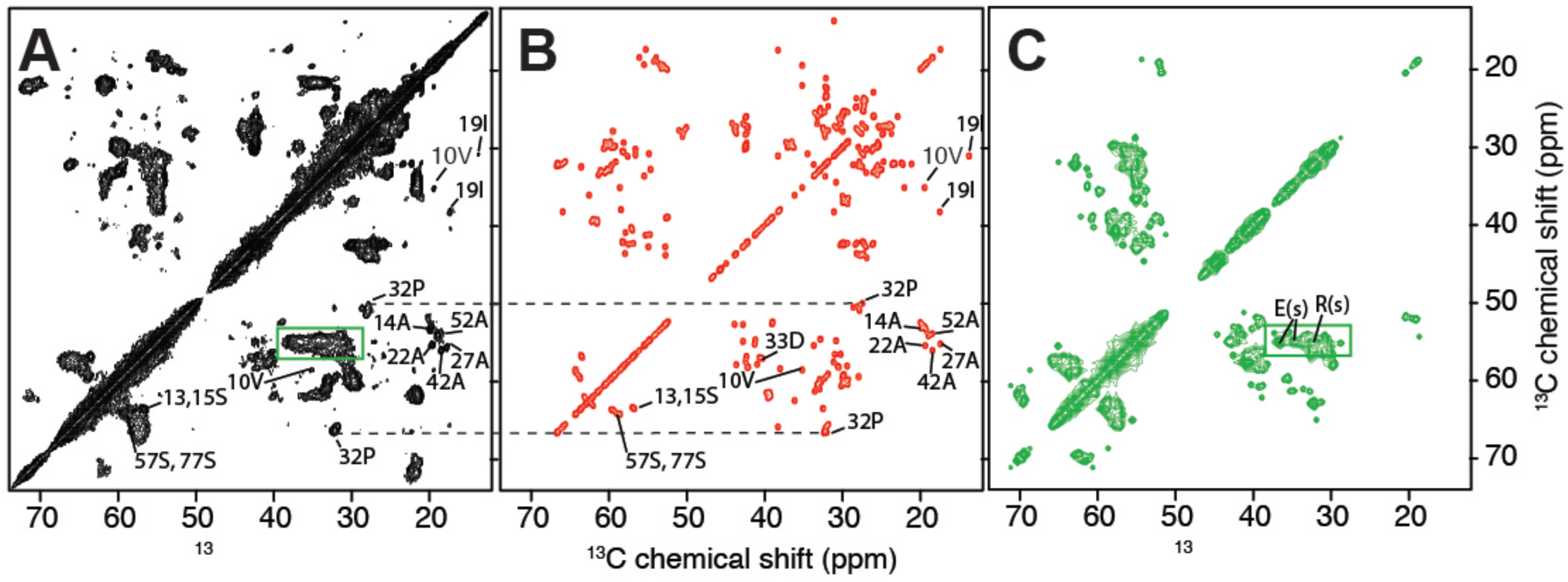
A
B
C
19I
10V
19I
32P
14A
52A
22A
27A
42A
10V
13,15S
57S, 77S
32P
33D
E(s)
R(s)
70
60
50
40
30
20
13
13C chemical shift (ppm)

Figure S5

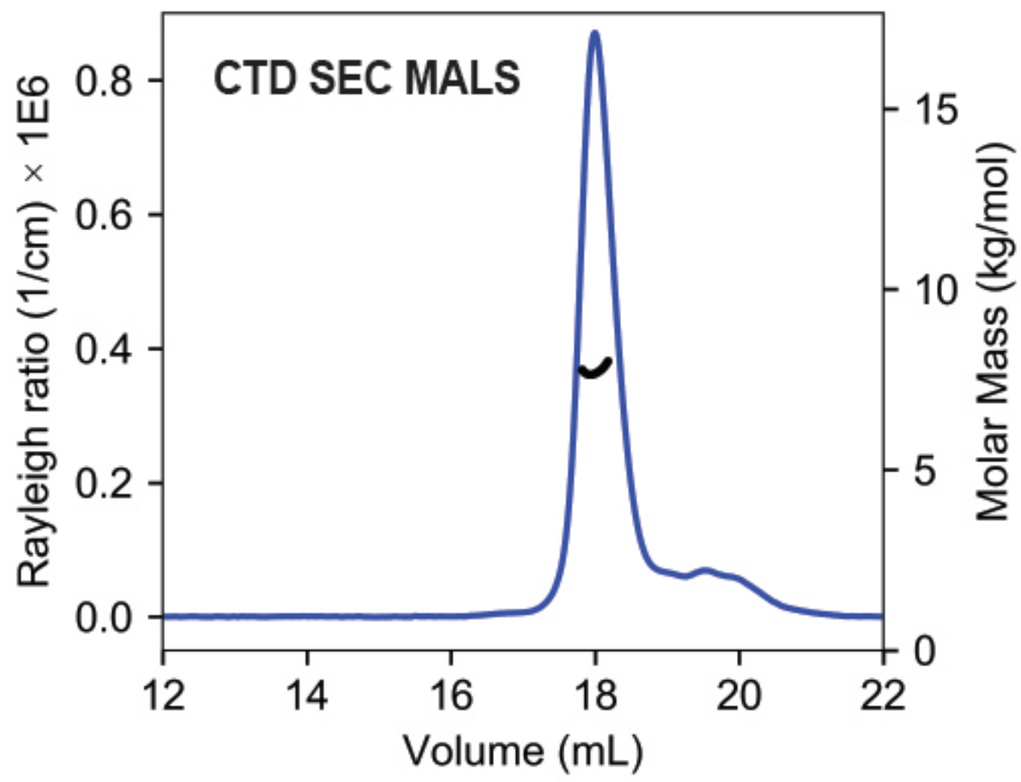
A
CTD SEC MALS
Rayleigh ratio (1/cm) × 1E6
Molar Mass (kg/mol)
Volume (mL)

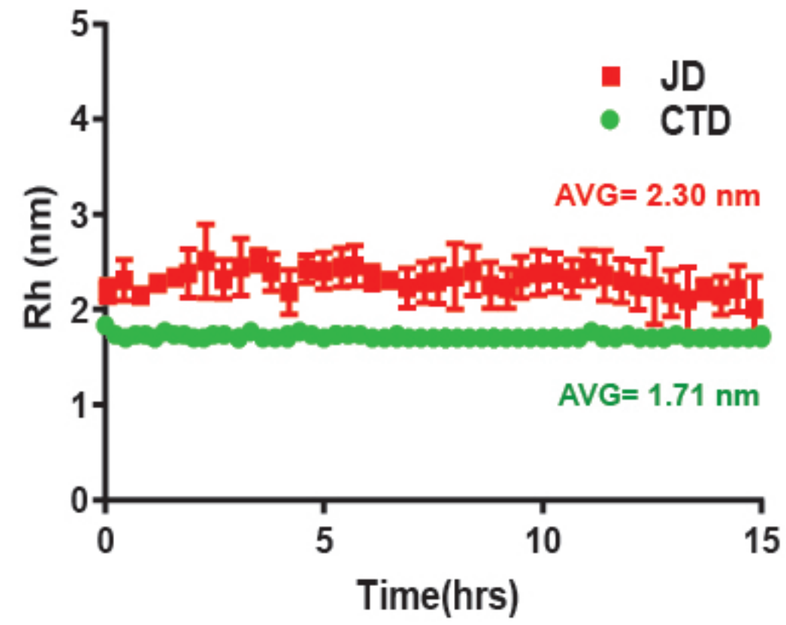
B
JD
CTD
AVG= 2.30 nm
AVG= 1.71 nm
Rh (nm)
Time(hrs)

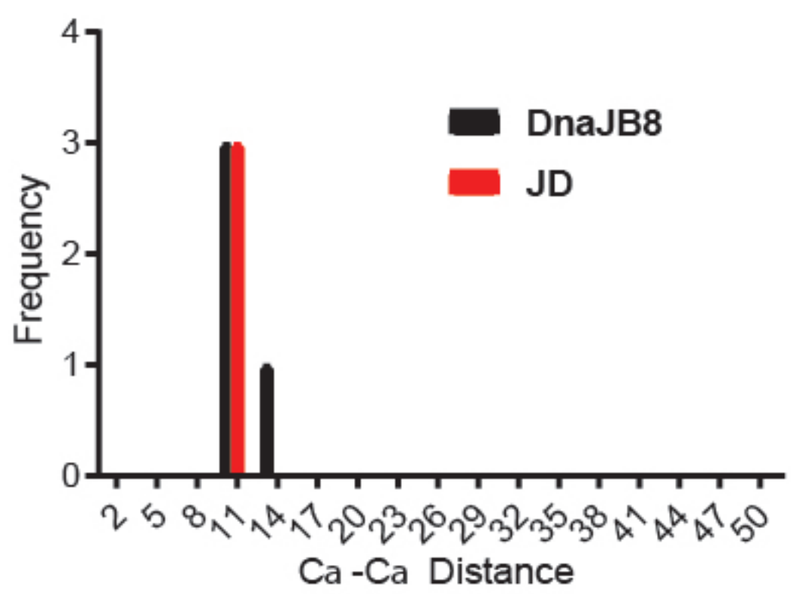
C
JD Intra-links
DnaJB8
JD
Frequency
Ca -Ca Distance

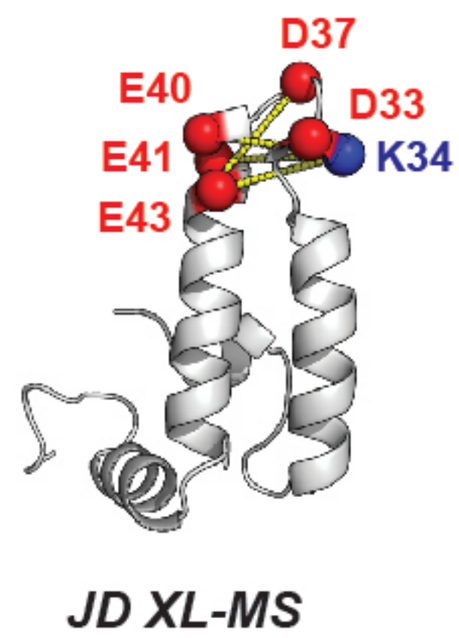
D
D37
E40
D33
E41
K34
E43
JD XL-MS

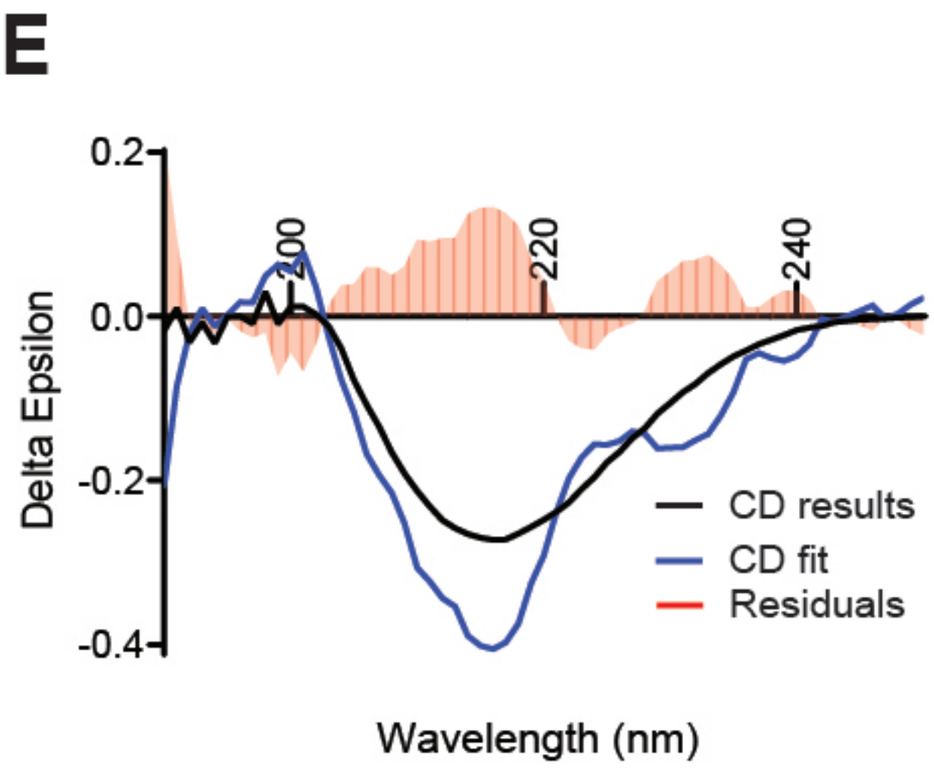
E
Delta Epsilon
CD results
CD fit
Residuals
Wavelength (nm)

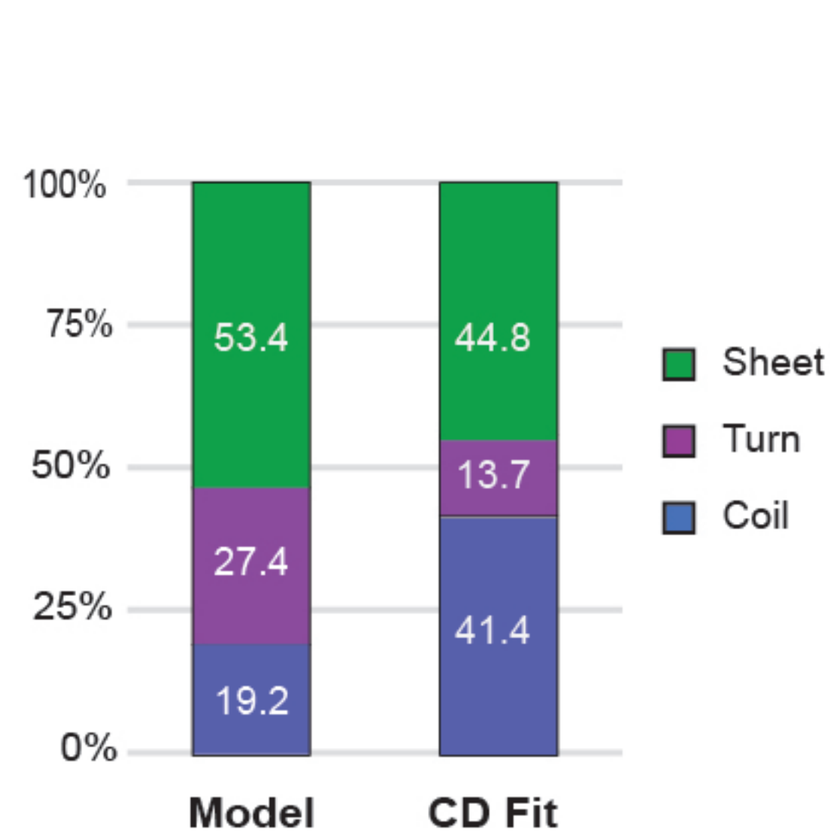
F
53.4
27.4
19.2
44.8
13.7
41.4
Sheet
Turn
Coil
Model
CD Fit

Figure S6

A

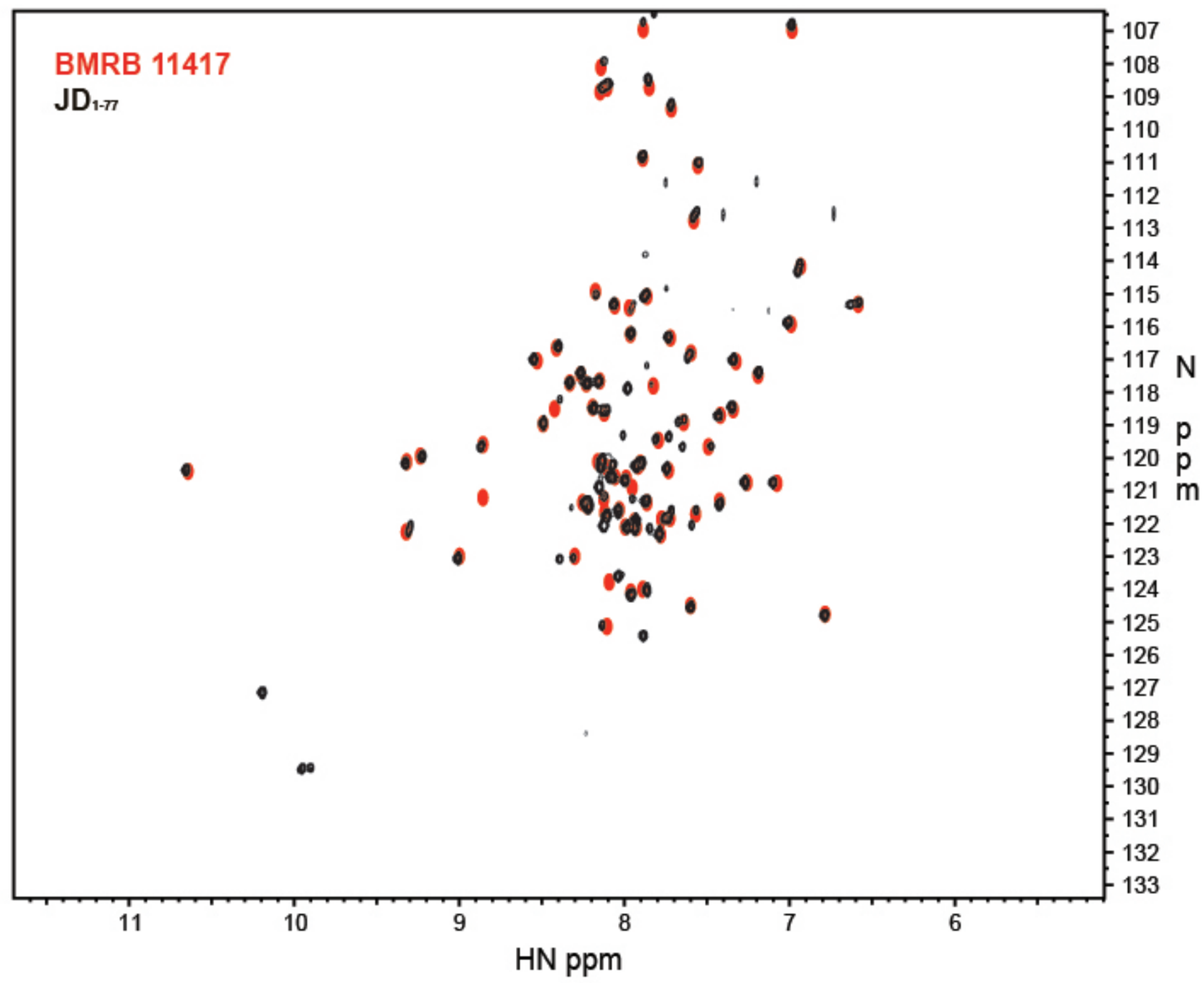
BMRB 11417
JD1-77
N
p
p
m
HN ppm

B

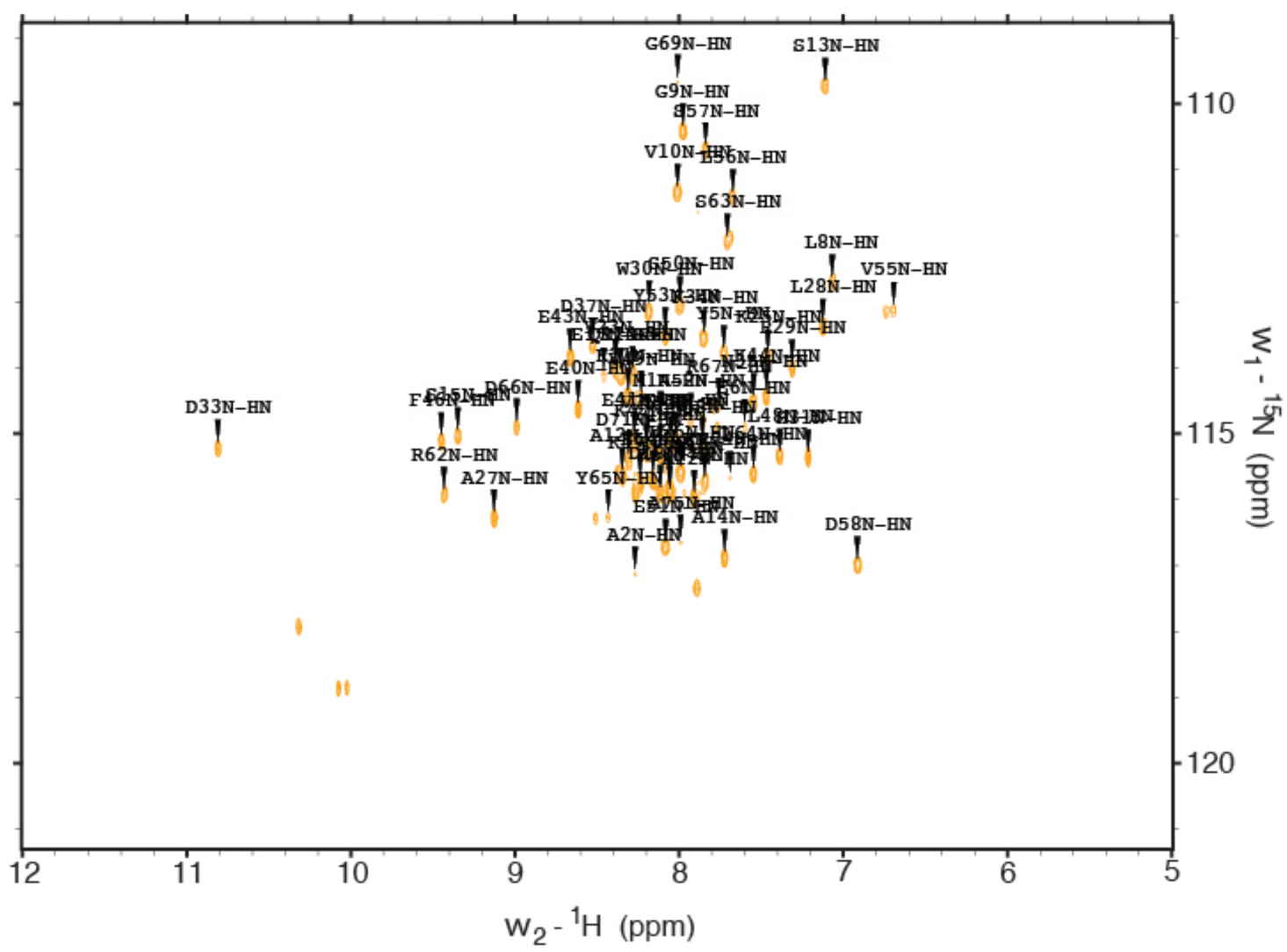
G69N-HN
S13N-HN
G9N-HN
S57N-HN
V10N-HN
S63N-HN
L8N-HN
V55N-HN
L28N-HN
D33N-HN
R62N-HN
A27N-HN
Y65N-HN
A14N-HN
A2N-HN
D58N-HN
w1 - 15N (ppm)
w2 - 1H (ppm)

Figure S7

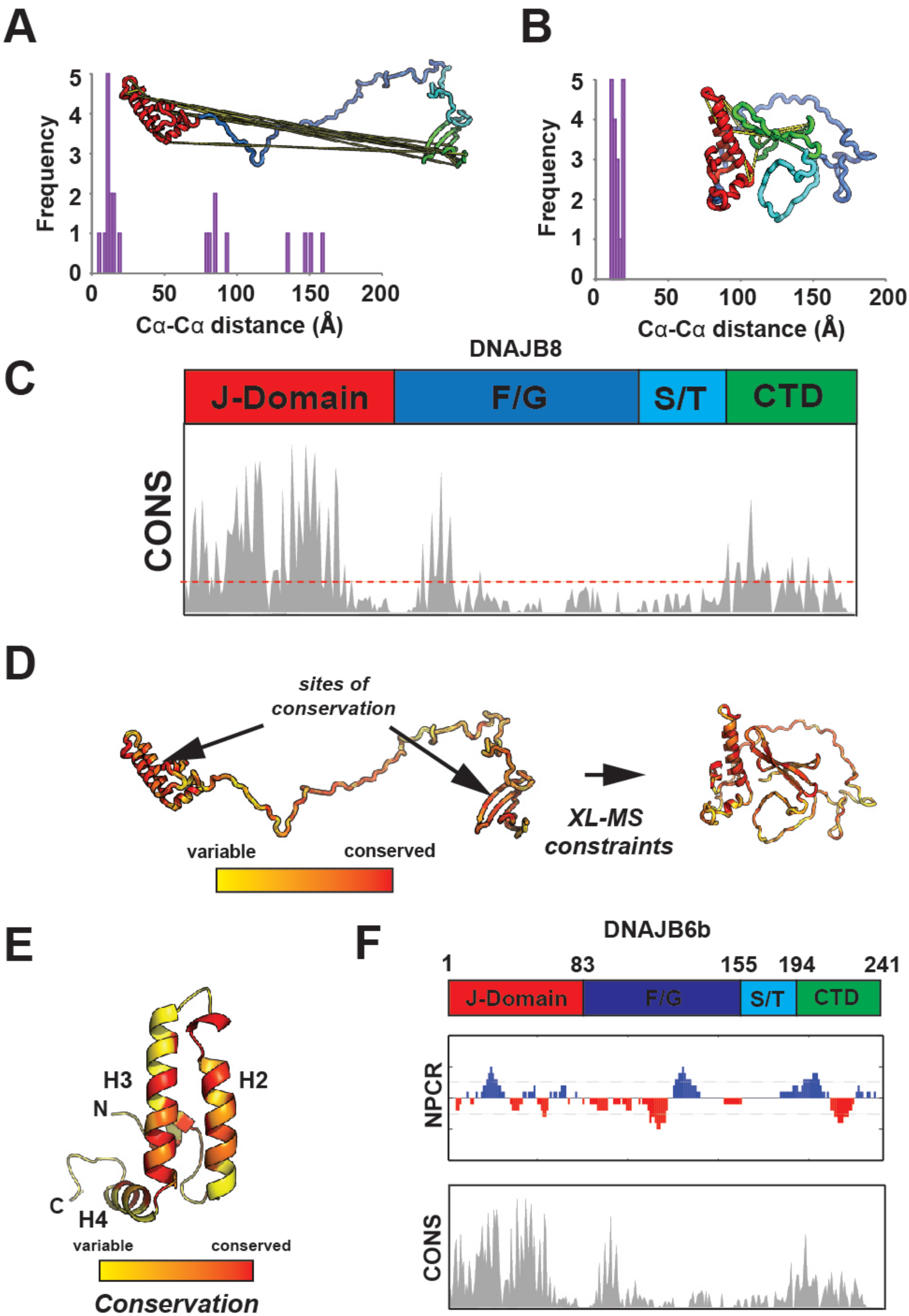
A
Frequency
Cα-Cα distance (Å)
B
Frequency
Cα-Cα distance (Å)
C
DNAJB8
J-Domain
F/G
S/T
CTD
CONS
D
sites of conservation
variable
conserved
XL-MS constraints
E
H3
H2
N
C
H4
variable
conserved
Conservation
F
DNAJB6b
1
83
155
194
241
J-Domain
F/G
S/T
CTD
NPCR
CONS

Figure S8

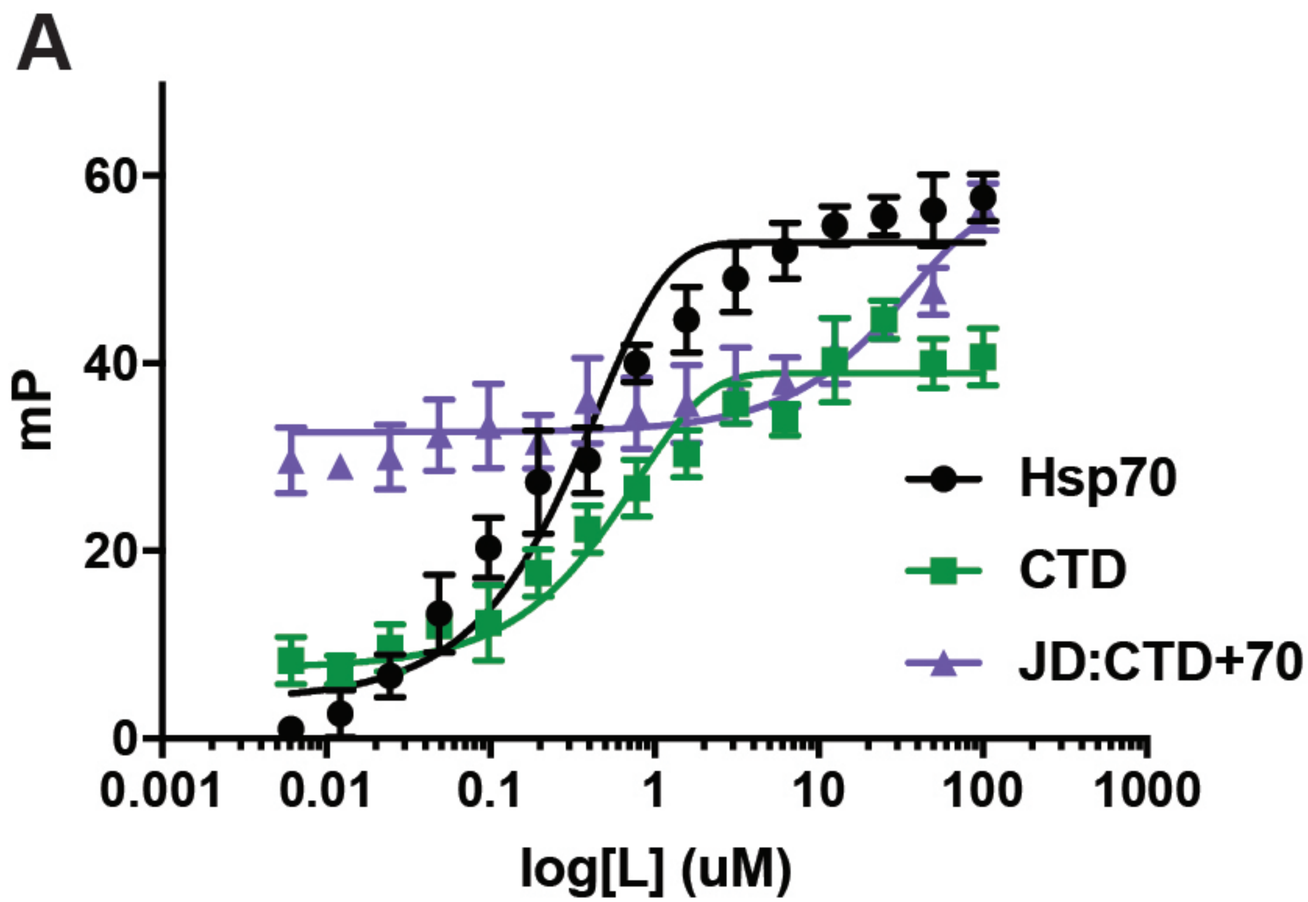
A
mP
60
40
20
0
0.001
0.01
0.1
1
10
100
1000
log[L] (uM)
Hsp70
CTD
JD:CTD+70